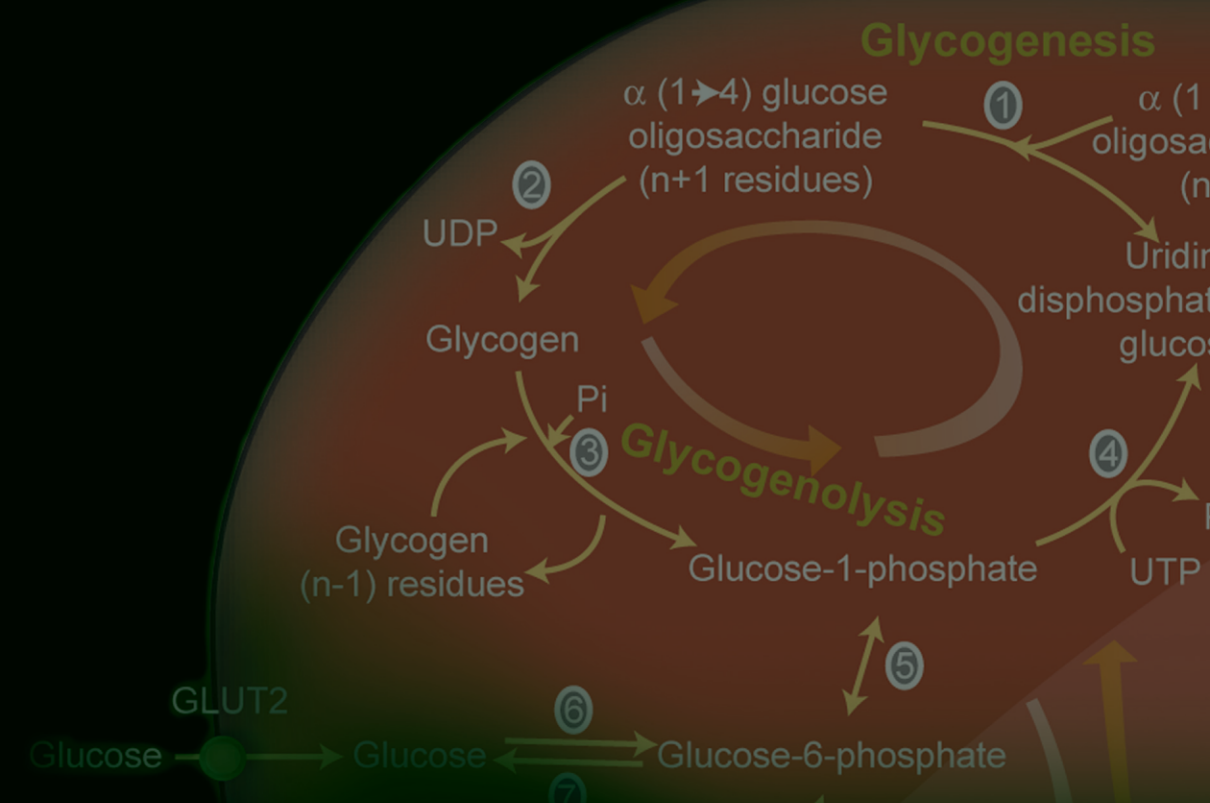

INSULIN RESISTANCE AND DIABETES

Insights from Magnetic Resonance studies of hepatic glucose and lipid metabolism

TERESA C. DELGADO

2008

UNIVERSIDADE DE COIMBRA

Insulin Resistance and Diabetes

Insights from Magnetic Resonance studies of hepatic glucose and lipid metabolism

Teresa C. Delgado
Universidade de Coimbra
2008

These studies were carried out at the Biochemistry Department of the Faculty of Sciences and Technology and at the NMR Laboratory of the Center for Neurosciences and Cell Biology of Coimbra, University of Coimbra, Portugal, under the supervision of Professor Doctor Carlos Frederico de Gusmão Campos Geraldes and co-supervision of Doctor John Griffith Jones. Part of the reported work took place at the Institute of Biomedical Research "Alberto Sols", Higher Council for Scientific Research, Autonomous University of Madrid, Madrid, Spain, under the guidance of Doctor Sebastián Cerdán García-Esteller. This Thesis was partially supported by a pre-doctoral fellowship from the Foundation of Science and Technology (FCT), Portugal (SFRH/BD/17010/2004).

Print Version:

Cover design: Javier Pérez
Special thanks to: Ana Delgado, Francesc Font, Inês Violante, Javier Pérez, Pedro Coxito, Valeria Righi.
Printed by: OGAMI, Serviços Multimédia, Coimbra, Portugal.

Departamento de Bioquímica
Faculdade de Ciências e Tecnologia
Universidade de Coimbra

Insulin Resistance and Diabetes

Insights from Magnetic Resonance studies of hepatic glucose and lipid metabolism

Dissertation presented to the Faculty of Sciences and Technology of the University of Coimbra for attribution of a Ph.D. degree in Biochemistry, speciality of Molecular Biophysics.

Resistência à Insulina e Diabetes

Estudos de Ressonância Magnética do metabolismo hepático da glicose e lipídico

Dissertação apresentada à Faculdade de Ciências e Tecnologia da Universidade de Coimbra para prestação de provas de Doutoramento em Bioquímica, especialidade de Biofísica Molecular.

Teresa C. Delgado

2008

Supervised by:

Carlos F.C.G. Geraldes, D.Phil.
Sebastián Cerdán García-Esteller, Ph.D.
John G. Jones, Ph.D.

Para os meus queridos pais, Francisco e Mª do Rosário

Para a melhor irmã do Mundo, Guida

Live as if you were to die tomorrow,
Learn as if you were to live forever

Mahatma Gandhi

CONTENTS

ABBREVIATIONS

γ	Gyromagnetic ratio
^{1}H	Proton
^{13}C	Carbon 13
^{14}C	Carbon 14
^{2}H	Deuterium
^{3}H	Tritrium
$^{2}H_2O$	Deuterated water
^{15}N	Nitrogen 15
^{31}P	Phosphorus 31
ADA	American Diabetes Association
ACP	Acyl carrier protein
ANOVA	Analysis of variance
ATP	Adenosine triphosphate
B_0 and B_1	Magnetic fields
BMI	Body mass index
C16	Palmitoyl
C18	Stearoyl
CLIX	Clamp like index
CNS	Central nervous system
CoA-SH	CoenzymeA
CsA	Cyclosporine A
CT	Computer-assisted Tomography
D_1	Pulse delay
DHAP	Dihydroxyacetone phosphate
DMSO	Dimethylsulfoxide
DNL	*De novo* lipogenesis
EGP	Endogenous glucose production
$F1,6P_2$	Fructose-1,6-bisphosphate
$F1,6P_2$ase	Fructose-1,6-bisphosphatase
F6P	Fructose-6-phosphate
FFA	Free fatty acids
FID	Free induction decay
Fk510	Tacrolimus
FT	Fourier transformed

G1P	Glucose-1-phosphate
G3P	Glyceraldehyde-3-phosphate
G6P	Glucose-6-phosphate
G6Pase	Glucose-6-phosphatase
GCs	Glucocorticoids
GC-MS	Gas Chromatography-Mass Spectrometry
GDM	Gestational diabetes *mellitus*
GTT	Glucose tolerance test
GLUT2	Hepatic non-insulin sensitive glucose transporter
GLUT4	Skeletal muscle insulin-sensitive glucose transporter
GK	Goto-Kakizaki
HDL	High density lipoprotein
HGP	Hepatic glucose production
HF	High fat
HOMA	Homeostasis Model Assessment
HPLC	High-Performance Liquid Chromatography
HSL	Hormone sensitive lipase
HTG	Hepatic triglycerides
IGT	Impaired glucose tolerance
IMCL	Intramyocellular lipids
i.p.	Intraperitoneal
IPGTT	Intraperitoneal glucose tolerance test
IR	Insulin resistance
IST	Insulin suppression test
ITT	Insulin tolerance test
i.v.	Intravenous
IVGTT	Intravenous glucose tolerance test
KTx	Kidney transplant
LDL	Low density lipoprotein
Li	Enrichment fraction of infusate tracer
Lp	Enrichment fraction of plasma glucose that is [3,4-^{13}C]glucose
LPL	Lipoprotein lipase
M6P	Mannose-6-phosphate
MAG	Monoacetone glucose
MAGL	Monoacetoneglucuronic lactone
MCMC	Markov Chain/Monte Carlo
MIDA	Mass isotopomer distribution analysis

MR	Magnetic Resonance
MRI	Magnetic Resonance Imaging
MRS	Magnetic Resonance Spectroscopy
MS	Mass Spectrometry
m/z	Mass to charge
NADH	Reduced nicotinamide adenine dinucleotide
NAFLD	Non-alcoholic fatty liver disease
NASH	Non-alcoholic steatohepatitis
NMR	Nuclear Magnetic Resonance
NOE	Nuclear Overhauser Effect
OGTT	Oral glucose tolerance test
PAGN	Phenylacetylglutamine
PEP	Phosphoenolpyruvate
PEPCK	Phosphoenolpyruvate carboxykinase
PET	Positron Emission Tomography
ppm	Parts *per* million
PRESS	Point-resolved spectroscopy
PTDM	Posttransplant diabetes *mellitus*
PW	Plasma water
QUICKI	Quantitative insulin check index
Ra	Rate of appearance
RF	Radio frequency
Ri	Infusion rate
ROI	Region of interest
SC	Standard chow
SEM	Standard error of the mean
SD	Standard deviation
SDBPP	Standard deviation of the Bayesian posterior probabilities
SMX	Sulfamethoxazole
SNR	Signal to noise ratio
SPECT	Single Photon Emission Computed Tomography
T	Tesla
T_1	Spin-lattice relaxation time
T_2	Spin-spin relaxation time
T1D	Type 1 diabetes
T2D	Type 2 diabetes
TA	Transaldolase

TCA	Tricarboxylic acids
TE	Echo time
TR	Repetition time
UDP-glucose	Uridine diphosphate-glucose
VLDL	Very low density lipoproteins
WHO	World Health Organization
ZDF	Zucker diabetic fatty

SUMMARY

In the last decades, insulin resistance (IR) and type 2 diabetes (T2D) are becoming more prevalent due to alterations in dietary and life-styles. Posttransplant diabetes *mellitus* (PTDM) has also become a subject of interest and importance in the wake of increased numbers and survival rates of solid organ transplantations. The liver is deeply involved in the regulation of whole body glucose and lipid homeostasis and hepatic glucose and lipid metabolic disruptions may play a central role in the onset of IR, T2D and PTDM. Changes in hepatic glucose and lipid fluxes using stable isotope tracers and Nuclear Magnetic Resonance (NMR) analysis both in animal models and patients with IR, T2D or PTDM were addressed in this Thesis. Moreover, further developments of techniques for the study of hepatic glucose metabolism from fasting to dynamic situations were challenged as well as for the integrated analysis of hepatic glucose and lipid metabolism.

In Chapter 1, whole body glucose and lipid metabolism were reviewed and integrated focusing on hepatic metabolic disruptions associated with IR and diabetes. Moreover, the stable isotope tracers and Magnetic Resonance techniques and their applications to hepatic metabolism evaluation were introduced.

In Chapter 2, fasting sources of endogenous glucose production (EGP) were evaluated in control and high fat (HF) diet induced-IR animal models by using [3,4-$^{13}C_2$]glucose and deuterated water ($^{2}H_2O$) combined with carbon 13 (^{13}C) and deuterium (^{2}H) NMR spectroscopy. Postabsorptive EGP from gluconeogenesis and glycogenolysis in HF diet-fed animals was essentially identical to the normally fed controls. The normal EGP rates found in HF diet-fed animals suggest that altered hepatic glucose fluxes are not involved in the development of IR secondary to HF diet feeding, at least in the early stages.

In Chapter 3, sources of fasting hepatic glucose production (HGP) were quantified in kidney transplant patients, undergoing cyclosporine A (CsA) immunosuppressant therapy. A novel Bayesian analysis of the position 2 and 5 ^{2}H NMR signals of monoacetone glucose derived from urinary acetaminophen glucuronide following $^{2}H_2O$ and acetominophen ingestion was proposed for quantification of gluconeogenesis and glycogenolysis relative contributions to HGP. For kidney transplant patients, the gluconeogenic contribution to HGP was significantly increased in the setting of PTDM. This metabolic alteration was found to be most strongly associated with adiposity and increased body mass index whereas CsA treatment *per se* provoked only modest alterations of HGP sources and was not shown to be associated with fasting hyperglycemia or hyperinsulinemia.

The fate of an intraperitoneal (i.p.) glucose load by ^{13}C and ^{2}H NMR analysis following administration of [U-^{13}C]glucose and $^{2}H_2O$ in healthy, HF diet-fed and CsA-treated rodents was addressed in Chapter 4. The contribution of HGP to total glucose was determined from the ^{2}H-enrichment of plasma glucose position 2 relative to that of plasma water and gluconeogenic sources were quantified from the ^{2}H-enrichment level at position 5 of plasma glucose relative to that of plasma water. The i.p. glucose load and "recycled" glucose from Cori cycle contributions to total glucose were estimated from the enrichment level of plasma [U- ^{13}C]glucose respective isotopomers relative to that of the load. Sources of total glucose after an i.p. glucose load were further evaluated in HF diet-fed and CsA-treated animals. Both groups of animals showed impaired glucose tolerance (IGT) relative to controls. HF diet did not promote impaired contribution from HGP and insulin secretion by pancreatic β-cells was not affected. Thus, the IGT of HF diet-fed animals can be attributed to decreased whole body glucose disposal secondary to peripheral insulin resistance rather than impaired HGP suppression. With CsA-treated animals the observed IGT was associated with a higher HGP contribution to plasma glucose levels, suggesting

that in this model impaired HGP suppression was a significant component of IGT.

Chapter 5 focused on postprandial hepatic glucose metabolism after a glucose load in healthy humans. Direct and indirect pathway contributions to hepatic glycogen synthesis during an oral glucose tolerance test (OGTT) were assessed by means of two isotopic tracers ([U-^{13}C]glucose and [U-$^{2}H_{7}$]glucose) following ingestion of peppermint oil and NMR analysis of plasma glucose and menthol glucuronide enrichments. Exchanges of both carbon and hydrogen moieties during the direct pathway metabolism of glucose were further revealed and quantified. During an OGTT in healthy humans, half of the hepatic glycogen synthesis was derived from 3-carbon precursors (indirect pathway) rather than directly from the glucose load. Furthermore, during an OGTT, ~20% of the direct pathway flux was involved in transaldolase exchange, hence the values derived from the [U-^{13}C]glucose tracer resulted in underestimates of the direct pathway contribution.

Sources of hepatic triglycerides accumulation in healthy and HF diet-fed rats, for evaluation of hepatic triglycerides content by using a novel $^{2}H_{2}O$ and ^{2}H NMR methodology combined with *in vivo* proton (^{1}H) Magnetic Resonance Spectroscopy (MRS), were determined in Chapter 6. In healthy rats, hepatic triglyceride levels can be acutely raised or lowered by altering the dietary fat content and these changes can be effectively monitored by ^{1}H MRS. During HF diet feeding, essentially all of the hepatic triglycerides were derived from dietary lipid with very little contribution from hepatic *de novo* lipogenesis.

Finally, Chapter 7 presents the concluding remarks where all the results described in this Thesis were integrated and further discussed.

RESUMO

Nas últimas décadas, a incidência de resistência à insulina e de diabetes tipo 2 têm aumentado principalmente devido a alterações de estilos de vida e na dieta. A diabetes pós-transplante é igualmente um tópico de crescente interesse considerando os números elevados e aumento das taxas de sobrevivência actuais de transplantes de orgãos. O fígado é um orgão profundamente envolvido na regulação da homeostase corporal da glicose e lipídica. Como tal, alterações hepáticas do metabolismo da glicose e lipídico poderão ocupar um papel central no desenvolvimento de patologias como a resistência à insulina, a diabetes tipo 2 ou a diabetes pós-transplante. Nesta Tese procedeu-se à avaliação do metabolismo hepático da glicose e lipídico em modelos animais e em pacientes com resistência à insulina, diabetes tipo 2 ou diabetes pós-transplante, utilizando-se marcadores de isótopos estáveis e análise por espectroscopia de Ressonância Magnética Nuclear (RMN). Adicionalmente, foram desenvolvidas novas metodologias para o estudo do metabolismo hepático da glicose em situações de jejum e em condições mais dinâmicas, e procedeu-se a uma análise integrativa do metabolismo hepático da glicose e lipídico.

No Capítulo 1, o metabolismo corporal da glicose e lípidos foi revisto e integrado focando as alterações do metabolismo hepático associadas à resistência à insulina e à diabetes. Os marcadores de isótopos estáveis e as técnicas de Ressonância Magnética assim como a sua aplicação à avaliação do metabolismo hepático foram introduzidos.

No Capítulo 2, as fontes endógenas de glicose durante o jejum foram avaliadas em ratos controlo e modelos animais de resistência à insulina induzida através de uma dieta rica em gordura. Para tal, utilizou-se [3,4-$^{13}C_2$]glicose e água deuterada ($^{2}H_2O$) em combinação com espectroscopia de RMN de carbono 13 (^{13}C) e deutério (^{2}H). A produção endógena de glicose resultante da

gluconeogénese e da glicogenólise determinada nos animais alimentados com uma dieta rica em gordura foi essencialmente idêntica à dos controlos com uma dieta normal. Os fluxos normais de produção endógena de glicose encontrados nos animais sujeitos a uma dieta rica em gordura sugerem que as alterações dos fluxos hepáticos da glicose não estão envolvidas, pelo menos nos estádios iniciais, no desenvolvimento da resistência à insulina como consequência de uma dieta rica em gordura.

No Capítulo 3, as fontes hepáticas de glicose durante o jejum foram quantificadas em pacientes com transplante renal e terapia imunossupressora baseada em Ciclosporina A (CsA). Foi proposta uma nova análise Bayesiana dos sinais de RMN de ^{2}H das posições 2 e 5 da monoacetona glicose derivada do glucuronado de paracetamol urinário, após ingestão de $^{2}H_2O$ e paracetamol, para a quantificação relativa das fontes gliconeogénicas e glicogenolíticas de produção hepática de glicose. Nos pacientes com transplante renal, a contribuição da gliconeogénese para a produção hepática de glicose é significativamente superior nos casos estabelecidos de diabetes pós-transplante. Esta alteração metabólica está principalmente relacionada com a crescente adiposidade e aumento do índice de massa corporal. Por outro lado, o tratamento com CsA *per se* provocou alterações modestas nas fontes hepáticas de glicose, não estando associado com a hiperglicémia ou hiperinsulinémia em jejum.

O destino de uma carga de glicose intra-peritoneal em ratos saudáveis foi estudado no Capítulo 4, utilizando a análise por espectroscopia de RMN de ^{13}C e ^{2}H após administração de [U-^{13}C]glicose e $^{2}H_2O$. A contribuição da produção hepática de glicose para a glicose total foi determinada a partir do enriquecimento em ^{2}H da posição 2 da glicose plasmática em relação ao enriquecimento da água plasmática. Por outro lado, a contribuição da gliconeogénese foi determinada pela quantificação da razão entre os enriquecimentos em ^{2}H da posição 5 do glicose plasmática e da água plasmática. As contribuições da carga intra-peritoneal de glicose e da glicose "reciclada" através do ciclo de Cori para a glicose total foram

estimadas a partir dos níveis de enriquecimento dos respectivos isotopómeros de [U-^{13}C]glicose presentes no plasma em relação ao enriquecimento inicial da carga de glicose. As fontes de glicose após a prova de tolerância à glicose intra-peritoneal foram avaliadas em animais sob uma dieta rica em gordura e com tratamento baseado em CsA. Ambos os grupos de animais mostraram intolerância à glicose relativamente aos controlos. Com a dieta rica em gordura, a produção hepática de glicose não foi alterada, tendo-se observado um padrão de secreção normal de insulina pelas células-β pancreáticas. Como tal, a hiperglicémia pós-prandial observada provavelmente reflecte uma ligeira resistência à insulina a nível dos orgãos periféricos em vez de produção hepática de glicose alterada. Por outro lado, nos animais tratados com CsA, a intolerância à glicose observada está associada com um aumento da contribuição da produção hepática de glicose.

O Capítulo 5 focou o metabolismo hepático pós-prandial de glicose após uma prova de tolerância à glicose oral (PTGO) em pessoas saudáveis. Foram avaliadas as contribuições relativas da via directa e indirecta de síntese de glicogénio durante a PTGO utilizando dois marcadores de isótopos estáveis ([U-^{13}C]glicose e [U-$^{2}H_7$]glicose), após ingestão de mentol e análise por espectroscopia de RMN dos enriquecimentos em ^{13}C e ^{2}H da glicose plasmática e do glucuronado de mentol urinário. As trocas existentes dos meios de carbono e de hidrogénio envolvidos foram reveladas e quantificadas. Durante a PTGO em pessoas saudáveis, cerca de metade da síntese de glicogénio hepático derivou de precursores de 3 carbonos (via indirecta) e não directamente da glicose oral fornecida. Durante a PTGO, ~20% do fluxo da via directa esteve envolvido em trocas promovidas pela transaldolase, pelo que os valores derivados a partir do marcador de [U-^{13}C]glicose resultam numa subestima das contribuições da via directa.

As fontes de triglicéridos hepáticos em ratos saudáveis e alimentados com uma dieta rica em gordura foram determinadas no Capítulo 6 utilizando uma nova metodologia baseada em $^{2}H_2O$ e análise por espectroscopia de RMN de ^{2}H juntamente com espectroscopia de Ressonância Magnética de protão (^{1}H)

in vivo para avaliação do conteúdo de triglicéridos no fígado. Em ratos saudáveis, os níveis de triglicéridos hepáticos podem ser rápidamente regulados alterando o conteúdo em gordura da dieta. Estas mudanças podem ser efectivamente monitorizadas usando espectroscopia de Ressonância Magnética de ^{1}H *in vivo*. Nos ratos com uma dieta rica em gordura, quase a totalidade dos triglicéridos hepáticos derivaram dos lípidos da dieta com uma contribuição residual da lipogénese *de novo* hepática.

Finalmente, o Capítulo 7 apresenta as conclusões gerais onde todos os resultados descritos nesta Tese foram discutidos e integrados.

Chapter 1

Hepatic glucose and lipid metabolism in insulin resistance and diabetes

1.1. Introduction

Diabetes *mellitus* is a widespread and growing public health problem affecting over 171 million people worldwide. The World Health Organization (WHO) predicts that by 2030 over 366 million people will be affected with diabetes. The growing worldwide prevalence of diabetes is highly associated with the increasingly sedentary life-style, together with access to energy-rich diets in genetically susceptible individuals. Diabetes is directly responsible for considerable morbidity and mortality, accounting for 5.2% of worldwide mortality in 2000 (Roglic *et al.* 2005). Moreover, the secondary complications of diabetes, including cardiovascular and microvascular dysfunction place a large burden on health care (i.e., heart failure, stroke, blindness and end-stage renal disease). Overall, treatment of diabetes and its secondary complications are estimated to consume up to 15% of the world's healthcare budget, hence its economic impact is considerable.

Diabetes is characterized by several metabolic disruptions that ultimately lead to hyperglycemia that can result either from impaired insulin secretion, type 1 diabetes (T1D) and/or abnormal insulin resistance (IR), type 2 diabetes (T2D) (Table 1.1). Insulin resistance can be defined as a state of reduced responsiveness of insulin-sensitive tissues to normal circulating levels of insulin. T2D accounts for the vast majority (85-95%) of diabetes worldwide incidence. In the wake of increased solid organ transplantation and improved survival rates, posttransplant diabetes *mellitus* (PTDM) and its adverse effects on organ rejection and quality of life is also a recent and rapidly growing concern. Of special interest is the possible role of cyclosporine A (CsA) and other immunosuppressive agents in the pathogenesis of PTDM. To the extent that PTDM is associated with IR and glucose intolerance, its pathophysiology resembles that of T2D but the underlying mechanisms, which like T2D may include disruptions of whole body glucose and lipid metabolism, remain unclear.

TABLE 1.1: Etiologic classification of diabetes *mellitus* (American Diabetes Association 2008).

I. Type 1 diabetes (T1D)	
Pancreatic β-cell destruction, usually leading to absolute insulin deficiency	
A. Immune mediated	
B. Idiopathic	
II. Type 2 diabetes (T2D)	
Predominantly insulin resistance with relative insulin deficiency	
III. Other specific types	
A. Genetic defects of β-cell function	
B. Genetic defects in insulin action	
C. Diseases of the exocrine pancreas	
D. Endocrinopathies	
E. Drug- or chemical-induced	Immunosuppressants and posttransplant diabetes *mellitus* (PTDM)
F. Infections	
G. Uncommon forms of immune-mediated diabetes	
H. Other genetic syndromes sometimes associated with diabetes	
IV. Gestational diabetes *mellitus* (GDM)	

The liver is an insulin sensitive organ that is highly involved in glucose and lipid biosynthesis. The effects of insulin in the liver are to appropriately alter metabolic fluxes of glucose and lipids to maintain whole body homeostasis. Mechanisms of hepatic metabolism regulation by insulin include alteration of metabolic gene expression and modulation of specific enzyme activities.

The development of IR and diabetes is closely linked with disruption of hepatic glucose and lipid metabolism. Classical approaches of hepatic metabolism assessment include rather invasive techniques such as liver biopsy or hepatic venous catheterization protocols. Currently, the development of techniques involving stable isotopes and Nuclear Magnetic Resonance (NMR) combined with the application of safe and noninvasive methods, such as Magnetic Resonance Imaging (MRI) and Spectroscopy (MRS) have made it possible to easily assess hepatic glucose and lipid metabolism *in vivo* in both animals and humans.

1.2. Integration of whole body glucose metabolism

Whole body glucose homeostasis is maintained over the daily feeding/fasting cycle through tight coordination between glucose appearance and disposal. Following carbohydrate ingestion, glucose is absorbed from the intestine into the hepatic portal vein. It then enters the liver, where a portion (~20%) is directly removed for storage as glycogen (Paquot *et al.* 2000, Petersen *et al.* 2001). The remaining glucose then enters the general circulation where it is consumed by peripheral tissues, such as skeletal muscle (Katz *et al.* 1983). The increased levels of plasma glucose promote pancreatic β-cells to secrete insulin which induces peripheral and splanchnic glucose uptake while at the same time, promoting hepatic glycogen synthesis and suppressing glucose production from the liver (Rizza *et al.* 1981) (Figure 1.1).

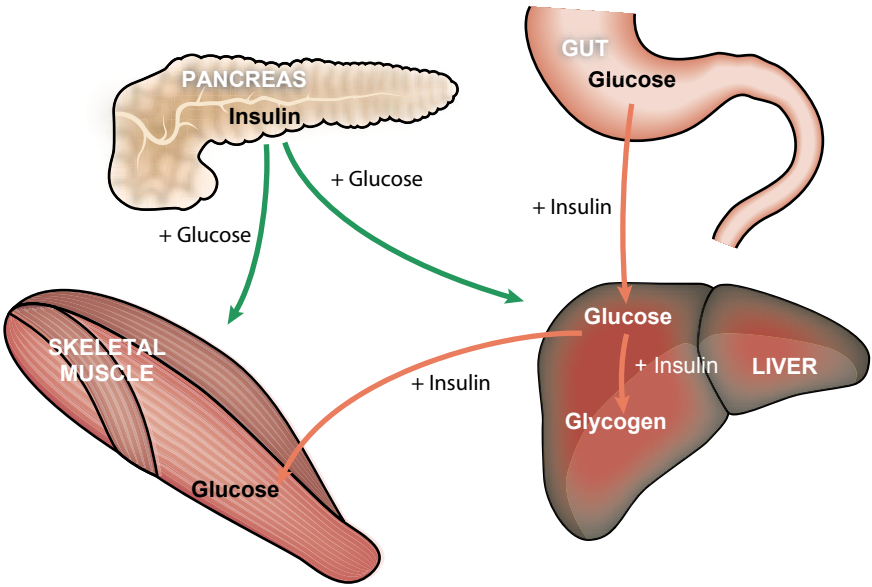

Figure 1.1. Patterns of whole body glucose metabolism in postprandial conditions.

In postabsorptive conditions, glucose appearance is entirely accounted for by endogenous glucose production (EGP) once digestive absorption has ceased. The ultimate step of glucose production from endogenous precursors involves the hydrolysis of glucose-6-phosphate (G6P) to glucose by glucose-6-phosphatase (G6Pase). Thus, only G6Pase expressing organs such as the liver and kidney can account for EGP (Van Schaftingen *et al.* 2002). While low levels of G6Pase activity have been found on other tissues such as pancreatic β-cells, intestine and skeletal muscle, these tissues do not represent significant sources of EGP (Ockerman *et al.* 1965, Khan *et al.* 1995, Gamberucci *et al.* 1996, Chatelain *et al.* 1998, Rajas *et al.* 1999, Croset *et al.* 2001). Under extreme conditions of acidosis or prolonged starvation, renal glucose production can contribute significantly to glucose production (Ekberg *et. al* 1999, Moller *et al.* 2001). However, under normal fasting conditions (i.e., overnight), hepatic glucose production (HGP) is the dominant source. HGP is regulated by insulin hence when insulin levels are low, as in the fasted state, HGP rates increase. Also, under these circumstances, glucagon is released from pancreatic α-cells, promoting the conversion of glycogen to glucose by the liver and further boosting HGP activity.

While liver, pancreas and skeletal muscle have long been considered to be the key tissues involved in glucose homeostasis, the role of other tissues (i.e., kidney, adipose tissue, gut and brain) is now being recognized. For example, after a meal, substrates stimulate the release of satiety signals, hormones and paracrine factors from the gut (i.e., ghrelin, amylin, peptide YY, apoliprotein A-1 and incretins (Holst and Gromada 2004)) and from the adipose tissue (leptin) (Buchanan *et al.* 1998). These signals then enter the circulation where they can directly stimulate the central nervous system (CNS) and inform about whole body energy availability. Subsequently, the CNS initiates and coordinates changes in energy and glucose homeostasis into peripheral tissues through changes in insulin secretion, HGP rates and glucose skeletal muscle uptake (Sandoval *et al.* 2008).

1.2.1. Hepatic glucose intermediary metabolism and endogenous glucose production

Hepatic glucose metabolism plays an important role in whole body glucose homeostasis by maintaining a balance between the uptake and storage of glucose and the release of glucose in response to the nutritional status.

After a meal, glucose is taken up by the liver predominantly by the non-insulin sensitive glucose transporter (GLUT2) (Leturque *et al.* 2005). The increase in hepatic portal vein glucose concentration activates glucokinase, through its rapid mobilization from the nucleus to the cytoplasm, and glucose is phosphorylated to G6P. G6P can be isomerized to fructose-6-phosphate (F6P) by phosphoglucose isomerase and further metabolized by glycolysis. Alternatively it can be stored as glycogen. Elevated G6P concentrations act synergistically with glucose and promote the inactivation of glycogen phosphorylase and activation of glycogen synthase (Agius 2008). Furthermore, hyperinsulinemia increases glycogen synthesis by counteracting the action of glycogenolytic hormones as glucagon and by activating glycogen synthase (Cohen *et al.* 1978).

Hepatic glycogen can be synthesized directly from G6P or through an indirect pathway where G6P is first metabolized to 3-carbon precursors before being deposited into glycogen (Hems *et al.* 1972, Newgard *et al.* 1983, Newgard *et al.* 1984, Kurland *et al.* 1989). Glycogen can also be synthesized from gluconeogenic precursors (i.e., lactate, gluconeogenic amino acids, glycerol) and these contribute to the indirect pathway flux. *In vivo* studies demonstrate that fluxes through direct and indirect pathways of glycogen synthesis are regulated by substrate and hormonal concentrations (Lang *et al.* 1986, Shulman *et al.* 1991). In healthy subjects, indirect pathway was found to contribute substantially (30-50%) to hepatic glycogen synthesis after a breakfast meal following an overnight fast (Taylor *et al.* 1996, Jones *et al.* 2006).

In postabsorptive conditions, when plasma glucose and insulin levels fall, the liver becomes a net producer of glucose through the conversion of G6P to glucose by G6Pase. Under these conditions, hepatic glycolytic fluxes drop due to decreased levels of the key glycolytic regulator fructose-2,6-biphosphatase and gluconeogenesis is promoted. Gluconeogenesis represents the generation of glucose from non-carbohydrate substrates (i.e., pyruvate, lactate, gluconeogenic amino acids and glycerol) and includes anaplerotic fluxes from the tricarboxylic acids (TCA) cycle. Gluconeogenesis is directly modified by insulin through inhibited expression of key gluconeogenic enzymes, namely phosphoenolpyruvate carboxykinase (PEPCK), fructose-1,6-bisphosphatase (F1,6P_2ase) and G6Pase (Barthel *et al.* 2003). In addition, insulin may inhibit gluconeogenesis by indirect mechanisms, as insulin-induced inhibition of adipose tissue lipolysis that reduces both free fatty acids (FFA) and glycerol availability for gluconeogenesis. Insulin also inhibits muscle proteolysis, resulting in a decreased availability of gluconeogenic amino acids (Umpleby *et al.* 1996).

Moreover, the increase in the circulating glucagon to insulin ratio, characteristic of fasting periods, activates glycogen phosphorylase and the concomitant mobilization of hepatic glycogen stores to generate glucose-1-phosphate (G1P), which is then converted to G6P and glucose (Figure 1.2). The relative contribution of gluconeogenesis and glycogenolysis to HGP depend on physiological conditions, hormonal factors and substrate availability. In healthy overnight fasted humans, gluconeogenesis and glycogenolysis contribute equally to HGP. As the fasting period increases, hepatic glycogen stores become depleted and the fraction of HGP derived from gluconeogenesis is increased (Landau *et al.* 1996). At 60 hours of fasting, gluconeogenesis accounts for more than 90% of HGP (Rothman *et al.* 1991).

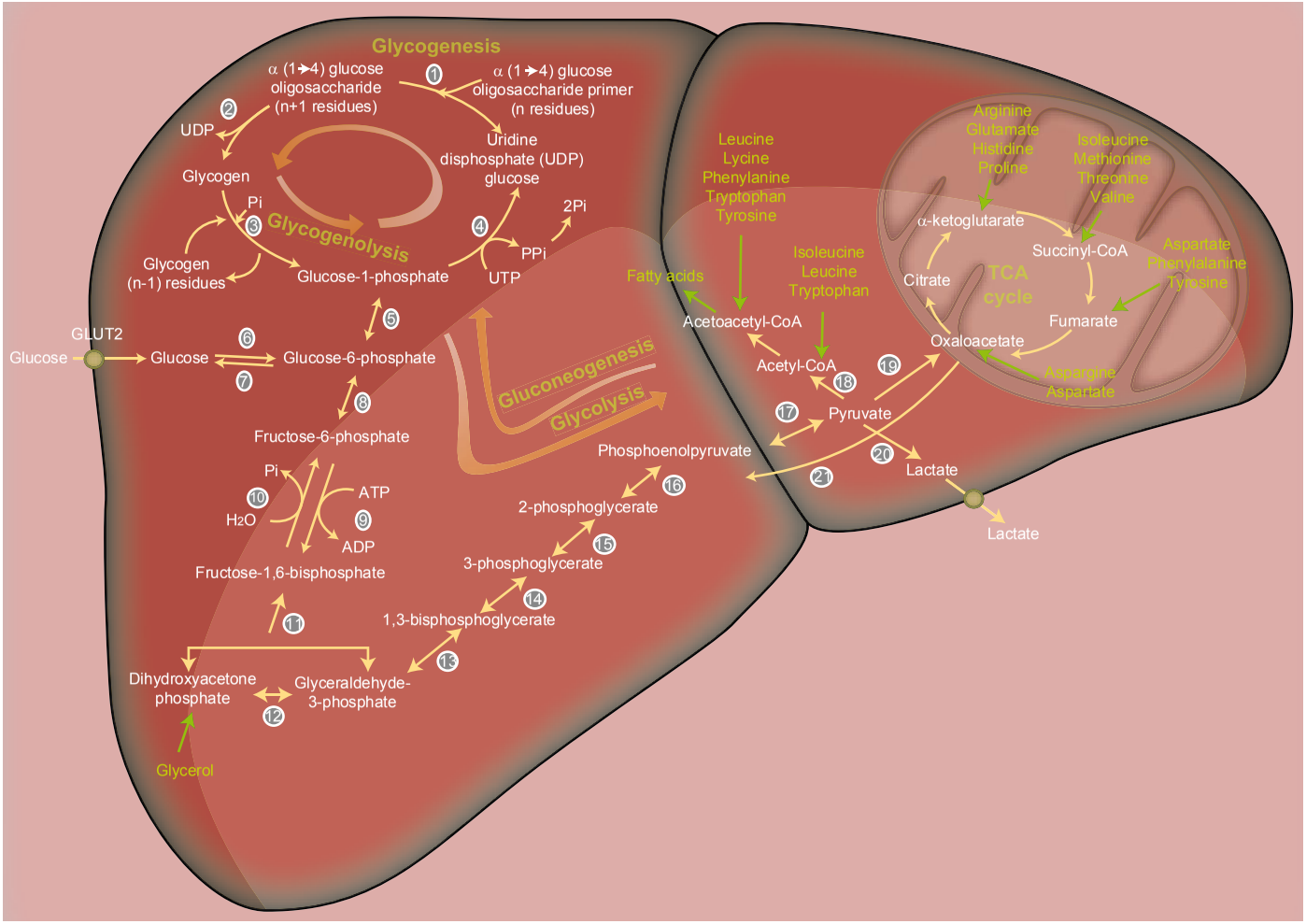
Glycogenesis
α (1➔4) glucose oligosaccharide (n+1 residues)
α (1➔4) glucose oligosaccharide primer (n residues)
UDP
Uridine disphosphate (UDP) glucose
Glycogen
Pi
2Pi
Glycogenolysis
PPi
UTP
Glycogen (n-1) residues
Glucose-1-phosphate
GLUT2
Glucose
Glucose
Glucose-6-phosphate
Gluconeogenesis
Glycolysis
Fructose-6-phosphate
Pi
ATP
H2O
ADP
Fructose-1,6-bisphosphate
Phosphoenolpyruvate
2-phosphoglycerate
3-phosphoglycerate
1,3-bisphosphoglycerate
Dihydroxyacetone phosphate
Glyceraldehyde-3-phosphate
Glycerol
Leucine
Lycine
Phenylanine
Tryptophan
Tyrosine
Fatty acids
Isoleucine
Leucine
Tryptophan
Acetoacetyl-CoA
Acetyl-CoA
Pyruvate
Lactate
Lactate
Arginine
Glutamate
Histidine
Proline
Isoleucine
Methionine
Threonine
Valine
α-ketoglutarate
Succinyl-CoA
Aspartate
Phenylalanine
Tyrosine
Citrate
TCA cycle
Fumarate
Oxaloacetate
Aspargine
Aspartate

Figure 1.2. Overview of hepatic glucose intermediary metabolism and hepatic glucose production. Glycolysis, gluconeogenesis, glycogenolysis, and glycogenesis are represented. 1. glycogen synthase; 2. glycogen branching-enzyme; 3. glycogen phosphorylase; 4. uridine diphosphate-glucose pyrophosphorylase; 5. phosphoglucomutase; 6. glucokinase; 7. glucose-6-phosphatase; 8. phosphoglucose isomerase; 9. phosphofuctokinase-1; 10. fructose-1,6-bisphosphatase; 11. fructose bisphosphate aldolase; 12. triose phosphate isomerase; 13. glyceraldehyde-3-phosphate dehydrogenase; 14. phosphoglycerate kinase; 15. phosphoglycerate mutase; 16. phosphoenolpyruvate hydratase; 17. pyruvate kinase; 18. pyruvate dehydrogenase; 19. pyruvate carboxylase; 20. lactate dehydrogenase; 21. phosphoenolpyruvate carboxykinase.

1.3. Integration of whole body lipid metabolism

Triglycerides account for the majority of dietary lipids. Ingested triglycerides are hydrolyzed in the gut and then absorbed in the small intestine where most of the fatty acids are resynthesized into triglycerides. Afterwards, triglycerides are released to the bloodstream through the lymphatic system in the form of chylomicron particles. Most of the triglycerides are further removed from chylomicrons by hydrolysis in non-hepatic tissues, such as adipose tissue by means of the insulin-stimulated lipoprotein lipase (LPL) (Sadur *et al.* 1982) whereas a minor percentage of triglycerides are taken up by skeletal muscle, by means of a LPL insensitive to insulin. After a meal, the net effect of insulin in adipose tissue is to enhance fatty acid storage as triglycerides with concomitant inhibition of fatty acids mobilization and oxidation. These stored triglycerides serve as a principal source of energy during fasting conditions.

In postabsorptive conditions, FFA are released from adipose tissue, through lipolysis of triglycerides. Lipolysis depends almost entirely on hormone-sensitive lipase (HSL) which is activated by a fall in insulin concentration and increase in glucagon levels (Meijssen *et al.* 2001). The rate of adipose tissue lipolysis exceeds that of fatty acid oxidation. Hence, a significant portion of fatty acids are reesterified into triglycerides within the adipose tissue, liver and skeletal muscle. Under normal circumstances, most FFA released from adipose

tissue are reesterified within the liver. Hepatic triglycerides can serve as local stores for hepatic needs or packaged in very low density lipoproteins (VLDL) for export into the bloodstream (Figure 1.3). Triglycerides accumulate in the liver when their synthesis exceeds their export *via* VLDL particles (Sanyal *et al.* 2005).

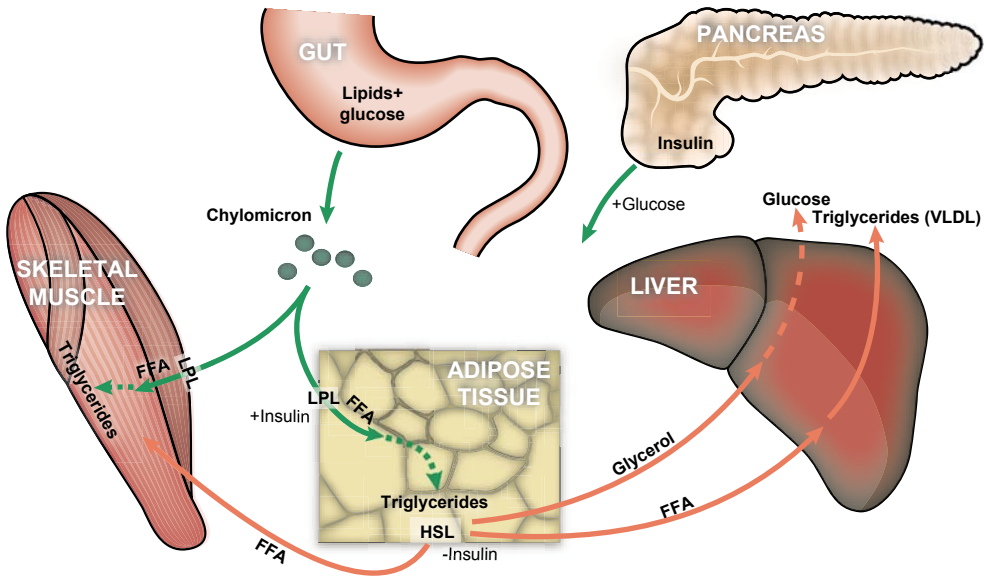

Figure 1.3. Patterns of whole body lipid metabolism in postprandial (in green) and postabsorptive conditions (in red). LPL. lipoprotein lipase; HSL. hormone-sensitive lipase; FFA. free fatty acids; VLDL. very low density lipoproteins.

There has been much interest in the role of fatty acids in whole body glucose homeostasis as they compete with glucose for substrates, as first described by Randle *et al.* (Randle *et al.* 1963). After a meal, elevated plasma glucose concentrations stimulate insulin secretion, which then suppresses FFA release from adipose tissue. This removes competition for substrate utilization in skeletal muscle and promotes whole body glucose disposal. Conversely, when plasma FFA concentration is high, usually as a result of low glucose and

insulin concentrations, fatty acids become the major fuel for skeletal muscle and glucose is spared for utilization by brain and CNS. Thus, the regulation of lipolysis enables FFA availability as an energy fuel to be inversely related to that of glucose.

1.3.1. Hepatic lipid intermediary metabolism

The major sources of hepatic fatty acids are: the uptake of fatty acids released by lipolysis of adipose tissue triglycerides, the uptake of triglycerides in VLDL and chylomicrons remnants, and hepatic *de novo* lipogenesis from acetyl-CoA. Long-term control of hepatic *de novo* lipogenesis involves changes in enzymatic activity and contributes to nutritional adaptations (i.e., increasing the capacity for endogenous triglyceride synthesis in response to a high carbohydrate and low fat diet). Short-term control over the daily feeding and fasting cycles involves modulation of enzyme activity by factors such as substrate supply and hormonal regulation. For example in the fed state, insulin promotes hepatic *de novo* lipogenesis by: 1) activation of pyruvate dehydrogenase and acetyl-CoA carboxylase to form acetyl-CoA and malonyl-CoA, respectively; 2) inactivation of pyruvate carboxylase and lactate dehydrogenase; and 3) stimulation of the fatty acid synthase (Wang *et al.* 1998, Sul *et al.* 2000), an enzymatic complex that catalyzes all reactions for the synthesis of fatty acids from acetyl-CoA and malonyl-CoA. After a meal, excess fatty acids are reesterified to triglycerides within the liver.

In postabsorptive conditions, the expression of fatty acid synthase is decreased with concomitant reduction of hepatic *de novo* lipogenesis. Under these conditions, hepatic fatty acids are mainly oxidized *via* β-oxidation to acetyl-CoA and the main function is energy production for liver many metabolic activities (i.e., gluconeogenesis). Fatty acids β-oxidation is regulated by malonyl-CoA levels that inhibit carnitine acyltranferase, responsible for the transport of fatty acids to mitochondria (where fatty acid β-oxidation occurs) (Figure 1.4).

Triglyceride synthesis
Fatty acid β-oxidation
Fatty acid activation
de novo lipogenesis
Fatty acid
ATP
PPi
Acyldenylate mixed anhidre
CoA-SH
AMP
Acyl-CoA
Fatty acyl-CoA
Acetoacetyl-ACP
E-SH+CO2
Malonyl-ACP
Malonyl-CoA
CE-SH
CoA-SH
Acetyl-ACP
CoA-SH
Acetyl-CoA
Non-lipidic percursors
CoA-SH
Lysophosphatidate
Fatty acyl-CoA
Glycerol-3-phosphate
CoA-SH
Phosphatidate
H2O
Pi
Diglyceride
Fatty acyl CoA
CoA-SH
Triglyceride
VLDL-Triglyceride
Fatty acyl-CoA
FAD
FADH2
Trans-enoyl--CoA
H20
3-L-hydroxyacyl-CoA
NAD+
NADH + H+
ß-Ketoacyl-CoA
CoA-SH
Acetyl-CoA
Fatty acyl-CoA (2C shorter)

Figure 1.4. Overview of hepatic lipid intermediary metabolism. Fatty acid *de novo* lipogenesis, activation and β-oxidation are represented as well as triglyceride synthesis and release. Abbreviations: ACP. acyl carrier protein; CoA-SH. CoenzymeA; 1. fatty acid synthase; 2. malonyl-CoA:ACP transacylase; 3. acyltransferase; 4. acyl-CoA dehydrogenase; 5. enoyl-CoA hydratase; 6. 3-L-hydroxyacyl-CoA dehydrogenase; 7. β-ketothiolase; 8. glycerol-3-phosphate acyltransferase; 9. phosphatidate phosphatase; 10. diglyceride acyltransferase.

1.4. Disruptions in glucose and lipid metabolism

1.4.1. Insulin resistance and type 2 diabetes

T2D is a heterogeneous and polygenic disorder resulting from the interaction of genetic and environmental factors (Romao *et al.* 2008). Several studies revealed altered gene expression associated with T2D including a number of genes that code for insulin signalling proteins. Apart from being a polygenic syndrome, T2D is also characterized by hyperglycemia and other metabolic perturbations secondary to IR and/or relative insulin deficiency. Hepatic and peripheral IR are key pathophysiological events in the onset of these metabolic disorders and may precede the onset of frank T2D by 10 to 20 years.

The majority of insulin-dependent glucose disposal occurs in skeletal muscle where insulin increases glucose uptake by stimulating the translocation of the insulin-sensitive glucose transporter, GLUT4, to the cell membrane. At a molecular level, multiple defects in insulin signalling have been implied in peripheral IR, including diminished insulin receptor number and affinity, altered insulin receptor kinase activity, decreased phosphorylation of intracellular substrates (i.e., IRS-1 and IRS-2) and abnormalities in glucose transporter translocation and activation (Saltiel and Khan 2001, Khan and Pessin 2002, Schinner *et al.* 2005). Thus, skeletal muscle IR is a consequence of abnormal insulin transduction pathways which culminates in the reduced uptake of glucose by GLUT4 and a substantial decrease in insulin stimulated muscle glycogen synthesis (Shulman *et al.* 1990, Cline *et al.* 1999, He *et al.* 2004).

In addition to impaired glucose clearance, there is also an excessive rate of fasting HGP in IR and T2D. Consoli *et al.* showed that about 90% of the increase in HGP in T2D can be accounted for enhanced gluconeogenesis (Consoli *et al.* 1989). Elevated gluconeogenesis in T2D can be attributed to several factors, such as increased circulating levels of gluconeogenic precursors, increased FFA oxidation, enhanced sensitivity to glucagon and decreased sensitivity to insulin. After a meal in healthy subjects, ~20% of total carbohydrate intake is stored as glycogen in the liver. Type 2 diabetics show decreased hepatic glycogen content (Magnusson *et al.* 1992). Defects in the process of hepatic glycogen synthesis secondary to hepatic IR may reduce the capacity of the liver to remove glucose from the circulation thus contributing to postprandial hyperglycemia. Moreover, inhibition of postprandial HGP is deffective in T2D.

Early in the development of IR, pancreatic β-cells secrete sufficient insulin to compensate for peripheral and splanchnic IR and normoglycemia is maintained (Saad *et al.* 1989). However, when pancreatic β-cells are unable to meet the increased demand for insulin secretion, hyperglycemia occurs (Szoke and Gerich 2005). In a vicious cycle, hyperglycemia *per se* (glucotoxicity) and the adverse effects of elevated fatty acids (lipotoxicity) (Shimabukuro *et al.* 1998, Grill *et al.* 2000) may also contribute to functional abnormalities and failure of pancreatic β-cells.

It is well known that disorders in fat storage and mobilization are associated with the pathophysiology of IR and T2D, hence obesity and T2D are often closely associated (Lewis *et al.* 2002, McGarry 2002, Kelley *et al.* 2003). In type 2 diabetics, the ability of insulin to suppress FFA release from adipose tissue by lipolysis is reduced (Coppack *et al.* 1994). The resultant excess circulating FFA will be reesterified to triglycerides in liver and skeletal muscle (Perseghin *et al.* 1999, Jacob *et al.* 1999, Virkamaki *et al.* 2001, Petersen and Shulman 2002, Machann *et al.* 2004). This ectopic accumulation of triglycerides interferes with insulin regulation of glucose metabolism (Miyazaki *et al.* 2002). For example, in

skeletal muscle, alterations in glucose transport activity are likely to result from the accumulation of intramyocellular lipids (IMCL) since this promotes altered insulin receptor kinase activity. Increased hepatic triglyceride (HTG) content is also implicated in hepatic IR (Ryysy *et al.* 2000, Marchesini *et al.* 2001, Kelley *et al.* 2003) since it is highly associated with excessive fasting and postprandial HGP rates (Boden *et al.* 2002). Mechanisms include the stimulation of gluconeogenesis and impaired insulin-mediated activation of glycogen synthase (Samuel *et al.* 2004).

Apart from metabolic alterations in the liver, skeletal muscle, pancreas and adipose tissue, increased glucose reabsorption in the kidney, decreased gut incretin effects (Knop *et al.* 2007) and neurotransmitter dysfunction (Schwartz *et al.* 2005) also contribute to hyperglycemia in T2D (Figure 1.5). More recently, the link between obesity and inflammation has raised the question of whether obesity-induced inflammation plays a role in the development of IR and T2D (Shoelson *et al.* 2006, Hotamisligil 2006). The concept that T2D has an immunological component provides the basis for formulating hypotheses that this syndrome and related factors as IR may be promoted in situations of immunodeficiency, as for instance patients on immunosuppressant therapy.

1.4.2. Posttransplant diabetes *mellitus*

PTDM is defined as the development of sustained hyperglycemia following an otherwise successful transplant procedure in patients without prior history of glucose intolerance or diabetes. The reported incidence of PTDM in literature is unclear, mainly due to a lack of consensus regarding the definition of the condition. Incidences as high as 25% have been reported (Reisæter and Hartmann 2001).

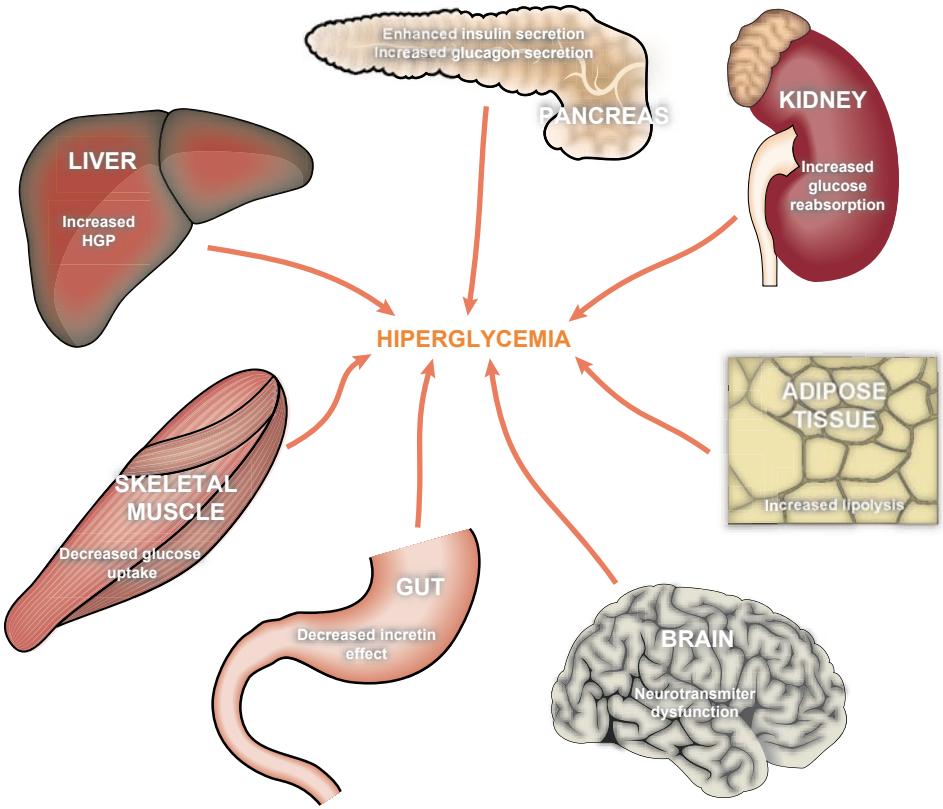

Figure 1.5. Whole body metabolic alterations leading to hyperglycemia in type 2 diabetes.

PTDM is generally accepted to be associated with a greater risk for morbidity and mortality from cardiovascular disease and a greater incidence of graft failure (Weir and Fink 1999, John *et al.* 2002, Salvadori *et al.* 2003, Markell 2004). Several PTDM risk factors have been identified including age, ethnicity, obesity, metabolic syndrome, hepatitis C infection and immunosuppressant regime (Jindal 1994, Weir and Fink 1999, Reisæter and Hartmann 2001, Salvadori 2003, Markell 2004, Marchetti 2004, Mora 2005). Throughout this Thesis, special attention will be given to one of the most widely used immunosuppressant drugs, the calcineurin inhibitor CsA, and particularly its effect on whole body glucose and lipid metabolism.

1.4.2.1. Calcineurin inhibitors

Under normal circunstances, calcineurin induces the transcription of interleukines which are citokines deeply involved in the immunological system activities. Calcineurin inhibitors bind to proteins called immunophilins forming complexes which bind to calcineurin promoting its inhibition. Thus, calcineurin inhibitors are associated with defective immune responses (Schreiber and Crabtree 1992, Kapturczak *et al.* 2004). The introduction of the calcineurin inhibitors, such as CsA and tacrolimus (Fk510), in immunosuppressive regimens was associated with a lower risk for PTDM. Nevertheless, CsA and Fk510 administration was shown to promote glucose intolerance, hence these drugs may also be diabetogenic, albeit to a lesser extent than for instance glucocorticoids (GCs).

In spite of some studies associating CsA with peripheral IR (Yale *et al.* 1988, Wahlstrom *et al.* 1990, Wahlstrom *et al.* 1992), the diabetogenic nature of CsA results mainly from it's disruption of pancreatic β-cell function (Doyle and Egan 2003), whether by affecting insulin synthesis or impairing the insulin secretory response of islet cells (Nielsen *et al.* 1986, Drachenberg *et al.* 1999, Hjelmesaeth *et al.* 2007). PTDM in patients on calcineurin inhibitors treatment indicate that calcineurin and its substrate (Nuclear Factor of Activated T-cells) may be required for β-cell function (Heit 2007). Furthermore, CsA administration is associated with dyslipidemia by increasing hepatic lipase activity and decreasing adipose tissue LPL hydrolysis thus resulting in impaired VLDL clearance (Subramanian *et al.* 2007). These disorders in fat storage and mobilization may in turn promote IR and contribute to PTDM.

1.5. Clinical assessment of hepatic metabolic disorders in insulin resistance and diabetes

In the development of T2D and PTDM, IR is predominant and underlies the failure in the stimulation of glucose uptake by skeletal muscle, and impaired control of HGP. Therefore, as a result of IR, fasting and/or postprandial hyperglycemia may prevail. Table 1.2 summarizes the current diabetes diagnostic criteria by the American Diabetes Association (ADA) (American Diabetes Association 2008). Typically, tests for assessment of IR can be separated into three different types: steady-state, fasting and dynamic measurement tests.

TABLE 1.2: Criteria diagnosis of diabetes *mellitus* by the American Diabetes Association (ADA) (American Diabetes Association 2008).

1) Symptoms of diabetes plus causal plasma glucose ≥ 11.1 mM
2) Fasting plasma glucose ≥ 7.0 mM
3) 2-h post-load glucose ≥ 11.1 mM during an oral glucose tolerance test (OGTT)

1.5.1. Steady-state measurement tests

Steady-state refers to the dynamic equilibrium of plasma glucose levels which implies that EGP and/or exogenously administered glucose equals the whole body glucose utilization rate. The gold standard method for quantifying IR is the hyperinsulinemic euglycemic clamp that was first introduced by Andres *et al.* (Andres *et al.* 1966) and later developed by DeFronzo *et al.* (DeFronzo *et al.* 1979). In the hyperinsulinemic euglycemic clamp technique, exogenous insulin is infused at constant levels to create hyperinsulinemia while the plasma glucose concentrations are kept at the euglycemic level using a variable glucose infusion. Thus, in these steady-state conditions, the rate of glucose infusion

is proportional to insulin sensitivity and inversely related to IR. Also, EGP is maximally suppressed such that the rate of glucose infusion approaches that of glucose disposal.

Under steady-state conditions, the insulin suppression test (IST), exploits the effect of insulin on glucose disposal after endogenous insulin is suppressed (i.e., by means of propranolol plus epinephrine or by infusing somatostatin). The increase in plasma glucose levels following suppression of insulin provides a measurement of insulin sensitivity.

1.5.2. Fasting measurement tests

Steady-state tests are quite laborious and time consuming, hence their routine implementation is not possible in clinical centers. Therefore, indicators of IR based on a basal measurement of fasting plasma glucose and insulin levels from a single blood sample have been developed. During fasting, glucose levels are a balance between EGP and whole body glucose disposal and both processes are regulated by insulin. Thus, elevated fasting plasma insulin and/or glucose are indicative of IR. Several models based on fasting insulin and glucose measurements have been developed, and validated against the hyperinsulinemic euglycemic clamp. For example, the homeostatic model assessment (HOMA), calculated from fasting plasma insulin and glucose, was first described by Matthews *et al.* (Matthews *et al.* 1985) and is indicative of IR. More recently, a quantitative insulin check index (QUICKI) was developed and is derived using the inverse of the sum of the logarithms of fasting plasma insulin and glucose (Katz *et al. 2*000). These indices are suitable for epidemiological studies where large study populations need to be sampled.

1.5.3. Dynamic measurement tests

To evaluate IR in dynamic conditions it is necessary to perturb the insulin/glucose system by providing glucose or insulin. During the intravenous

glucose tolerance test (IVGTT), metabolism is perturbed by infusing exogenous glucose and glucose clearance from plasma is assessed. The glucose clearance rates are proportional to peripheral IR. Alternatively, exogenous glucose can be provided by means of an oral load, such as in an oral glucose tolerance test (OGTT), or included in a more physiological mixed meal. Several models have been proposed for analytical interpretation of the OGTT empirical results, such as the model-based insulin sensitivity (OGIS) (Mari *et al.* 2001) and the clamp like index (CLIX) (Anderwald *et al.* 2007). Finally, glucose homeostasis can be perturbed by providing exogenous insulin and evaluating changes in plasma glucose levels, the insulin tolerance test (ITT).

The tests described in here, in spite of useful for assessment of peripheral insulin sensitivity and glucose disposal do not provide insights into the sources of plasma glucose and therefore hepatic glucose metabolism. For this purpose, metabolic tracers need to be incorporated into these assays.

1.6. Isotopic tracers in metabolic studies

Until recently, assessment of hepatic glucose and lipid metabolism was based on rather invasive studies. These include needle liver biopsies, which allow a direct quantification of hepatic metabolite concentrations (Beringer and Thaler 1964, Nilsson 1973, Nilsson and Hultman 1973, Nilsson and Hultman 1974), and catheterization protocols, which measure net uptake and release of substrates by the liver (Madison 1969, Wahren *et al.* 1972). The introduction of metabolic tracers was of fundamental importance for establishing the metabolic intermediates in the pathways of hepatic glucose and lipid metabolism as well as for determining pathway fluxes.

Following the development of Mass Spectrometry (MS) and the purification of hydrogen and other isotopes, the deuterium (^2H) stable isotope

was one of the first tracers used for *in vivo* metabolic studies (Schoenheimer *et al.* 1935). With the advent of simple instruments for quantifying radioactivity *via* scintillation counting and the availability of a wide range of carbon 14 (^{14}C) and tritrium (^{3}H) tracers, most of the pioneering studies in mammalian intermediary metabolism used radioactive tracers. The development of routine radioactivity measurements coincided with the development of paper and column chromatography techniques for separating complex metabolite mixtures. A resurgence in the use of stable isotopes followed the coupling of chromatographic separation with MS analysis in the form of the Gas Chromatography-Mass Spectrometry (GC-MS) instrument and the development of improved sensitivity for the detection of carbon 13 (^{13}C), ^{2}H and nitrogen 15 (^{15}N) nuclei by NMR. The replacement of radioactive with stable isotopes is required for most studies involving humans and is mandatory for all studies in children or women of child-bearing potential.

Considering the composition of biological substrates, ^{13}C and ^{2}H are widely used stable isotopes for *in vivo* studies. ^{13}C has natural background abundance of 1.11% while that of ^{2}H is 0.015%. Metabolic substrates for tracer studies are enriched to a high level (99%) with ^{13}C, ^{2}H or both. Hence, for a singly-labeled substrate, the highest attainable enrichment relative to the background level for that position is ~90-fold for ^{13}C and ~6,000-fold for ^{2}H. Since metabolic tracers may be diluted by 2-3 orders of magnitude by endogenous metabolites, the background abundance may contribute significantly to the detected isotope levels. For ^{13}C in particular, multi-labeled tracer substrates are preferred for metabolic studies as the enrichment of n positions in a given molecule results in a substantially reduction of background ^{13}C-signals of $(0.011)^{n}$.

1.7. Tracing glucose metabolism with stable isotopes

In postabsorptive conditions, liver is a net producer of glucose through gluconeogenesis and glycogenolysis. EGP fluxes can be evaluated by the constant infusion-isotope dilution technique. Briefly, after a constant infusion of a known concentration solution of a ^{13}C labeled glucose tracer, the infused labeled glucose will be diluted as a result of unlabeled glucose from EGP. Thus, the rate of appearance (R_a) of labeled glucose in plasma is proportional to EGP fluxes. However, glucose carbons are recycled during their metabolism *in vivo* thus resulting in a higher enrichment than would otherwise be expected leading to lower dilution and concomitant increased EGP estimates. To avoid these effects, non-recyclable tracers as [U-^{13}C]glucose or hydrogen isotope tracers (i.e., [2-^{2}H], [6,6-$^{2}H_2$], [2,3,6,6-$^{2}H_4$]glucose) are used where the carbon skeleton is broken or the hydrogens are removed during glucose recycling. Relative contributions of gluconeogenesis and glycogenolysis sources to glucose production can be estimated by using ^{13}C labeled gluconeogenic precursors (i.e., alanine, lactate or pyruvate) and measurement of plasma precursor and glucose enrichment at isotopic equilibrium.

However, the use of labeled glucose and ^{13}C labeled gluconeogenic precursors present some drawbacks such as: 1) difficulties in determining true precursor enrichments since plasma and liver enrichments of the tracer may differ; and 2) the zonation of hepatic metabolism could imply that the incorporation of the tracer into glucose is not representative of all hepatic substrates.

In the last decade, deuterated water ($^{2}H_2O$), has been widely used for evaluation of fasting glucose production sources. $^{2}H_2O$ is considered a safe and relative non-expensive tracer that can be used in humans as long as body water ^{2}H-enrichment level is limited to 0.3-0.5%. The main advantage of $^{2}H_2O$ is the fact that rapidly equilibrates with total body water implying that precursor enrichment can be determined precisely from plasma or urine enrichments.

Moreover, $^{2}H_2O$ is not affected by zonation of hepatic metabolism as it rapidly distributes through all tissues. After ingestion of $^{2}H_2O$, plasma glucose becomes enriched with ^{2}H at predictable positions depending upon the metabolic pathway that resulted in the formation of the glucose molecule. The quantification of the different plasma glucose ^{2}H positional enrichments can provide information on the gluconeogenic and glycogenolysis contributions to EGP (Landau *et al.* 1995, Landau *et al.* 1996).

After a meal, glucose is taken up by the liver, used for glycogen synthesis and EGP is inhibited. Consequently, the evaluation of hepatic glucose metabolism using stable isotopes in postprandial conditions is more complex. In postprandial conditions, when there is absorption of a meal or a glucose load, simultaneously with the intravenous (i.v.) infusion of a tracer, the newly absorbed glucose enters the portal vein and a fraction is removed by the liver, prior to entering peripheral circulation. Clearly, glucose meal and infusion tracers are not entering at equivalent points and the use of a second tracer is usually necessary, the dual-tracer method (Radziuk *et al.* 1978, Radziuk *et al.* 1987). Whereas the first tracer is infused intravenously, the second tracer is added to the glucose as part of the meal in order to calculate the systemic appearance rate of both ingested tracer and total glucose. More recently, a triple-tracer technique was suggested for estimation of postprandial appearance of total and ingested glucose, and the suppression of EGP. The first tracer is infused at a constant rate during the basal period and the second tracer is infused during the basal and in the postprandial period, being its infusion rate altered in the later to simulate the decline in postprandial EGP; finally, the third tracer is added to the meal (Basu *et al.* 2003). To date, dual- and triple-tracer methodologies, although very informative, are quite laborious and require complicated mathematical models for correct data extrapolation. Thus, in order to fully understand postprandial hepatic glucose metabolism, there is an urge for simpler protocols.

Hepatic glucose metabolism assessment using stable isotopes is based

on the assessment of plasma glucose, rather than by direct analysis of hepatic glucose metabolites. To the extent that other organs (i.e., kidney) may contribute to plasma glucose appearance, the analysis of plasma glucose enrichment may not represent hepatic metabolism. To address this, xenobiotic agents can be used for probing hepatic glucose metabolism. Xenobiotics are substances foreign to the body that are conjugated to specific glucose metabolic intermediates in the liver by several processes (i.e., glucuronidation, glutamination, ribosylation and others). For example, acetominophen and peppermint oil bind directly to hepatic uridine diphosphate-glucose (UDP-glucose) forming glucuronide that is excreted as urinary acetaminophen and menthol glucuronide, respectively (Landau *et al.* 1991, Jones *et al.* 2001, Burgess *et al.* 2003, Ribeiro *et al.* 2005, Mendes *et al.* 2006). The analysis of the urinary conjugated xenobiotics provides a means of noninvasively assess hepatic glucose metabolism. In addition, by using these biopsy agents, hepatic glycogen metabolism can be further assessed (i.e., direct and indirect pathway relative contributions to hepatic glycogen synthesis after a glucose load (Petersen *et al.* 2001, Jones *et al.* 2006)).

However, xenobiotic agents are not appropriate for liver failure patients and may reflect hepatic zonation as the xenobiotic agent may only be sampling one hepatic region. For example, hepatic glutamine is sampled by phenylacetate or phenylbutyrate as urinary phenyalcetylglutamine (PAGN) (Magnusson *et al.* 1991, Cline *et al.* 1994, Jones *et al.* 1998, Jones *et al.* 2001) only in the perivenous region of the liver. Thus, the enrichment patterns of glutamine may reflect that region and not the whole hepatic metabolism.

1.8. Tracing lipid metabolism with stable isotopes

During fasting, adipose tissue triglycerides are hydrolized to fatty acids that are released into the bloodstream. The fatty acids rate of appearance into

the bloodstream can be measured by the constant infusion-isotope dilution technique. Following infusion of labeled fatty acids (i.e., [U-^{13}C]palmitate or [U-^{13}C]oleate), the Ra of endogenous unlabeled fatty acids into the bloodstream can be determined by calculating the dilution of the infused fatty acid tracer. However, due to the reesterification of fatty acids within the adipose tissue, the rate of appearance of fatty acids does not always reflect lipolytic rates. Under fasting conditions, plasma glycerol is all derived from lipolysis and is utilized exclusively by the liver as other tissues lack glycerol kinase. Thus, the Ra of labeled glycerol determined after a primed constant infusion of [U-^{13}C]glycerol or [U-^{2}H]glycerol gives a direct measurement of adipose tissue lipolysis rates.

Excess fatty acids in the bloodstream can be uptaken by the liver, reesterified to triglycerides, and then released from the liver as VLDL triglycerides. Whole body triglyceride turnover is usually assessed by infusing a labeled fatty acid (i.e. [U-^{13}C]palmitate, [U-^{13}C]oleate) or glycerol and the appearance of labeled fatty acids in VLDL triglycerides is used to calculate the rate of triglycerides synthesis (Wolfe *et al.* 1973). Another approach is to pre-label the VLDL triglycerides with labeled glycerol or fatty acids. Afterwards, the VLDL are harvested by plasmapheresis and again infused into the subject for measurement of fractional VLDL turnover rates (Wolfe *et al.* 1985, Sidossis *et al.* 2004).

The fraction of hepatic fatty acids derived from acetyl-CoA by *de novo* lipogenesis can be assessed by using [1-^{13}C]acetate combined with the acetylated-xenobiotic probe technique, sulfamethoxazole (SMX) and analysis of the secreted VLDL. The SMX conjugates to hepatic acetyl-CoA and is later excreted in urine allowing the possibility to noninvasively assess hepatic acetyl-CoA ^{13}C-enrichment (Hellerstein *et al.* 1991). Blood VLDL triglycerides are then further analyzed and the ^{13}C-enrichment in fatty acids from triglycerides determined. The ratio of enrichments in fatty acids from VLDL triglycerides and acetyl-CoA reflects hepatic fatty acids *de novo* lipogenesis turnover rates.

$^{2}H_2O$ measurements have been applied with success to the study of lipid metabolism. For example, following $^{2}H_2O$ ingestion, the Ra of deuterium in whole body fatty acids is proportional to their synthetic rate (Schoenheimer *et al.* 1935, Lee *et al.* 2000, Bassilian *et al.* 2002).

^{2}H and ^{13}C-enrichments in lipid molecules are typically quantified by GC-MS, a technique where ions are sorted out by their mass to charge (m/z) ratio. Molecules that incorporate heavy isotopes, for example ^{13}C or ^{2}H, will have a higher m/z ratio that can be resolved by GC-MS. Moreover, mass isotopomer distribution analysis (MIDA) can be used for enrichment quantification of polymers synthesized from repeating monomeric units (i.e., fatty acids from acetyl-CoA units or triglycerides from fatty acids). MIDA is a mass spectrometric technique based on combinatorial probabilities. The theoretical advantage of MIDA is that the precursor enrichment can be inferred from that of the product (Hellerstein and Neese 1999). Hence, there is no need to measure precursor acetyl-CoA enrichments when measuring hepatic *de novo* lipogenesis rates.

1.9. Stable isotopes analysis by Nuclear Magnetic Resonance (NMR)

Because of the ^{13}C and ^{2}H nuclear spin properties, these isotopes can be monitored and detected using GC-MS and NMR spectroscopy for quantification of isotopic enrichment. GC-MS, is usually chosen because is more sensitive than NMR and due to its widespread application as a result of the relatively low instrumentation cost. However, if multiple stable isotopes or labeling patterns are used to probe additional metabolic pathways, NMR has a significant advantage, provided that its poor sensitivity is overcome by larger samples (10-100 μmol). In humans, 5 mL of blood and a urine sample easily fulfil this requirement for most of glucose and lipid metabolites. NMR is a non-destructive technique, ideally for repeated measurements. NMR principles are summarized schematically in Figure 1.6.

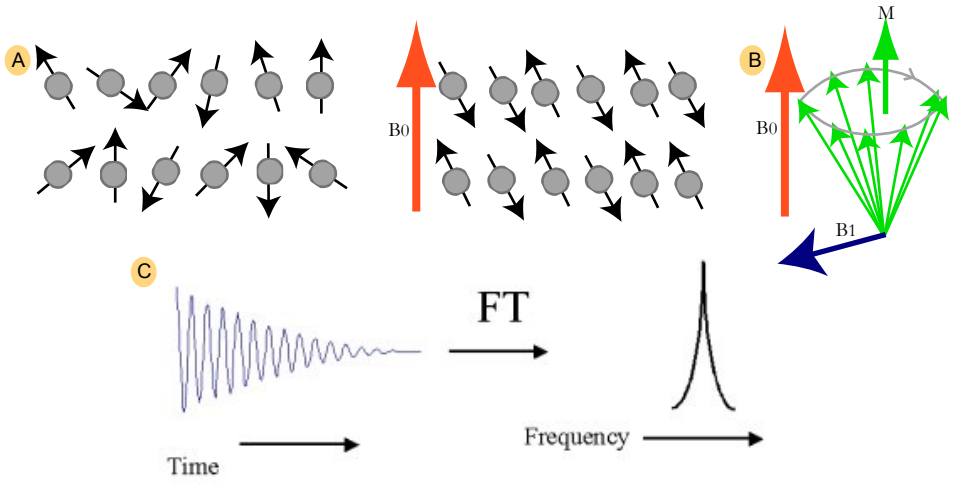

Figure 1.6. Principles of NMR Spectroscopy. NMR is a physical phenomenon based upon the quantum mechanical magnetic properties of certain atoms' nucleus (spin≠0) when placed in a strong static magnetic field (B_0) generated by a NMR spectrometer. **A.** The constant force applied, B_0, to the nucleus magnetic momentum induces an alignment. If the spin of the nucelus =1/2, parallel and anti-parallel alignment corresponds to the two energy levels allowed for each particular nucleus in presence of a magnetic field. **B.** Stimulation of the nuclei by an additional orthognal oscillating radio frequency (RF) magnetic field (B_1) at the nuclei Larmor frequency ($\omega_L = \gamma \times B_0$, where γ is the gyromagnetic ratio) transiently swings these nuclei out of alignment producing a magnetization vector, M. **C.** When the RF pulse is turned off, the return to the low energy state (spin-lattice T_1 relaxation) is associated with emission of non-radiative energy in the form of radiowaves that are detected by a receiver coil, the free induction decay (FID). Moreover, the nuclei can also fall out of alignment with each other (spin-spin T_2 relaxation). The length of T_1 and T_2 is closely related to molecular motion. The mathematical operation Fourier transformed (FT) of the FID originates the corresponding spectrum. Importantly, nuclei in a molecule resonate at a given but unique frequency, depending on the molecular structure. This is known as chemical shift and occurs because nuclei in different chemical environments experience slightly different magnetic field strengths resultant from the shielding offered by the nearby electrons.

1.9.1. ^{13}C NMR

^{13}C has a favourable nuclear spin (I=1/2) to NMR spectroscopy. Additionally, ^{13}C NMR displays a wide chemical shift range (~200 parts *per* million (ppm)), allowing a good resolution of the ^{13}C resonances. Moreover, peak signals in the ^{13}C NMR spectra display narrow lineshapes, due to slow T_1 relaxation, allowing a better separation of the distinct peak signals with appropriate correction for T_1 and Nuclear Overhauser Effect (NOE). A signal increase in the ^{13}C NMR spectrum corresponds to an increase in the ^{13}C-enrichment and therefore can be interpreted as an incorporation of label into the carbon position under observation. These ^{13}C-enrichments are referred to as positional enrichments and are easily quantified by ^{13}C NMR spectroscopy.

During metabolism, an isotopic tracer is submitted to pathway-specific carbon rearrangements and, upon labeling with ^{13}C, a specific range of isotopomers is produced. For a molecule with n carbons a maximum of 2^n different isotopomers exist. Multi-labeled isotopes are usually preferred for metabolic studies as the simultaneously enrichment of two covalently bound carbon positions in the same molecule not only increases the signal intensity for the two carbons positions but leads to homonuclear ^{13}C-^{13}C spin coupling, *J*-coupling, resulting in new signals called multiplets (Figure 1.7). The appearance of multiplets permits the resolution of background ^{13}C from ^{13}C tracer enrichments.

1.9.2. ^{2}H NMR

^{2}H is a nucleus with a quadrupolar moment and a spin of 1, resulting in broad signals in the ^{2}H NMR spectrum except for small molecules where ^{2}H signals are relatively narrow. Moreover, ^{2}H signals have low frequency dispersion (low gyromagnetic ratio- $\gamma/2\pi = 1/6.52$ that of proton (^{1}H)). This requires high magnetic fields and/or derivatization of molecules to forms where the signals are better resolved (i.e., glucose to monoacetone glucose (MAG)).

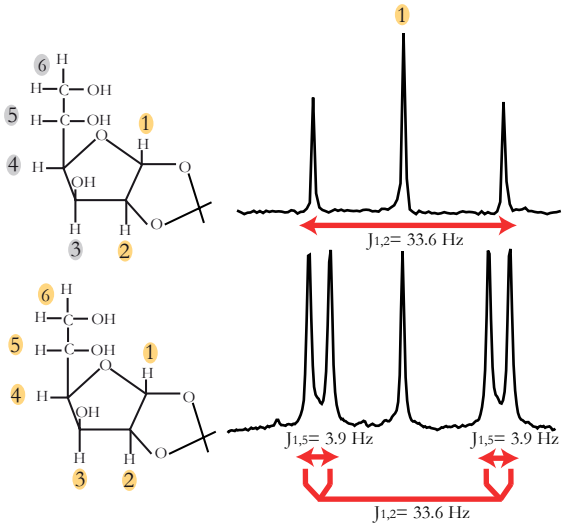

Figure 1.7. *J*-coupling arises from the interaction of different spin states through the chemical bonds of a molecule and results in the splitting of NMR signals. Coupling between n equivalent nuclei splits the signal into (n + 1) multiplets with intensity ratios following Pascal's triangle. Coupling between chemically equivalent nuclei (with equal chemical shift) has no effect in the NMR spectra and coupling between nuclei that are distant are usually too small to cause observable splittings. Long-range couplings over more than three bonds can often be observed in cyclic and aromatic compounds, leading to more complex splitting patterns. For example, in the monoacetone glucose (MAG) molecule, spin coupling between positions 1 and 2 is detected in the form of line splitting of the resonances of carbon 1 position into doublets and is characterized by the line separation within the doublets, $J_{1,2}$. When MAG is labeled in all the carbon positions, the resonance in carbon 1 will be split into a doublet due to the spin coupling between positions 1 and 2. Further splitting will occur due to coupling with carbon 5 of MAG, resulting in a superposition of both couplings, namely a doublet of doublets (Perdigoto *et al.* 2003).

At last, as the natural abundance of deuterium is much lower than of ^{13}C it can usually be neglected. Following the administration of a deuterated tracer, different positional ^{2}H-enrichments in a molecule of interest can be associated with different metabolic pathway fluxes, similar to what is observed with ^{13}C isotopomers. ^{2}H NMR spectroscopy allows the quantification of the different ^{2}H positional enrichments.

1.9.3. ^{1}H NMR

The proton (^{1}H) nucleus (spin=1/2) is the second most sensitive nucleus for NMR, in terms of intrinsic NMR sensitivity (high gyromagnetic ratio) and has high natural abundance (>99.9%). Since nearly all metabolites contain protons, ^{1}H NMR is a powerful technique to observe, identify and quantify a large number of biologically important metabolites. Due to ^{1}H high sensitivity, it's a suitable nucleus for *in vivo* studies by MRI and ^{1}H MRS.

1.10. *In vivo* Magnetic Resonance Imaging and Spectroscopy (MRI/MRS)

There are many tools available to assess the anatomy, dynamic and metabolism *in vivo*. Whereas X-ray and Computer-assisted Tomography (CT) can provide high-resolution structural images, Positron Emission Tomography (PET) and Single Photon Emission Computed Tomography (SPECT) present relatively low-resolution functional images. MRI is a relatively safe, as no ionizing radiation is used, and suitable technique for the noninvasive investigation of anatomy and morphology. Moreover, due to excellent chemical specificity as expressed in the chemical shift, MRS can be applied to the monitorization of particular intracellular metabolite concentrations and kinetics. MRI and MRS techniques are based on the principles of NMR and spatial localization of the MRI signal is achieved by using magnetic field gradients that are used to create position-dependent magnetic fields. The principal nuclei studied are ^{13}C and phosphorus (^{31}P) (for MRS) and especially ^{1}H (for MRI and ^{1}H MRS). MRI exploits the fact that proton concentration varies in the different types of body tissues. Also, different structures present distinct T_1 and T_2 values. Thus, different structures are revealed as these parameters can influence the intensity of the proton signal in a predictable manner with certain pulsing/acquisition conditions.

1.10.1. Assessment of hepatic glucose metabolism by *in vivo* ^{13}C MRS

Hepatic glucose metabolism is altered in diabetic states and assessment of hepatic glucose metabolism is therefore crucial. The 1.11% natural abundance of the ^{13}C nucleus allows observation of metabolites that are present in relatively high concentrations, such as glycogen. *In vivo* ^{13}C MRS can be used for assessment of hepatic glycogen metabolism. For example, the sharp signal at 100.4 ppm of carbon C1 of glycogen can be used to measure hepatic glycogen at different time points thus allowing the quantification of *in vivo* glycogenolysis or glycogen synthesis rates without any tracers (Rothman *et al.* 1991, Grueter *et al.* 1994) (Figure 1.8). Increased sensitivity of ^{13}C MRS can be attained by tracing ^{13}C incorporation into glycogen during infusion or ingestion of labeled glucose (Magnusson *et al.* 1994, Choi *et al.* 2002, Krssak *et al.* 2004).

Moreover, the development of technology that applies dynamic nuclear polarization to generate hyperpolarized ^{13}C labeled metabolic substrates can totally change the clinical potential of MRS of ^{13}C labeled metabolic substrates by increasing dramatically the sensitivity of ^{13}C MRS *in vivo*.

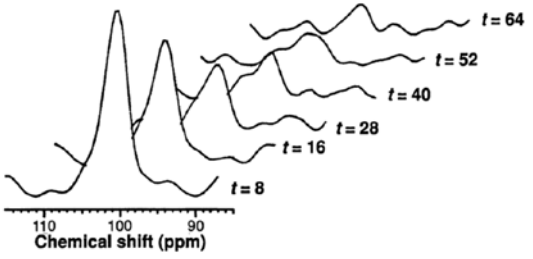

Figure 1.8. *In vivo* **^{13}C Magnetic Resonance spectra obtained from a healthy subject at different fasting times (h).** Reproduced from (Rothman *et al.* 1991) with permission of the publisher.

1.10.2. Assessment of hepatic lipid metabolism by *in vivo* MRI and ^{1}H MRS

Whole body and particularly hepatic triglyceride accumulation are closely associated with the onset of IR and diabetes. Whole body lipid metabolism disorders can be assessed by anthropometric methods of subcutaneous fat tissue and volume displacement measurements (Field *et al.* 2002). For measurement of whole body fat distribution, bioelectrical impedance analysis, ultrasound waves, double energy X-ray absorption, CT and MRI (T_1-relaxation based contrast images) can be used. On the other hand, before the introduction of Magnetic Resonance (MR) techniques (Szczepaniak *et al.* 1999), hepatic triglycerides accumulation was measured by means of rather invasive liver biopsies or by qualitative ultrasound measurements.

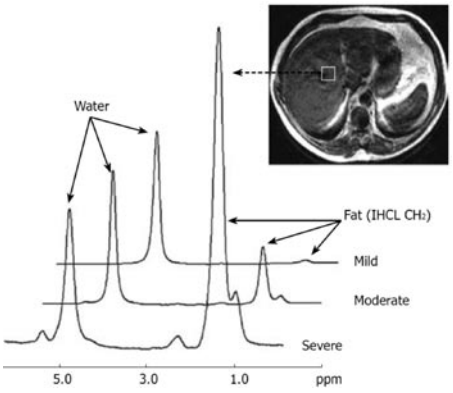

Figure 1.9. Hepatic ^{1}H Magnetic Resonance spectra of different subjects with progressive degrees of hepatic fatty infiltration. A single-voxel volume is defined in the region of interest (ROI) of liver and the ^{1}H Magnetic Resonance spectrum obtained from this region. Resonances from water at 4.7 ppm and lipid at 1.0-1.5 ppm can be clearly observed in the ^{1}H spectra. Reproduced from (Mehta *et al.* 2008) with permission of the publisher.

^{1}H MRS can be applied to the noninvasive measurement of hepatic triglycerides (Figure 1.9). However, by using single-voxel spectroscopy, only a small volume of the liver region of interest (ROI) is analyzed, not accounting for

intrinsic organ heterogeneity. More recently, the development of more potent spectrometers together with continuous research on pulse sequence design, made it possible to perform multi-voxel spectroscopy. In here, different volumes within the ROI are chosen and in a relatively short time, multi-voxel spectra obtained. The quantification of the intensity of the relative signals from water and lipids in each spectrum allows the performance of specific metabolite maps, chemical shift imaging (Venkataraman *et al.* 2002).

1.11. Scope, Aim and Outline of Thesis

In the last decades, IR and T2D are becoming more prevalent mainly due to alterations in dietary and life-styles. PTDM has also become a subject of interest considering the elevated incidences that prevail in posttransplant patients under immunosuppressant therapy after solid organ transplantation. Hepatic glucose and lipid metabolic disruptions appear to play a central role in the onset of IR, T2D and PTDM. Thus, by using novel stable isotope techniques combined with MR methodologies it is possible to study hepatic and glucose metabolism disruptions which are associated with the development of these pathologies. The aim of this Thesis is to define changes in hepatic glucose and lipid fluxes using stable isotope tracers and NMR analysis both in animal models and patients with IR, T2D or PTDM. Moreover, further developments of techniques for the study of hepatic glucose metabolism from fasting to dynamic situations are challenged as well as for the integrated analysis of hepatic glucose and lipid metabolism.

In Chapter 2, fasting sources of EGP are evaluated in rodents by using [3,4-$^{13}C_2$]glucose and $^{2}H_2O$ combined with ^{13}C and ^{2}H NMR spectroscopy. In addition, gluconeogenesis and glycogenolysis relative contributions to EGP are assessed in a HF diet induced-IR animal model.

In Chapter 3, contributions of gluconeogenesis and glycogenolysis to fasting HGP are quantified in kidney transplant patients undergoing CsA immunosuppressant therapy. A novel Bayesian analysis of the position 2 and 5 ^{2}H NMR of MAG derived from urinary acetaminophen glucuronide following $^{2}H_2O$ and acetominophen ingestion is used.

The fate of a glucose load by ^{13}C and ^{2}H NMR analysis following administration of [U-^{13}C]glucose and $^{2}H_2O$ in healthy, HF diet-fed and CsA treated rodents is addressed in Chapter 4.

Chapter 5 describes postprandial hepatic glucose metabolism after a glucose load in healthy humans. Direct and indirect pathway contributions to hepatic glycogen synthesis during an OGTT are assessed by means of two isotopic tracers ([U-^{13}C]glucose and [U-$^{2}H_7$]glucose), following ingestion of peppermint oil and NMR analysis of plasma glucose and menthol glucuronide ^{13}C and ^{2}H-enrichments, respectively.

Sources of hepatic triglycerides accumulation in healthy and HF diet-fed rats by using a novel $^{2}H_2O$ and ^{2}H NMR methodology combined with *in vivo* ^{1}H MRS for evaluation of hepatic triglycerides content are determined in Chapter 6. Finally, all the principal results of the previous chapters are integrated and further discussed in Chapter 7.

1.12. References

Agius L. Glucokinase and molecular aspects of liver glycogen metabolism. Biochem J 2008;414(1):1-18.

American Diabetes Association. Diagnosis and classification of diabetes *mellitus*. Diabetes Care 2008;31(Supplement_1):S55-S60.

Anderwald C, Anderwald-Stadler M, Promintzer M, Prager G, Mandl M, Nowotny P, Bischof MG, Wolzt M, Ludvik B, Kastenbauer T, Pacini G, Luger A, Krebs M. The Clamp-like index: A novel and highly sensitive insulin sensitivity index to calculate hyperinsulinemic clamp glucose infusion rates from oral glucose tolerance tests in nondiabetic subjects. Diabetes Care 2007;30(9):2374-2380.

Andres R, Swerdloff R, Pozefsky T, Coleman D. Manual feedback technique for the control of blood glucose concentration. Automation in Analytical Chemistry. 1966. 486-491.

Barthel A, Schmoll D. Novel concepts in insulin regulation of hepatic gluconeogenesis. Am J Physiol Endocrinol Metab 2003;285(4):E685-E692.

Bassilian S, Ahmed S, Lim SK, Boros LG, Mao CS, Lee W-NP. Loss of regulation of lipogenesis in the Zucker diabetic rat. II. Changes in stearate and oleate synthesis. Am J Physiol Endocrinol Metab 2002;282(3):E507-E513.

Basu R, Di Camillo B, Toffolo G, Basu A, Shah P, Vella A, Rizza R, Cobelli C. Use of a novel triple-tracer approach to assess postprandial glucose metabolism. Am J Physiol Endocrinol Metab 2003;284(1):E55-E69.

Beringer A, Thaler H. Quanitative studies of glycogen content of the liver in normal and sick persons. II. The influence of fructose and glucose on glycogen storage. Wien Klin Wochenschr 1964;76:627-630.

Boden G, Shulman GI. Free fatty acids in obesity and type 2 diabetes: defining their role in the development of insulin resistance and beta-cell dysfunction. Eur J Clin Invest 2002;32 Suppl 3:14-23.

Buchanan C, Mahesh V, Zamorano P, Brann D. Central nervous system effects of leptin. Trends Endocrinol Metab 1998;9(4):146-150.

Burgess SC, Weis B, Jones JG, Smith E, Merritt ME, Margolis D, Dean Sherry A, Malloy CR. Noninvasive evaluation of liver metabolism by ^{2}H and ^{13}C NMR isotopomer analysis of human urine. Anal Biochem. 2003;312(2):228-34.

Chatelain F, Pegorier JP, Minassian C, Bruni N, Tarpin S, Girard J, Mithieux G. Development and regulation of glucose-6-phosphatase gene expression in rat liver, intestine, and kidney: *in vivo* and *in vitro* studies in cultured fetal hepatocytes. Diabetes 1998;47(6):882-889.

Choi IY, Wu C, Okar DA, Lange AJ, Gruetter R. Elucidation of the role of fructose 2,6-bisphosphate in the regulation of glucose fluxes in mice using *in vivo* (13)C NMR measurements of hepatic carbohydrate metabolism. Eur J Biochem 2002;269(18):4418-4426.

Cline GW, Petersen KF, Krssak M, Shen J, Hundal RS, Trajanoski Z, Inzucchi S, Dresner A, Rothman DL, Shulman GI. Impaired glucose transport as a cause of decreased insulin-stimulated muscle glycogen synthesis in type 2 diabetes. N Engl J Med 1999;341(4):240-246.

Cline GW, Rothman DL, Magnusson I, Katz LD, Shulman GI. ^{13}C-nuclear magnetic resonance spectroscopy studies of hepatic glucose metabolism in normal subjects and subjects with insulin-dependent diabetes *mellitus*. J Clin Invest 1994;94(6):2369-2376.

Cohen P, Nimmo HG, Proud CG. How does insulin stimulate glycogen synthesis? Biochem Soc Symp 1978;(43):69-95.

Consoli A, Nurjhan N, Capani F, Gerich J. Predominant role of gluconeogenesis in increased hepatic glucose production in NIDDM. Diabetes 1989;38(5):550-557.

Coppack SW, Jensen MD, Miles JM. *In vivo* regulation of lipolysis in humans. J Lipid Res 1994;35(2):177-193.

Croset M, Rajas F, Zitoun C, Hurot JM, Montano S, Mithieux G. Rat small intestine is an insulin-sensitive gluconeogenic organ. Diabetes 2001;50(4):740-746.

DeFronzo RA, Tobin JD, Andres R. Glucose clamp technique: a method for quantifying insulin secretion and resistance. Am J Physiol Endocrinol Metab 1979;237(3):E214-E223.

Doyle ME, Egan JM. Pharmacological agents that directly modulate insulin secretion. Pharmacol Rev 2003;55(1):105-131.

Drachenberg CB, Klassen DK, Weir MR, Wiland A, Fink JC, Bartlett ST, Cangro CB, Blahut S, Papadimitriou JC. Islet cell damage associated with tacrolimus and cyclosporine: morphological features in pancreas allograft biopsies and clinical correlation. Transplantation 1999;68(3):396-402.

Ekberg K, Landau BR, Wajngot A, Chandramouli V, Efendic S, Brunengraber H, Wahren J. Contributions by kidney and liver to glucose production in the postabsorptive state and after 60 h of fasting. Diabetes 1999;48(2):292-298.

Fields DA, Goran MI, McCrory MA. Body-composition assessment *via* air-displacement plethysmography in adults and children: a review. Am J Clinical Nutrition 2002;75(3):453-467.

Gamberucci A, Marcolongo P, Fulceri R, Giunti R, Watkins SL, Waddell ID, Burchell A, Benedetti A. Low levels of glucose-6-phosphate hydrolysis in the sarcoplasmic reticulum of skeletal muscle: involvement of glucose-6-phosphatase. Mol Membr Biol 1996;13(2):103-108.

Grill V, Bjorklund A. Dysfunctional insulin secretion in type 2 diabetes: role of metabolic abnormalities. Cell Mol Life Sci 2000;57(3):429-440.

Gruetter R, Magnusson I, Rothman DL, Avison MJ, Shulman RG, Shulman GI. Validation of ^{13}C NMR measurements of liver glycogen *in vivo*. Magn Reson Med 1994;31(6):583-588.

He J, Kelley DE. Muscle glycogen content in type 2 diabetes *mellitus*. Am J Physiol Endocrinol Metab 2004;287(5):E1002-E1007.

Heit JJ. Calcineurin/NFAT signaling in the beta-cell: From diabetes to new therapeutics. Bioessays 2007;29(10):1011-1021.

Hellerstein MK, Christiansen M, Kaempfer S, Kletke C, Wu K, Reid JS, Mulligan K, Hellerstein NS, Shackleton CH. Measurement of *de novo* hepatic lipogenesis in humans using stable isotopes. J Clin Invest 1991;87(5):1841-1852.

Hellerstein MK, Neese RA. Mass isotopomer distribution analysis at eight years: theoretical, analytic, and experimental considerations. Am J Physiol Endocrinol Metab 1999;276(6):E1146-E1170.

Hems DA, Whitton PD, Taylor EA. Glycogen synthesis in the perfused liver of the starved rat. Biochem J 1972;129(3):529-538.

Hjelmesaeth J, Hagen LT, Asberg A, Midtvedt K, Storset O, Halvorsen CE, Morkrid L, Hartmann A, Jenssen T. The impact of short-term ciclosporin A treatment on insulin secretion and insulin sensitivity in man. Nephrol Dial Transplant 2007;22(6):1743-1749.

Holst JJ, Gromada J. Role of incretin hormones in the regulation of insulin secretion in diabetic and nondiabetic humans. Am J Physiol Endocrinol Metab 2004;287(2):E199-E206.

Hotamisligil GS. Inflammation and metabolic disorders. Nature 2006:860-867.

Jacob S, Machann J, Rett K, Brechtel K, Volk A, Renn W, Maerker E, Matthaei S, Schick F, Claussen CD, Haring HU. Association of increased intramyocellular lipid content with insulin resistance in lean nondiabetic offspring of type 2 diabetic subjects. Diabetes 1999;48(5):1113-1119.

Jindal RM. Posttransplant diabetes *mellitus*- a review. Transplantation 1994;58(12):1289-1298.

John PR, Thuluvath PJ. Outcome of patients with new-onset diabetes *mellitus* after liver transplantation compared with those without diabetes *mellitus*. Liver Transpl 2002;8(8):708-713.

Jones JG, Fagulha A, Barosa C, Bastos M, Barros L, Baptista C, Caldeira MM, Carvalheiro M. Noninvasive analysis of hepatic glycogen kinetics before and after breakfast with deuterated water and acetaminophen. Diabetes 2006;55(8):2294-2300.

Jones JG, Solomon MA, Sherry AD, Jeffrey FM, Malloy CR. ^{13}C NMR measurements of human gluconeogenic fluxes after ingestion of [U-13C]propionate, phenylacetate, and acetaminophen. Am J Physiol. 1998;275(5 Pt 1):E843-52.

Kapturczak MH, Meier-Kriesche HU, Kaplan B. Pharmacology of calcineurin antagonists. Transplant Proc 2004;36(2 Suppl):25S-32S.

Katz A, Nambi SS, Mather K, Baron AD, Follmann DA, Sullivan G, Quon MJ. Quantitative insulin sensitivity check index: A simple, accurate method for assessing insulin sensitivity in humans. J Clin Endocrinol Metab 2000;85(7):2402-2410.

Katz LD, Glickman MG, Rapoport S, Ferrannini E, DeFronzo RA. Splanchnic and peripheral disposal of oral glucose in man. Diabetes 1983;32(7):675-679.

Kelley DE, McKolanis TM, Hegazi RAF, Kuller LH, Kalhan SC. Fatty liver in type 2 diabetes *mellitus*: relation to regional adiposity, fatty acids, and insulin resistance. Am J Physiol Endocrinol Metab 2003;285(4):E906-E916.

Khan A, Hong-Lie C, Landau BR. Glucose-6-phosphatase activity in islets from ob/ob and lean mice and the effect of dexamethasone. Endocrinology 1995;136(5):1934-1938.

Khan AH, Pessin JE. Insulin regulation of glucose uptake: a complex interplay of intracellular signalling pathways. Diabetologia 2002;45(11):1475-1483.

Knop FK, Vilsboll T, Hojberg PV, Larsen S, Madsbad S, Volund A, Holst JJ, Krarup T. Reduced incretin effect in type 2 diabetes: cause or consequence of the diabetic state? Diabetes 2007;56(8):1951-1959.

Krssak M, Brehm A, Bernroider E, Anderwald C, Nowotny P, Man CD, Cobelli C, Cline GW, Shulman GI, Waldhausl W, Roden M. Alterations in postprandial hepatic glycogen metabolism in type 2 diabetes. Diabetes 2004;53(12):3048-3056.

Kurland IJ, Pilkis SJ. Indirect *versus* direct routes of hepatic glycogen synthesis. FASEB J 1989;3(11):2277-2281.

Landau BR. Noninvasive approaches to tracing pathways in carbohydrate metabolism. J Parenter Enteral Nutr 1991;15(3):74S-777.

Landau BR, Chandramouli V, Schumann WC, Ekberg K, Kumaran K, Kalhan SC, Wahren J. Estimates of krebs cycle activity and contributions of gluconeogenesis to hepatic glucose production in fasting healthy-subjects and IDDM patients. Diabetologia 1995;38(7):831-838.

Landau BR, Fernandez CA, Previs SF, Ekberg K, Chandramouli V, Wahren J, Kalhan SC, Brunengraber H. A limitation in the use of mass isotopomer distributions to measure gluconeogenesis in fasting humans. Am J Physiol Endocrinol Metab 1995;32(1):E18-E26.

Landau BR, Wahren J, Chandramouli V, Schumann WC, Ekberg K, Kalhan SC. Contributions of gluconeogenesis to glucose production in the fasted state. J Clin Invest 1996;98(2):378-385.

Lang CH, Bagby GJ, Blakesley HL, Johnson JL, Spitzer JJ. Plasma glucose concentration determines direct *versus* indirect liver glycogen synthesis. Am J Physiol Endocrinol Metab 1986;251(5):E584-E590.

Lee W-NP, Bassilian S, Lim S, Boros LG. Loss of regulation of lipogenesis in the Zucker diabetic (ZDF) rat. Am J Physiol Endocrinol Metab 2000;279(2):E425-E432.

Leturque A, Brot-Laroche E, Le Gall M, Stolarczyk E, Tobin V. The role of GLUT2 in dietary sugar handling. J Physiol Biochem 2005;61(4):529-537.

Lewis GF, Carpentier A, Adeli K, Giacca A. Disordered fat storage and mobilization in the pathogenesis of insulin resistance and type 2 diabetes. Endocr Rev 2002;23(2):201-229.

Machann J, Haring H, Schick F, Stumvoll M. Intramyocellular lipids and insulin resistance. Diabetes Obes Metab 2004;6(4):239-248.

Madison LL. Role of insulin in the hepatic handling of glucose. Arch Intern Med 1969;123(3):284-292.

Magnusson I, Rothman DL, Jucker B, Cline GW, Shulman RG, Shulman GI. Liver glycogen turnover in fed and fasted humans. Am J Physiol Endocrinol Metab 1994;266(5): E796-E803.

Magnusson I, Rothman DL, Katz LD, Shulman RG, Shulman GI. Increased rate of gluconeogenesis in type II diabetes *mellitus*. A ^{13}C nuclear magnetic resonance study. J Clin Invest 1992;90(4):1323-1327.

Magnusson I, Schumann WC, Bartsch GE, Chandramouli V, Kumaran K, Wahren J, Landau BR. Noninvasive tracing of krebs cycle metabolism in liver. J Biol Chem. 1991;266(11):6975-84.

Marchesini G, Brizi M, Bianchi G, Tomassetti S, Bugianesi E, Lenzi M, McCullough AJ, Natale S, Forlani G, Melchionda N. Nonalcoholic fatty liver disease: A feature of the metabolic syndrome. Diabetes 2001;50(8):1844-1850.

Marchetti P. New-onset diabetes after transplantation. J Heart Lung Transplant 2004;23(5 Suppl):S194-S201.

Mari A, Pacini G, Murphy E, Ludvik B, Nolan JJ. A model-based method for assessing insulin sensitivity from the oral glucose tolerance test. Diabetes Care 2001;24(3):539-548.

Markell M. New-onset diabetes *mellitus* in transplant patients: pathogenesis, complications, and management. Am J Kidney Dis 2004;43(6):953-965.

Matthews DR, Hosker JP, Rudenski AS, Naylor BA, Treacher DF, Turner RC. Homeostasis model assessment: insulin resistance and beta-cell function from fasting plasma glucose and insulin concentrations in man. Diabetologia 1985;28(7):412-419.

McGarry JD. Banting Lecture 2001: Dysregulation of fatty acid metabolism in the etiology of type 2 diabetes. Diabetes 2002;51(1):7-18.

Mehta SR, Thomas EL, Bell JD, Johnston DG, Taylor-Robinson SD. Non-invasive means of measuring hepatic fat content. World J Gastroenterol 2008;14(22):3476-3483.

Meijssen S, Cabezas MC, Ballieux CGM, Derksen RJ, Bilecen S, Erkelens DW. Insulin mediated inhibition of hormone sensitive lipase activity *in vivo* in relation to endogenous catecholamines in healthy subjects. J Clin Endocrinol Metab 2001;86(9):4193-4197.

Mendes AC, Caldeira MM, Silva C, Burgess SC, Merritt ME, Gomes F, Barosa C, Delgado TC, Franco F, Monteiro P, Providencia L, Jones JG. Hepatic UDP-glucose ^{13}C isotopomers from [U-^{13}C]glucose: a simple analysis by ^{13}C NMR of urinary menthol glucuronide. Magn Reson Med. 2006;56(5):1121-5.

Miyazaki Y, Glass L, Triplitt C, Wajcberg E, Mandarino LJ, DeFronzo RA. Abdominal fat distribution and peripheral and hepatic insulin resistance in type 2 diabetes *mellitus*. Am J Physiol Endocrinol Metab 2002;283(6):E1135-E1143.

Moller N, Rizza RA, Ford GC, Nair KS. Assessment of postabsorptive renal glucose metabolism in humans with multiple glucose tracers. Diabetes 2001;50(4):747-751.

Mora PF. Post-transplantation diabetes *mellitus*. Am J Med Sci 2005;329(2):86-94.

Newgard CB, Hirsch LJ, Foster DW, Mcgarry JD. Studies on the mechanism by which exogenous glucose is converted into liver glycogen in the rat. A direct or an indirect pathway? J Biol Chem 1983;258(13):8046-8052.

Newgard CB, Moore SV, Foster DW, Mcgarry JD. Efficient hepatic glycogen synthesis in refeeding rats requires continued carbon flow through the gluconeogenic pathway. J Biol Chem 1984;259(11):6958-6963.

Nielsen JH, Mandrup-Poulsen T, Nerup J. Direct effects of cyclosporin A on human pancreatic beta-cells. Diabetes 1986;35(9):1049-1052.

Nilsson LH. Liver glycogen content in man in the postabsorptive state. Scand J Clin Lab Invest 1973;32(4):317-323.

Nilsson LH, Hultman E. Liver glycogen in man- the effect of total starvation or a carbohydrate-poor diet followed by carbohydrate refeeding. Scand J Clin Lab Invest 1973;32(4):325-330.

Nilsson LH, Hultman E. Liver and muscle glycogen in man after glucose and fructose infusion. Scand J Clin Lab Invest 1974;33(1):5-10.

Ockerman PA. Glucose-6-phosphatase in human jejunal mucosa properties demonstrating the specific character of the enzyme activity. Biochim Biophys Acta 1965;105(1):22-33.

Paquot N, Schneiter P, Scheen AJ, Lefebvre PJ, Tappy L. Assessment of postprandial hepatic glycogen synthesis from uridine diphosphoglucose kinetics in obese and lean non-diabetic subjects. Int J Obes Relat Metab Disord 2000;24(10):1297-1302.

Perdigoto R, Rodrigues TB, Furtado AL, Porto A, Geraldes CFGC, Jones JG. Integration of [U-C-13]glucose and (H_2O)-H-2 for quantification of hepatic glucose production and gluconeogenesis. NMR in Biomedicine 2003;16(4):189-198.

Perseghin G, Scifo P, De Cobelli F, Pagliato E, Battezzati A, Arcelloni C, Vanzulli A, Testolin G, Pozza G, Del Maschio A, Luzi L. Intramyocellular triglyceride content is a determinant of *in vivo* insulin resistance in humans: a ^{1}H-^{13}C nuclear magnetic resonance spectroscopy assessment in offspring of type 2 diabetic parents. Diabetes 1999;48(8):1600-1606.

Petersen KF, Cline GW, Gerard DP, Magnusson I, Rothman DL, Shulman GI. Contribution of net hepatic glycogen synthesis to disposal of an oral glucose load in humans. Metabolism 2001;50(5):598-601.

Petersen KF, Shulman GI. Pathogenesis of skeletal muscle insulin resistance in type 2 diabetes *mellitus*. Am J Cardiol 2002;90(5A):11G-18G.

Radziuk J. Tracer methods and the metabolic disposal of a carbohydrate load in man. Diabetes Metab Rev 1987;3(1):231-267.

Radziuk J, Norwich KH, Vranic M. Experimental validation of measurements of glucose turnover in nonsteady state. Am J Physiol Endocrinol Metab 1978;234(1):E84-E93.

Randle PJ, Garland PB, Hales CN, Newsholme EA. The glucose fatty-acid cycle. Its role in insulin sensitivity and the metabolic disturbances of diabetes *mellitus*. Lancet 1963;1(7285):785-789.

Rajas F, Bruni N, Montano S, Zitoun C, Mithieux G. The glucose-6 phosphatase gene is expressed in human and rat small intestine: regulation of expression in fasted and diabetic rats. Gastroenterology 1999;117(1):132-139.

Reisæter AV, Hartmann A. Risk factors and incidence of posttransplant diabetes *mellitus*. Trans Proc 2001;33(5, Supplement 1):S8-S18.

Ribeiro A, Caldeira MM, Carvalheiro M, Bastos M, Baptista C, Fagulha A, Barros L, Barosa C, Jones JG. Simple measurement of gluconeogenesis by direct ^{2}H NMR analysis of menthol glucuronide enrichment from $^{2}H_2O$. Magn Reson Med. 2005;54(2):429-34.

Rizza RA, Mandarino LJ, Gerich JE. Dose-response characteristics for effects of insulin on production and utilization of glucose in man. Am J Physiol Endocrinol Metab 1981;240(6):E630-E639.

Roglic G, Unwin N, Bennett PH, Mathers C, Tuomilehto J, Nag S, Connolly V, King H. The burden of mortality attributable to diabetes: Realistic estimates for the year 2000. Diabetes Care 2005;28(9):2130-2135.

Romao I, Roth J. Genetic and environmental interactions in obesity and type 2 diabetes. J Am Diet Assoc 2008;108(4 Suppl 1):S24-S28.

Rothman DL, Magnusson I, Katz LD, Shulman RG, Shulman GI. Quantitation of hepatic glycogenolysis and gluconeogenesis in fasting humans with ^{13}C NMR. Science 1991;254(5031):573-576.

Ryysy L, Hakkinen AM, Goto T, Vehkavaara S, Westerbacka J, Halavaara J, Yki-Jarvinen H. Hepatic fat content and insulin action on free fatty acids and glucose metabolism rather than insulin absorption are associated with insulin requirements during insulin therapy in type 2 diabetic patients. Diabetes 2000;49(5):749-758.

Saad MF, Knowler WC, Pettitt DJ, Nelson RG, Mott DM, Bennett PH. Sequential changes in serum insulin concentration during development of non-insulin-dependent diabetes. Lancet 1989;1(8651):1356-1359.

Sadur CN, Eckel RH. Insulin stimulation of adipose tissue lipoprotein lipase. Use of the euglycemic clamp technique. J Clin Invest 1982;69(5):1119-1125.

Saltiel AR, Kahn CR. Insulin signalling and the regulation of glucose and lipid metabolism. Nature 2001;414(6865):799-806.

Salvadori M, Bertoni E, Rosati A, Zanazzi M. Post-transplant diabetes *mellitus*. J Nephrol 2003;16(5):626-634.

Samuel VT, Liu ZX, Qu XQ, Elder BD, Bilz S, Befroy D, Romanelli AJ, Shulman GI. Mechanism of hepatic insulin resistance in non-alcoholic fatty liver disease. J Biol Chem 2004;279(31):32345-32353.

Sandoval D, Cota D, Seeley RJ. The integrative role of CNS fuel-sensing mechanisms in energy balance and glucose regulation. Annu Rev Physiol 2008;70:513-535.

Sanyal AJ. Mechanisms of disease: pathogenesis of nonalcoholic fatty liver disease. Nat Clin Pract Gastroenterol Hepatol 2005;2(1):46-53.

Schinner S, Scherbaum WA, Bornstein SR, Barthel A. Molecular mechanisms of insulin resistance. Diabet Med 2005;22(6):674-682.

Schoenheimer R, Rittenberg D. Deuterium as an indicator in the study of intermediate metabolism. Science 1935;82(2120):156-157.

Schoenheimer R, Rittenberg D. Deuterium as an indicator in the study of intermediate metabolism. VI. Synthesis and destruction of fatty acids in the organism. J Biol Chem 1936;114(2):381-396.

Schreiber SL, Crabtree GR. The mechanism of action of cyclosporin A and FK506. Immunol Today 1992;13(4):136-142.

Schwartz MW, Porte D, Jr. Diabetes, obesity, and the brain. Science 2005;307(5708):375-379.

Shimabukuro M, Zhou YT, Levi M, Unger RH. Fatty acid-induced beta cell apoptosis: A link between obesity and diabetes. PNAS 1998;95(5):2498-2502.

Shoelson S.E., Lee J, Goldfine AB. Inflammation and insulin resistance. J Clin Invest 2006:1793-1801.

Shulman GI, DeFronzo RA, Rossetti L. Differential effect of hyperglycemia and hyperinsulinemia on pathways of hepatic glycogen repletion. Am J Physiol Endocrinol Metab 1991;260(5):E731-E735.

Shulman GI, Rothman DL, Jue T, Stein P, DeFronzo RA, Shulman RG. Quantitation of muscle glycogen synthesis in normal subjects and subjects with non-insulin-dependent diabetes by ^{13}C nuclear magnetic resonance spectroscopy. N Engl J Med 1990;322(4):223-228.

Sidossis LS, Magkos F, Mittendorfer B, Wolfe RR. Stable isotope tracer dilution for quantifying very low-density lipoprotein-triacylglycerol kinetics in man. Clin Nutr 2004;23(4):457-466.

Subramanian S, Trence DL. Immunosuppressive agents: effects on glucose and lipid metabolism. Endocrinol Metab Clin North Am 2007;36(4):891-905.

Sul HS, Latasa MJ, Moon Y, Kim KH. Regulation of the fatty acid synthase promoter by insulin. J Nutr 2000;130(2):315.

Szczepaniak LS, Babcock EE, Schick F, Dobbins RL, Garg A, Burns DK, McGarry JD, Stein DT. Measurement of intracellular triglyceride stores by ^{1}H spectroscopy: validation *in vivo*. Am J Physiol Endocrinol Metab 1999;276(5):E977-E989.

Szoke E, Gerich JE. Role of impaired insulin secretion and insulin resistance in the pathogenesis of type 2 diabetes *mellitus*. Compr Ther 2005;31(2):106-112.

Taylor Roy, Magnusson I, Rudenski AS, Cline GW, Caumo Andrea, Cobelli C, Shulman GI. Direct assessment of liver glycogen storage by ^{13}C nuclear magnetic resonance spectroscopy and regulation of glucose homeostasis after a mixed meal in normal subjects. J Clin Invest 1996;97:126-132.

Umpleby AM, Russell-Jones DL. The hormonal control of protein metabolism. Baillieres Clin Endocrinol Metab 1996;10(4):551-570.

Van Schaftingen E, Gerin I. The glucose-6-phosphatase system. Biochem J 2002;362(Pt 3):513-532.

Venkataraman S, Braga L, Semelka RC. Imaging the fatty liver. Magn Reson Imaging Clin N Am 2002;10(1):93-103.

Virkamaki A, Korsheninnikova E, Seppala-Lindroos A, Vehkavaara S, Goto T, Halavaara J, Hakkinen AM, Yki-Jarvinen H. Intramyocellular lipid is associated with resistance to *in vivo* insulin actions on glucose uptake, antilipolysis, and early insulin signaling pathways in human skeletal muscle. Diabetes 2001;50(10):2337-2343.

Wahlstrom HE, Akimoto R, Endres D, Kolterman O, Moossa AR. Recovery and hypersecretion of insulin and reversal of insulin resistance after withdrawal of short-term cyclosporine treatment. Transplantation 1992;53(6):1190-1195.

Wahlstrom HE, Lavelle-Jones M, Endres D, Akimoto R, Kolterman O, Moossa AR. Inhibition of insulin release by cyclosporine and production of peripheral insulin resistance in the dog. Transplantation 1990;49(3):600-604.

Wahren J, Felig P, Cerasi E, Luft R. Splanchnic and peripheral glucose and amino acid metabolism in diabetes *mellitus*. J Clin Invest 1972;51(7):1870-1878.

Wang D, Sul HS. Insulin Stimulation of the fatty acid synthase promoter is mediated by the phosphatidylinositol 3-kinase pathway. Involvement of protein kinase B/Akt. J Biol Chem 1998;273(39):25420-25426.

Weir MR, Fink JC. Risk for posttransplant diabetes *mellitus* with current immunosuppressive medications. Am J Kidney Dis 1999;34(1):1-13.
Wolfe BM, Kane JP, Havel RJ, Brewster HP. Mechanism of the hypolipemic effect of clofibrate in postabsorptive man. J Clin Invest 1973;52(9):2146-2159.

Wolfe RR, Shaw JH, Durkot MJ. Effect of sepsis on VLDL kinetics: responses in basal state and during glucose infusion. Am J Physiol Endocrinol Metab 1985;248(6):E732-E740.

Yale JF, Chamelian M, Courchesne S, Vigeant C. Peripheral insulin resistance and decreased insulin-secretion after cyclosporine-A treatment. Transplant Proc 1988;20(3):985-988.

Chapter 2

Endogenous glucose production in fasting

Effects of high fat dietary food intake in rats

2.1. Introduction

Type 2 diabetes (T2D) is a heterogenous syndrome with metabolic disruptions that ultimately lead to hyperglycemia. While there are genetic factors that contribute to T2D, it can also be induced by environmental factors, such as oversupply of dietary fat. Studies in both humans and animals have shown that an increased dietary fat intake results in reduced peripheral glucose uptake and/or impaired suppression of endogenous glucose production (EGP) (Thiebaud *et al.* 1982, Ferrannini *et al.* 1983, Kraegen *et al.* 1991, Boden *et al.* 1994).

In normal fasting conditions, the liver accounts for the bulk of EGP through the hydrolysis of glucose-6-phosphate (G6P) to glucose *via* glucose-6-phosphatase and the release of glucose into the circulation. Hepatic gluconeogenesis and glycogenolysis generate G6P and hence both pathways contribute to EGP. Synthesis of G6P from these sources is influenced by both substrate availability and endocrine status. In healthy overnight-fasted humans, EGP accounts for ~10 μmol $kg^{-1}min^{-1}$ with gluconeogenesis and glycogenolysis each contributing with ~5 μmol $kg^{-1}min^{-1}$. In extended fasting (40-60 hours) hepatic glycogen stores are severely depleted and glycogenolysis fluxes are limited to ~ 1 μmol $kg^{-1}min^{-1}$. To sustain EGP, gluconeogenic flux is enhanced and becomes the dominant contributor (Rothman *et al.* 1991, Chandramouli *et al.* 1997). Gluconeogenesis results in the generation of glucose from non-carbohydrate precursors: the glycerol that enters at the level of the triose-phosphates and all other precursors (i.e., pyruvate, lactate and gluconeogenic amino acids) which are metabolised *via* the anaplerotic fluxes of the tricarboxylic acids (TCA) cycle.

Flux changes from either gluconeogenesis or glycogenolysis can alter EGP rates, and if EGP exceeds the rate of whole body glucose disposal, hyperglycemia occurs. In poorly controlled type 2 diabetics, overt fasting hyperglycemia is believed to result from enhanced EGP, mainly due to increased

gluconeogenesis (Consoli *et al.* 1989, Hundal *et al.* 2000, Magnusson *et al.* 2002, Kunert *et al.* 2003). Gluconeogenesis may be stimulated in part by increased plasma free fatty acids (FFA) which supply the hepatic TCA cycle with an abundant supply of oxidizable substrate that can fuel the synthesis of glucose from pyruvate and other precursors (Coppack *et al* 1994). Moreover, the excess circulating FFA will be reesterified in the liver, thus boosting hepatic triglyceride levels and contributing to hepatic insulin resistance (DeFronzo 2004). Hepatic insulin resistance refers to the inability of insulin to suppress postprandial EGP and may be a key factor in the loss of glucose homeostasis associated with obesity (Kim *et al.* 2003).

In animal models, a high fat (HF) diet leads to insulin resistance and increased hepatic triglyceride levels. Therefore, the HF diet induced-insulin resistance animal model is widely used for the study of the pathological events that characterize the onset of T2D. HF diet-fed animals show normal fasting blood glucose levels, but are glucose intolerant and mildly insulin resistant as demonstrated by impaired clearance of a glucose load (Kraegen *et al.* 1986, Storlien *et al.* 1986). Given the role of systemic lipids in promoting EGP and gluconeogenesis, it is hypothesized that these fluxes would be increased in HF diet-fed rats compared to animals fed with a standard chow (SC) diet. Possibly, elevated fasting EGP rates reflect a loss of hepatic glucose control and contributes to glucose intolerance through a less effective suppression of EGP during a meal or a glucose load. If the glucose intolerance induced by HF-diet is not accompanied by higher fasting EGP rates, the principal mechanism may lie with defective peripheral glucose clearance rather than with hepatic glucose control.

In order to investigate postabsorptive EGP rates, and the contributing fluxes from glycerol and TCA cycle gluconeogenesis, and glycogenolysis, 6-h fasted adult Sprague-Dawley rats fed with a HF diet for 20 days were infused with a mixture of [3,4-$^{13}C_2$]glucose and deuterated water (^2H_2O) tracers. EGP was

quantified by isotope dilution measurement of infused [3,4-$^{13}C_2$]glucose and the contributions of TCA cycle and glycerol gluconeogenesis, and glycogenolysis to EGP were estimated from the ^{2}H-enrichment pattern of monoacetone glucose (MAG) derived from plasma glucose. EGP rates and sources were also assessed in control animals fasted for 6-h as well as a second control group fasted for 12 hours in order to determine if the performed measurements appropriately represented EGP rates and sources during the fed to fasted transition.

2.2. Materials and Methods

2.2.1. Materials

[3,4-$^{13}C_2$]glucose (99%) was purchased from Omicron Biochemicals (South Bend, IN). Deuterated water (99.9%) and deuterated acetonitrile (99.8%) were obtained from Cambridge Isotope Laboratories Inc. (Andover, MA, USA). Other common chemicals were purchased from Sigma-Aldrich.

2.2.2. Protocol

The study was approved by the Institutional Animal Care and Use Committee. Sprague-Dawley rats were housed in a room on a 12-h light-dark cycle under constant temperature (22-25 ºC) and with *ad libitum* access to food and water. Animals were divided into 3 groups: Group 1, five (5) 12-h fasted control animals; Group 2, five (5) 6-h fasted control rats; Group 3, 6-h fasted animals (n=6) maintained on a HF diet for 20 days. The HF diet used contained 45% of calories from fat, 35% from carbohydrate and 20% derived from protein (E15744-34, SSNIFF, Specialdiäten GmbH)®, whereas the SC diet given to control animals consists of 2.7% of fat, 60% carbohydrate and 16% protein. At the day of experiment, animals from all groups showed matched body weight (340-380 g). After the corresponding fast, ketamine-(2-(2,6-xylidine)-5,6-dihydro-4H-1,3-

tiazine chlorhydrate) anesthetized animals were cannulated in the jugular vein. Then, rats were submitted to an intravenous (i.v.) prime consisting of 2 mg of [3,4-$^{13}C_2$]glucose and an intraperitoneal (i.p.) injection of 4 mL 70% saline ^2H_2O followed by infusion. 2.1 mg/mL of [3,4-$^{13}C_2$]glucose solution were infused at a constant rate of 0.33 mL/min. After a 60 min infusion, blood was immediately withdrawn from the descending aorta and the liver weighed, freeze-clamped and kept at -80ºC until further analysis.

2.2.3. Blood processing

Blood was immediately deproteinized with a final volume of 4% perchloric acid (70%) and centrifuged at 13,000 *g* at 4ºC for plasma separation. The plasma supernatant was separated from erythrocytes and neutralized with concentrated KOH. Samples were further purified by anionic-cationic exchange chromatography and evaporated to dryness. The conversion of plasma glucose to MAG was performed according to the literature (Jones *et al.* 2001). A mixture of 0.5 mL acetone/mL original plasma and concentrated anhydrous H_2SO_4 (40 µL/mL acetone) was added to the sample and stirred vigorously for 4 h. 10 mL of H_2O were added and the pH adjusted to 2.2-2.3 followed by incubation at 40 ºC for 5 h. The pH was then adjusted to ~8.0 with Na_2CO_3 and the solution evaporated to dryness. MAG was extracted from the dry residue with 5 mL of boiling ethyl acetate, removal of insoluble salts by centrifugation, and evaporation of ethyl acetate. MAG molecules show the same labeling patterns as plasma glucose but with completely resolved ^2H and ^{13}C NMR signals.

2.2.4. Liver Processing

Frozen livers were freeze-dried and then powdered. 30% KOH (at 70 ºC) was added to each sample in 2:1 final volume ratio. After 30 minutes, 8 mL of Na_2SO_4 6% and 50 mL of absolute ethanol were added and the sample incubated overnight at 4ºC. The precipitated glycogen is separated from the supernatant

by centrifugation at 3,000 *g*. The dried glycogen samples were dissolved in 5 mL of acetate buffer 0.05 M (pH 4.5). 16 U of amyloglucosidase were added to each sample and incubated for 10 hours at 55 ºC. The containing glucose supernatant was then separated by centrifugation. Finally, glucose concentration in each sample was quantified enzymatically by the glucose oxidase method using a commercial kit (Invitrogen).

2.2.5. NMR Spectroscopy

2.2.5.1. ^{13}C NMR Spectroscopy

MAG samples were dissolved in 90% deuterated acetonitrile/10% H_2O for carbon 13 (^{13}C) Nuclear Magnetic Resonance (NMR) analysis. Proton-decoupled ^{13}C NMR spectra were obtained with a Varian 11.75 Tesla (T) system (Varian Instruments, Palo Alto, CA, USA) equipped with a 5-mm broadband probe. Spectra were acquired at 25ºC using a 90º pulse and a 2.5 s acquisition time. Typically 4,000-40,000 scans were averaged.

2.2.5.1. ^{2}H NMR Spectroscopy

While ^{13}C NMR signals of MAG were adequate for accurate quantification in each blood sample, initial deuterium (^{2}H) NMR spectra had poor signal to noise ratio (SNR) and were deemed unacceptable for reliable quantification of the H2, H5 and H6 signals (data not shown). Therefore, it was decided to pool the MAG samples for each group for ^{2}H NMR spectroscopy after acquiring individual ^{13}C NMR spectra. ^{2}H NMR spectra of pooled MAG samples were obtained using a Varian 14.1 T spectrometer (Varian Instruments, Palo Alto, CA, USA) equipped with a 3-mm broadband probe. MAG was dissolved in 90% acetonitrile/10% water and shimming was performed on selected proton (^{1}H) resonances of MAG. ^{1}H-decoupled ^{2}H NMR spectra were acquired at 50ºC using a 90º pulse and a 1.5 s acquisition time. Typically 6,000-20,000 scans were averaged.

2.2.5.3. NMR Analysis

^{13}C NMR spectra were analyzed using the curve-fitting routine supplied with the NUTS PC-based NMR spectral analysis program (Acorn NMR Inc., Fremont CA). Analysis of ^{2}H-enrichments was performed in an automated way by using Bayesian analysis (Varian Instruments) of a ^{2}H free induction decay (FID) signal from MAG pooled samples.

2.2.6. Metabolic flux calculations

Glucose rate of appearance (Ra) was calculated from the known infusion rate (Ri), the enrichment fraction of infusate [3,4-$^{13}C_2$]glucose (Li), and the fraction of plasma glucose that was [3,4-$^{13}C_2$]glucose (Lp), using Eq. 2.1 (Jin *et al.* 2003, Jin *et al.* 2004, Jin *et al.* 2005b). The fraction of [3,4-$^{13}C_2$]glucose in the plasma glucose (Lp) was determined from the ratio of the areas of the doublet due to ^{13}C-^{13}C spin-spin coupling between carbons 3 and 4 (J_{34}=37.8 Hz) compared with the area of the singlet that reflects ^{13}C natural abundance (1.11%). EGP was calculated from Eq. 2.2 and is equal to Ra minus Ri. The contribution of gluconeogenesis and glycogenolysis to EGP was derived from the ratio of ^{2}H-enrichment at positions 2, 5 and 6S of MAG (H2, H5, H6S), as shown in Eqs. 2.3 and 2.4. G6P derived from glycogenolysis has deuterium in position 2 only, as a result of exchange between G6P and fructose-6-phosphate (F6P), whereas G6P derived from any gluconeogenic precursor has deuterium incorporated in both position 2 and 5 due to additional exchanges at the triose phosphate level (see Figure 2.1). Hence, the ratios of ^{2}H-enrichment in positions 5 and 2 (H5/H2) of G6P and plasma glucose reflect the fractional contribution of gluconeogenesis to fasting EGP. The contribution of gluconeogenesis was resolved into glycerol and TCA cycle sources as shown by Eqs 2.5 and 2.6 (Schleucher *et al.* 1998, Jones *et al.* 2001).

$Ra = Ri \times (Li - Lp) / Lp$ ($\mu mol\ kg^{-1} min^{-1}$) *[Eq. 2.1]*

$EGP = Ra - Ri$ ($\mu mol\ kg^{-1} min^{-1}$) *[Eq. 2.2]*

Glycogenolysis= [1-(H5/H2)]× 100 (%) *[Eq. 2.3]*

Gluconeogenesis= (H5/H2) × 100 (%) *[Eq. 2.4]*

Gluconeogenesis from glycerol= {1-[(H5-H6S)/H2]} × 100 (%) *[Eq. 2.5]*

Gluconeogenesis from TCA cycle= [1-(H6S/H2)] × 100 (%) *[Eq. 2.6]*

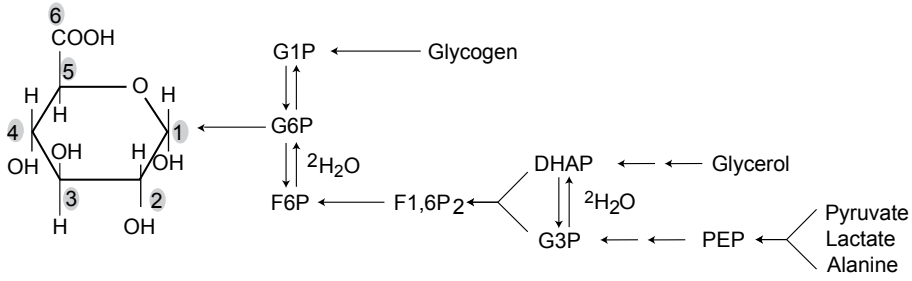

Figure 2.1. Metabolic pathways of fasting endogenous glucose poduction after ^2H_2O administration. G1P. glucose-1-phosphate; G6P. glucose-6-phosphate; F6P. frutose-6-phosphate; F1,6P$_2$, fructose-1,6-bisphosphate; DHAP. dihydroxyacetone phosphate; PEP. phosphonolpuruvate; G3P. glyceraldehyde-3-phosphate.

2.2.7. Statistical analysis

Data are expressed as means ± standard deviation (SD) and one-way analysis of variance (ANOVA) was used to compare EGP and hepatic glycogen content between groups. The difference was considered statistical significant when $p<0.05$. Gluconeogenesis from TCA cycle and glycerol, and glycogenolysis estimated by Bayesian analysis are associated with an uncertainty, SD, given by the Markov Chain/Monte Carlo (MCMC) simulations (Merritt *et al.* 2003). Comparison of gluconeogenic and glycogenolysis fluxes was accomplished by using the means and SD for the relative fluxes obtained by the Bayesian analysis of the ^{2}H-enrichments of pooled MAG samples. In a normal distribution, ± 1.96 SD of the mean corresponds to an interval likely to include the real parameter value with a 95% confidence.

2.3. Results

As illustrated by the spectra of Figure 2.2, ^{13}C NMR spectra obtained from the MAG derivative of plasma glucose had well-defined doublet signals from the [3,4-$^{13}C_2$]glucose isotopomer allowing confident quantification of plasma [3,4-$^{13}C_2$]glucose enrichments, shown in Table 2.1. Whereas control rats and rats on a HF diet fasted for 6-h showed similar EGP rates, the 12-h fasted control rats EGP rates were significantly lower, as seen by higher plasma [3,4-$^{13}C_2$]glucose enrichments.

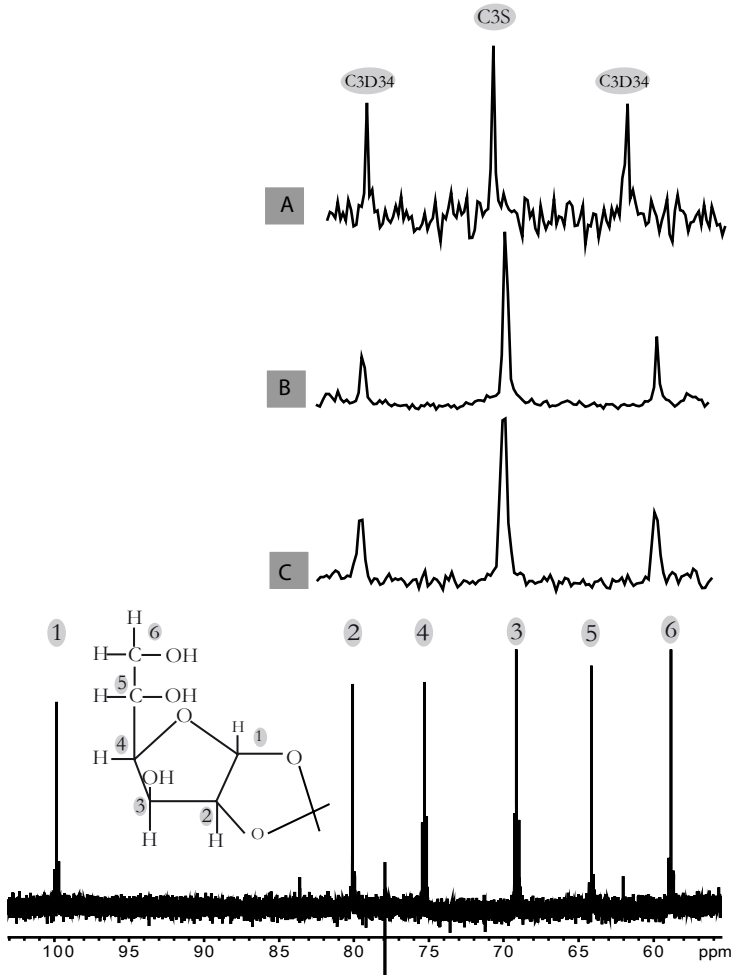

Figure 2.2. ^{13}C NMR spectra of monoacetone glucose (MAG) derived from plasma glucose of rats infused with [3,4-$^{13}C_2$]glucose. Carbon 3 signals are expanded and a doublet resulting from coupling of carbon 3 with 4 (C3D34) is observed. **A.** 12-h fasted control rat; **B.** 6-h fasted control; **C.** 6-h fast HF diet-fed animals. Carbon 3 natural abundance singlets (C3S) and carbon 3-carbon 4 coupling doublets (C3D34) are identified.

Pooled ^2H NMR spectra of MAG derived from plasma glucose samples had well-resolved ^2H-signals with high SNR for all seven aliphatic hydrogens of glucose (Figure 2.3) allowing the precise quantification of the relative ^2H-enrichments and the respective metabolic fluxes. Generally, the precision of the flux estimates, as determined by the size of the SD, is highest for spectra with high SNR (Merritt *et al.* 2003). From the relative enrichments of hydrogens 2, 5 and 6S, the contributions from glycerol and TCA cycle gluconeogenesis, and glycogenolysis to EGP were estimated by Bayesian analysis and are shown in Figure 2.4

For 6-h fasted control animals, EGP rates and gluconeogenic contributions were similar to other reports from early postabsorptive stage (5-6 hours) (Sena *et al.* 2007). Gluconeogenesis contributed about half of EGP with the TCA cycle accounting for the majority of gluconeogenic sources and glycerol gluconeogenesis only accounting for ~9% of EGP. This profile reflects the abundance of hepatic glycogen and low rates of net lipolysis - the source of endogenous glycerol that is characteristic of the initial hours of fasting. Given the paucity of published EGP values during early postabsorptive conditions and the fact that a 60-min primed infusion of [3,4-$^{13}C_2$]glucose was used rather than the more usual 90 min an additional group of 12-hour fasted control animals was studied to determine if these measurements appropriately represented EGP rates and sources during the fed to fasted transition.

TABLE 2.1. ^{13}C NMR multiplet ratios from the monoacetone glucose (MAG) derived from plasma glucose and [3,4-$^{13}C_2$]glucose enrichment, glucose Ra and EGP flux for: Group 1. 12-h fasted animals; Group 2. 6-h fasted control animals and Group 3. 6-h fasted rats on a high fat (HF) diet.

	^{13}C NMR multiplet ratios enrichments					Glucose R_a μmol kg^{-1}min^{-1}	E GP μmol kg^{-1}min^{-1}
	C3S %	C3D34 %	C4S %	C4D34 %	[3,4$^{13}C_2$]glucose enrichment % (Lp)		
Group 1 12-h fast							
Rat 1	1.11	1.61	1.11	1.64	1.63	59.97	58.98
Rat 2	1.11	1.11	1.11	1.60	1.35	74.03	73.02
Rat 3	1.11	1.25	1.11	1.16	1.21	68.11	67.27
Rat 4	1.11	0.84	1.11	0.84	0.84	78.31	77.64
Rat 5	1.11	1.08	1.11	1.12	1.10	60.6	59.94
Average±STD	-	-	-	-	-	-	67.37 ± 8.11 *
Group 2 6-h fast							
Rat 1	1.11	0.86	1.11	0.87	0.87	90.56	89.76
Rat 2	1.11	0.63	1.11	0.78	0.70	116.48	115.66
Rat 3	1.11	0.65	1.11	0.82	0.74	105.17	104.39
Rat 4	1.11	0.82	1.11	0.83	0.83	99.79	98.95
Rat 5	1.11	0.83	1.11	0.58	0.70	89.14	88.51
Average±STD	-	-	-	-	-	-	99.45 ± 11.19
Group 3 HF 6 -h fast							
Rat 1	1.11	0.78	1.11	0.87	0.82	111.21	110.30
Rat 2	1.11	0.80	1.11	0.98	0.89	89.92	89.11
Rat 3	1.11	0.91	1.11	0.73	0.82	108.53	107.63
Rat 4	1.11	0.69	1.11	0.82	0.73	114.23	113.37
Rat 5	1.11	0.72	1.11	0.59	0.66	120.21	119.41
Rat 6	1.11	0.94	1.11	1.05	1.00	83.01	82.17
Average ± STD	-	-	-	-	-	-	103.67 ± 14.67

* $p<0.01$ relative to 6-h fasted controls.

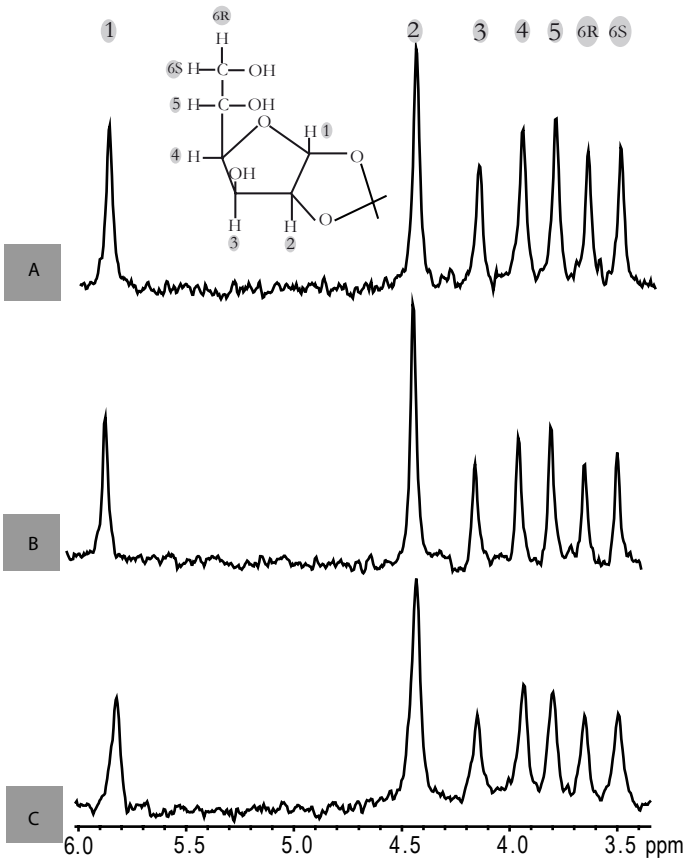

Figure 2.3. ^{2}H NMR spectra of monoacetone glucose (MAG) derived from rat plasma glucose after deuterated water ($^{2}H_2O$) administration. Seven aliphatic hydrogens derived from plasma MAG are shown and identified respectively, from **A**. 12-h fasted control rat; **B.** 6-h fasted control; **C.** 6-h fast HF diet-fed animals.

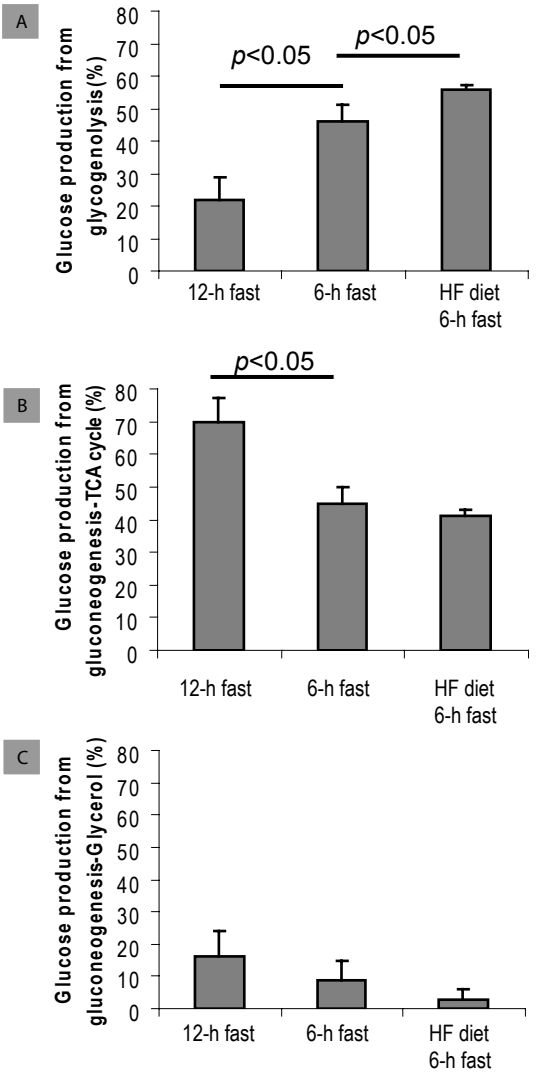

Figure 2.4. A. Glycogenolysis, B. TCA cycle and C. glycerol gluconeogenesis relative contributions for 12-h fasted animals, 6-h fasted control animals and 6-h fasted HF diet-fed rats. Statistical significant differences ($p<0.05$) are indicated.

The progression of fasting is characterized by a well defined reduction of glucose disposal rates as plasma glucose and insulin levels subside. The decline in whole body glucose disposal is matched by a reduction in EGP, principally as a result of reduced hepatic glycogen levels and glycogenolytic fluxes. For the 12-h fasted animals, hepatic glycogen was significantly depleted relative to the 6-h fasting controls (0.05 ± 0.07 *vs.* 0.35 ± 0.04 mmol/g liver wet weight, $p<0.01$). Consistent with reduced liver glycogen levels, the glycogenolytic contribution was sharply lower in the 12-h fasted animals, contributing only for 22% ± 7% of EGP. While the total gluconeogenic contribution was significantly different between 6 and 12-h fasted (54% *vs.* 78%), the contribution from glycerol was not significantly altered between 6 and 12 hours of fasting (9% ± 6% *vs.* 16% ± 8%). The 12 hour fast was not sufficient to induce extensive lipolysis and an increase in glycerol availability. However, there is a significant drop in the relative gluconeogenic contribution from the TCA cycle (70% ± 7% compared to 45% ± 5% for the 6-h fasted control group). In terms of absolute fluxes, the dramatic drop in glycogenolysis contribution (15 *vs.* 45 μmol $kg^{-1}min^{-1}$) appears to be the principal responsible for decreased EGP fluxes in 12-h fasted rats whereas gluconeogenesis from the TCA cycle flux is similar between 6 and 12-h fasted rats (45 *vs.* 47 μmol $kg^{-1}min^{-1}$, respectively). In conclusion, the measurements described in here appropriately describe the changes in EGP rates and sources that occur in healthy animals during the progression of fasting.

Animals on a HF diet showed comparable EGP rates to 6-h fasted controls with minor shifts in the EGP sources. Glycogenolysis contribution, although significantly elevated in HF diet-fed animals relative to 6-h fasted controls (56% ± 1% *vs.* 46% ± 5%, $p<0.05$), only accounts for a modest increase to EGP whereas the gluconeogenic contribution from TCA cycle and glycerol to EGP was not significantly different. Hepatic glycogen levels were similar between the HF diet and the 6-h fasted controls (0.25 ± 0.12 *vs.* 0.35 ± 0.10 mmol/g liver wet weight).

2.4. Discussion

Fasting hyperglycemia in T2D is often associated with enhanced EGP rates. Previously, postabsorptive EGP was found to be increased in animal models of T2D. In the Zucker diabetic fatty (ZDF) animals, EGP was shown to be increased due to elevated glycogenolysis as a result of elevated hepatic glycogen content (Jin *et al.* 2005a) whereas in Goto-Kakizaki (GK) rats increased EGP is due to enhanced gluconeogenesis from TCA cycle (Sena *et al.* 2007). Thus, in ZDF and GK rats with well developed T2D, enhanced EGP contributes to fasting hyperglycemia. To determine if EGP is altered in glucose intolerant rats that show normal fasting glycemia, a rodent model of HF-induced insulin resistance was studied.

From the [3,4-$^{13}C_2$]glucose isotope dilution measurements, postabsorptive EGP was found not to be significantly different between HF diet-fed and control animals. Furthermore, there was no indication of increased gluconeogenic fluxes in the HF diet-fed group. These results are not in agreement with a previous study where EGP was found to be increased in overnight-fasted HF diet-fed animals (Song *et al.* 2001), determined by using [6-^{3}H]glucose as a tracer. However, their published EGP values of 20-30 μmol kg^{-1}min^{-1} are far below from the 50-70 μmol kg^{-1}min^{-1} range from many studies (Jin *et al.* 2003, Jin *et al.* 2004, Nakahara *et al.* 2004) and the value of 67 ± 8 μmol kg^{-1}min^{-1} reported in here.

The results presented in here show that for HF diet-fed animals, postabsorptive EGP from gluconeogenesis and glycogenolysis was essentially identical to the normally fed controls. These data therefore provide no indication of stimulated hepatic gluconeogenesis in the fasted state as a result of the HF diet. However, further studies are necessary to determine if HF diet induced glucose intolerance results from altered whole body glucose disposal, failure of normal inhibition of postprandial EGP or a combination of both. HF diet-fed animals present some important early markers of T2D pathology including

glucose intolerance and increased hepatic triglyceride levels. However, the normal EGP and gluconeogenesis rates that were found in glucose-intolerant HF diet-fed animals suggest that altered hepatic glucose fluxes are not involved in the development of fasting hyperglycemia and insulin resistance secondary to high fat feeding, at least in the early stages.

These conclusions concur with clinical studies where postabsorptive EGP and gluconeogenic rates are normal in mildly hyperglycemic diabetics and are only significantly enhanced in severe hyperglycemic type 2 diabetics (Boden *et al.* 2001). These studies suggest that increases in postabsorptive EGP and gluconeogenesis rates are preceded by other defects of glucose homeostasis such as insulin resistance and glucose intolerance in the pathogenesis of T2D. Rather, the involvement of elevated EGP and gluconeogenesis is associated with the onset of severe fasting hyperglycemia, a relatively late event in the development of T2D.

2.5. References

Boden G, Chen X, Ruiz J, White JV, Rossetti L. Mechanisms of fatty acid-induced inhibition of glucose uptake. J Clin Invest 1994;93(6):2438-2446.

Boden G, Chen XH, Stein TP. Gluconeogenesis in moderately and severely hyperglycemic patients with type 2 diabetes *mellitus*. Am J Physiol Endocrinol Metab 2001;280(1):E23-E30.

Chandramouli V, Ekberg K, Schumann WC, Kalhan SC, Wahren J, Landau BR. Quantifying gluconeogenesis during fasting. Am J Physiol Endocrinol Metab 1997;36(6): E1209-E1215.

Consoli A, Nurjhan N, Capani F, Gerich J. Predominant role of gluconeogenesis in increased hepatic glucose production in NIDDM. Diabetes 1989;38(5):550-557.

Coppack SW, Jensen MD, Miles JM. *In vivo* regulation of lipolysis in humans. J Lipid Res 1994;35(2):177-193.

DeFronzo RA. Dysfunctional fat cells, lipotoxicity and type 2 diabetes. Int J Clin Pract Suppl 2004;(143):9-21.

Ferrannini E, Barrett EJ, Bevilacqua S, DeFronzo RA. Effect of fatty acids on glucose production and utilization in man. J Clin Invest 1983;72(5):1737-1747.

Hundal RS, Krssak M, Dufour S, Laurent D, Lebon V, Chandramouli V, Inzucchi SE, Schumann WC, Petersen KF, Landau BR, Shulman GI. Mechanism by which metformin reduces glucose production in type 2 diabetes. Diabetes 2000;49(12):2063-2069.

Jin ES, Burgess SC, Merritt ME, Sherry AD, Malloy CR. Differing mechanisms of hepatic glucose overproduction in triiodothyronine-treated rats *vs.* Zucker diabetic fatty rats by NMR analysis of plasma glucose. Am J Physiol Endocrinol Metab 2005;288(4):E654-E662.

Jin ES, Jones JG, Merritt M, Burgess SC, Malloy CR, Sherry AD. Glucose production, gluconeogenesis, and hepatic tricarboxylic acid cycle fluxes measured by nuclear magnetic resonance analysis of a single glucose derivative. Anal Biochem 2004;327(2):149-155.

Jin ES, Jones JG, Burgess SC, Merritt ME, Sherry AD, Malloy CR. Comparison of [3,4-C-13(2)]glucose to [6,6-H-2(2)]glucose as a tracer for glucose turnover by nuclear magnetic resonance. Magn Reson Med 2005;53(6):1479-1483.

Jin ES, Uyeda K, Kawaguchi T, Burgess SC, Malloy CR, Sherry AD. Increased hepatic fructose 2,6-bisphosphate after an oral glucose load does not affect gluconeogenesis. J Biol Chem 2003;278(31):28427-28433.

Jones JG, Solomon MA, Cole SM, Sherry AD, Malloy CR. An integrated H-2 and C-13 NMR study of gluconeogenesis and TCA cycle flux in humans. Am J Physiol Endocrinol Metab 2001;281(4):E848-E856.

Kim SP, Ellmerer M, Van Citters GW, Bergman RN. Primacy of hepatic insulin resistance in the development of the metabolic syndrome induced by an isocaloric moderate-fat diet in the dog. Diabetes 2003;52(10):2453-2460.

Kraegen EW, Clark PW, Jenkins AB, Daley EA, Chisholm DJ, Storlien LH. Development of muscle insulin resistance after liver insulin resistance in high-fat-fed rats. Diabetes 1991; 40(11):1397-1403.

Kraegen EW, James DE, Storlien LH, Burleigh KM, Chisholm DJ. *In vivo* insulin resistance in individual peripheral tissues of the high fat fed rat: assessment by euglycaemic clamp plus deoxyglucose administration. Diabetologia 1986;29(3):192-198.

Kunert O, Stingl H, Rosian E, Krssak M, Bernroider E, Seebacher W, Zangger K, Staehr P, Chandramouli V, Landau BR, Nowotny P, Waldhausl W, Haslinger E, Roden M. Measurement of fractional whole-body gluconeogenesis in humans from blood samples using H-2 nuclear magnetic resonance spectroscopy. Diabetes 2003;52(10):2475-2482.

Magnusson I, Rothman DL, Katz LD, Shulman RG, Shulman GI. Increased rate of gluconeogenesis in type II diabetes *mellitus* - A C13 nuclear magnetic resonance study. J Clin Invest 1992;90(4):1323-1327.

Merritt M, Bretthorst GL, Burgess SC, Sherry AD, Malloy CR. Sources of plasma glucose by automated Bayesian analysis of H-2 NMR spectra. Magn Reson Med 2003;50(4):659-663.

Nakahara I, Matsuhisa M, Shiba Y, Kuroda A, Nakatani Y, Hatazaki M, Kajimoto Y, Kubota M, Yamasaki Y, Hori M. Acute elevation of free fatty acids impairs hepatic glucose uptake in conscious rats. Diabetes Res Clin Pract 2004;66(2):109-118.

Rothman DL, Magnusson I, Katz LD, Shulman RG, Shulman GI. Quantitation of hepatic glycogenolysis and gluconeogenesis in fasting humans with ^{13}C NMR. Science 1991;254(5031):573-576.

Schleucher J, Vanderveer PJ, Sharkey TD. Export of carbon from chloroplasts at night. Plant Physiol 1998;118(4):1439-1445.

Sena CM, Barosa C, Nunes E, Seica R, Jones JG. Sources of endogenous glucose production in the Goto-Kakizaki diabetic rat. Diabetes & Metabolism 2007;33(4):296-302.

Song S, Andrikopoulos S, Filippis C, Thorburn AW, Khan D, Proietto J. Mechanism of fat-induced hepatic gluconeogenesis: effect of metformin. Am J Physiol Endocrinol Metab 2001;281(2):E275-E282.

Storlien LH, James DE, Burleigh KM, Chisholm DJ, Kraegen EW. Fat feeding causes widespread *in vivo* insulin resistance, decreased energy expenditure, and obesity in rats. Am J Physiol Endocrinol Metab 1986;251(5):E576-E583.

Thiebaud D, DeFronzo RA, Jacot E, Golay A, Acheson K, Maeder E, Jequier E, Felber JP. Effect of long chain triglyceride infusion on glucose metabolism in man. Metabolism 1982;31(11):1128-1136.

Chapter 3

Sources of hepatic glucose production in fasting

Effects of obesity and cyclosporine A treatment in humans

This chapter is based on:

Delgado TC, Barosa C, Castro MMCA, Geraldes CFGC, Bastos M, Baptista C, Fagulha A, Barros L, Mota A, Carvalheiro M, Jones JG, Merritt M. Sources of hepatic glucose production by $^{2}H_2O$ ingestion and Bayesian analysis of ^{2}H glucuronide enrichment. Magn Reson Med 2008;60(3):517-523.

3.1. Introduction

Plasma glucose levels are maintained over the daily feeding/fasting cycle through tight coordination of glucose appearance and disposal. During overnight fasting, glucose appearance is entirely accounted for by endogenous glucose production (EGP) once digestive absorption has ceased. Hepatic glucose production (HGP) is the principal contributor to EGP and both gluconeogenesis and glycogenolysis contribute to fasting HGP. The occurrence of hyperglycemia after overnight fasting is a hallmark of defective glucose metabolism and indicates a mismatch between glucose production and plasma glucose clearance. Impaired glucose uptake by peripheral tissues and inappropriately high levels of HGP can both contribute to this condition. Among other things, resolving these underlying defects could prove useful for guiding and evaluating interventions of fasting hyperglycemia since some antihyperglycemic medications act by inhibiting HGP while others function by improving whole body glucose uptake.

Systemic glucose metabolism is typically assessed in the clinical setting by quantifying plasma glucose levels before and after an oral glucose load but this approach does not provide any information about hepatic glucose metabolism. Assessment of HGP with stable isotope tracers could provide useful information to complement measurements of plasma glucose clearance but current methods are poorly suited for routine clinical studies. This is due to several factors including high tracer cost, the requirement for lengthy infusion times for administration of the tracer, and extensive sample processing and analysis.

Deuterated water (^2H_2O) is an inexpensive tracer of gluconeogenesis that can be administered orally and is therefore well suited for routine clinical study procedures. The metabolic information is derived from the analysis of the deuterium (^2H)-enrichment distribution of plasma glucose (Jones *et al.* 2001, Boden *et al.* 2001, Landau *et al.* 1996, Chandramouli *et al.* 1997, Perdigoto *et al.* 2003, Weis *et al.* 2004, Chevalier *et al.* 2006). Current Gas Chromatography-

Mass Spectrometry (GC-MS) methods, while highly sensitive and therefore applicable to small blood samples, are labor intensive and poorly suited for high sample throughputs. Analysis by ^{2}H Nuclear Magnetic Resonance (NMR) spectroscopy of the monoacetone glucose (MAG) derivative of plasma glucose is less sensitive but far simpler to the extent that both sample preparation and NMR spectroscopy can be extensively automated with current technologies. Conversion of plasma glucose to MAG has been successfully performed with a commercially available robotic chemical synthesizer (Burgess *et al.* 2002) and high-resolution ^{2}H NMR spectra of the product can be obtained with automated tuning/shimming routines and minimal technical oversight. The contribution of gluconeogenic and glycogenolytic fluxes to HGP can be automatically obtained from the ^{2}H NMR signal by Bayesian/Markov Chain Monte Carlo (MCMC) analysis of the free induction decay (FID) (Merritt *et al.* 2003). The analysis also provides estimates of uncertainty levels for the flux parameters. Data modeling studies indicate that these uncertainty levels are heavily influenced by the signal to noise ratio (SNR) of the ^{2}H NMR signals. Obtention of ^{2}H NMR signals with suitable SNR for Bayesian analysis requires a large sample size (~30 mL of whole blood) and/or long NMR collection times thereby limiting the practicality and throughput of the method.

When acetaminophen is provided and due to rapid exchange between hepatic glucose-6-phosphate (G6P) and glucose-1-phosphate (G1P) the ^{2}H-enrichment distribution of plasma glucose is also reflected in hydrogens 1-5 of the acetaminophen glucuronide excreted in urine (Burgess *et al.* 2003) (Figure 3.1). In addition to eliminating the need to collect and rapidly process blood samples, the quantity of urinary glucuronide that is available for analysis is typically 5-10 times that of plasma glucose. Under these conditions, it is anticipated that ^{2}H NMR spectra with sufficient SNR to yield reasonably precise estimates of gluconeogenesis by Bayesian analysis could be obtained without prohibitively long NMR collection times. The Bayesian method is ideal for analyzing data of

this type. Experimental time constraints prevent repeated measurements upon the same sample in order to construct a more traditional statistical estimate of the uncertainty, i.e., the mean and standard deviation (SD) of repeated NMR spectra for a given sample. The Bayesian formulation of this problem uses prior knowledge regarding the shifts and amplitudes of the relevant resonances as well as a model for the "nuisance" resonances that are not important for the metabolic measurements. A MCMC simulation makes multiple independent analyses of the posterior probability distribution that define the metabolic measurement. This provides an estimate of the most probable values of the metabolic parameters as well as the uncertainty value for each parameter.

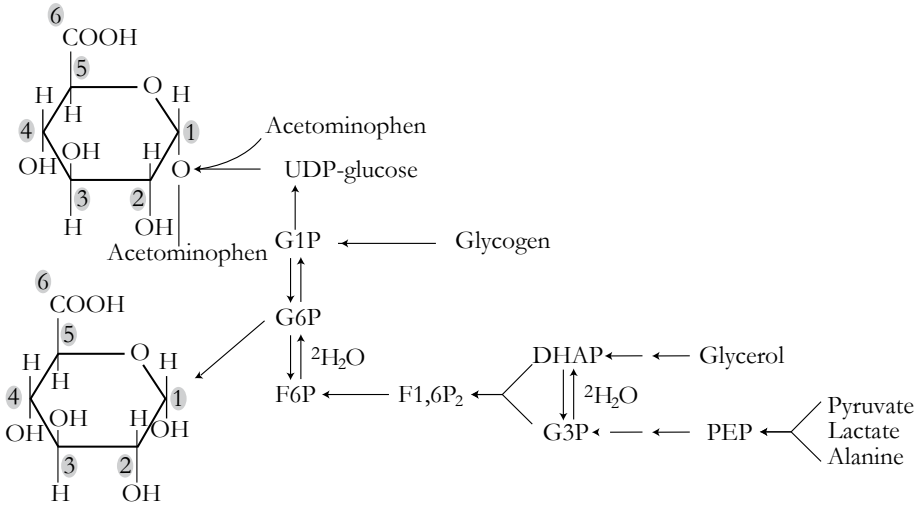

Figure 3.1. Metabolic pathways involved in fasting hepatic glucose production after ^2H_2O and acetaminophen ingestion. UDP-glucose. uridine diphosphate-glucose; G1P. glucose-1-phosphate; G6P. glucose-6-phosphate; F6P. fructose-1-phosphate; $F1,6P_2$. fructose-1,6-bisphosphate; DHAP. dihydroxyacetone phosphate; G3P. glyceraldehyde-3-phosphate; PEP. phosphoenolpyruvate.

In this study, the gluconeogenic contribution to HGP was estimated by Bayesian analysis of the ^{2}H NMR signals of MAG derived from urinary acetaminophen glucuronide collected after overnight fasting and ingestion of $^{2}H_2O$ and acetaminophen. The analysis was applied to healthy subjects and to kidney transplant (KTx) recipients, including a subgroup diagnosed with posttransplant diabetes *mellitus* (PTDM). The development of hyperglycemia and PTDM is a frequent event following kidney transplantation (Salvadori *et al.* 2003, Markell 2004). This may involve several factors, including increased adiposity, and glucose intolerance resulting from posttransplant weight gain, age and ethnicity (Salvadori *et al.* 2003), as well as the direct action of immunosuppressive agents such as glucocorticoids (GCs) and the calcineurin inhibitor, cyclosporine A (CsA), on insulin secretion and sensitivity (Jindal *et al.* 1997, Markell 2001). The activity of hepatic gluconeogenesis and its contribution to posttransplant fasting hyperglycemia under these conditions is not known. In this study, sources of fasting HGP derived by Bayesian analysis were collated with plasma metabolite and insulin sensitivity measurements.

3.2. Materials and methods

3.2.1. Human studies

The study protocol was approved by the University Hospital of Coimbra Ethics Committee and was performed in accordance with the ethical standards laid down in the Helsinki Declaration. Subjects were studied in the Department of Endocrinology, Metabolism and Diabetes in the University Hospital of Coimbra after informed consent. Three groups were studied as follows: Group 1, six healthy, lean normoglycemic controls; Group 2, seven lean, normoglycemic patients with a functional KTx with stable ongoing CsA-based therapy; and Group 3, three obese and hyperglycemic patients with a functional

renal transplant and CsA-based therapy. All KTx patients received 200-400 mg/day of CsA in conjunction with a low dose of GCs (5 mg/day).

3.2.2. ^2H_2O administration and sampling

Fasting was started at 20:00 (24-h clock) on the previous evening after a normal dinner meal. At 01:00 and 03:00 on the next day, patients were given two loading doses of ^2H_2O (2.5 g/kg of body water) to achieve a target body water enrichment of 0.5% ^2H_2O. Body water was assumed to be 60% of body weight for males and 50% of body weight for females. To improve palatability and decrease the risk of vertigo each loading was diluted with bottled spring water to give a final enrichment of 35% ^2H_2O. Acetaminophen (1000 mg) was also taken at 03:00 h. At 06:00 h the patients were asked to empty their bladder and all urine was collected from 06:00-08:00 h. Blood for clinical analysis was also drawn at 06:00 and 08:00 (Figure 3.2).

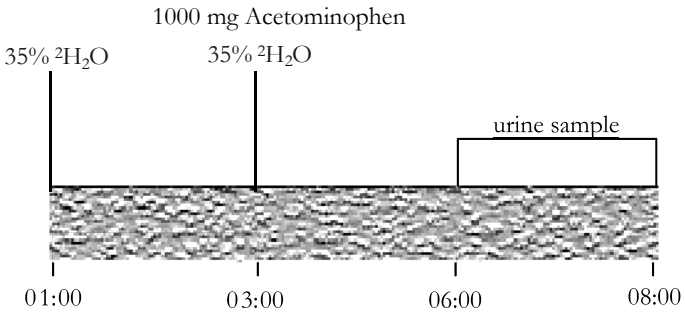

Figure 3.2. Schematic protocol design. Volunteers were given deuterated water (^2H_2O) and acetaminophen for assessment of fasting gluconeogenesis and glycogenolysis contributions to hepatic glucose production.

3.2.3. Biochemical analysis

Blood collected after 10 h of fasting was analyzed for plasma glucose, insulin, C peptide, cholesterol, high-density lipoprotein (HDL) cholesterol, low-density lipoprotein (LDL) cholesterol, triglycerides, glycosylated hemoglobin, creatinine and ureic nitrogen levels in the laboratories of the University Hospital of Coimbra. Plasma free fatty acids (FFA) were determined independently, using an enzymatic colorimetric method kit from Wako Chemicals GmbH, in plasma collected after 12 h of fasting.

3.2.4. Sample processing

Acetaminophen glucuronide from the 06:00-08:00 h urine samples was derived to MAG as previously described (Jones *et al.* 2006a, Jones *et al.* 2006b). Briefly, urine was concentrated by evaporation to 10% of its original volume and this portion was mixed with 9 volumes of ethanol (100%). The precipitate was centrifuged, the supernatant was evaporated to ~10 mL and the pH was adjusted to 8.0-9.0 with 1M NaOH. The supernatant was applied to an 18 × 1 cm diameter Dowex-1X8-200-acetate column. The column was washed with 35 mL of water, the glucuronide eluted with 35 mL of 10 M acetic acid, and the collected acetic acid fraction was evaporated to dryness at 40-50 ºC. The residue was resuspended in 50 mL water and the pH was adjusted to 4.5-5.0. The acetaminophen glucuronide in this solution was derivatized to monoacetoneglucuronic lactone (MAGL). Two thousand units of β-glucuronidase (*H. Pomatia,* Sigma Chemical Company) were added and the solution was incubated at 45ºC for 48 h. The solution was then passed through 10 mL Dowex-50X8-200 H^+ ion-exchange resin and evaporated to complete dryness at 40 ºC resulting in the conversion of free glucuronic acid to glucuronolactone. The lactone was converted to MAGL by stirring for 24 h with 5 mL of anhydrous acetone and 0.1 mL concentrated H_2SO_4. The yellow solution was mixed with 5 mL water, the pH adjusted to between 4 and 5 with 0.5 M Na_2CO_3 and the solution evaporated to dryness at room temperature.

MAGL was extracted from the salt products with 2-3 mL acetonitrile and reduced to MAG with lithium borohydride using tetrahydrofuran as the solvent. MAG molecules show the same labeling patterns as urinary acetominophen glucuronide but with completely resolved ^{2}H NMR signals.

3.2.5. ^{2}H NMR spectroscopy

^{2}H NMR spectra were acquired at 11.75 Tesla (T) with a Varian spectrometer equipped with a 5-mm broadband "switchable" probe with z-gradient (Varian, Palo Alto, CA, USA). MAG was dissolved in 90% acetonitrile/10% water and shimming was performed on selected proton (^{1}H) resonances of MAG. ^{1}H-decoupled ^{2}H NMR spectra were acquired without field-frequency lock at 50ºC using a 90º pulse and a 1.6 s acquisition time. Typically 6,000-30,000 FID were collected (2.7-13.5 h total collection time). For the determination of urine water ^{2}H-enrichment, spectra were obtained at 25ºC using a 22.5º pulse and a 4 s acquisition time (Jones *et al.* 2001b).

3.2.6. Bayesian/MCMC analysis of glucuronide metabolic fluxes

G6P derived from glycogenolysis has deuterium in position 2, as a result of exchange between G6P and fructose-6-phosphate (F6P) whereas G6P derived from any gluconeogenic precursor has deuterium incorporated in both position 2 and 5 due to additional exchanges at the triose phosphate level (Figure 3.1). Hence, the ratios of ^{2}H-enrichment in positions 5 and 2 (H5/H2) of G6P and plasma glucose reflect the fractional contribution of gluconeogenesis to fasting glucose production. The glucuronide moiety of acetaminophen is assumed to be derived from the hepatic uridine diphosphate-glucose (UDP-glucose) pool that is in isotopic steady state with hepatic G6P as a result of rapid G6P-G1P exchange (Schwenk and Kahl 1996). On this basis, glucuronide H5/H2 is identical to that of hepatic G6P and the fractional contributions of gluconeogenesis and glycogenolysis to HGP are given by the following equations:

Gluconeogenesis fraction = Glucuronide H5/Glucuronide H2 ×100 (%) *[Eq. 3.1]*

Glycogenolysis fraction = 1 – (Glucuronide H5/Glucuronide H2) ×100 (%) *[Eq. 3.2]*

The H5/H2 parameter is thus obtained from the ratio of the glucuronide ^{2}H NMR signals for these positions. This parameter can be obtained in an operator-independent manner by Bayesian analysis of the FID as previously described (Merritt *et al.* 2003). The posterior probability distribution for the gluconeogenesis and glycogenolysis fractions was obtained from a MCMC simulation consisting of 50 independent Markov chains, from each of which 50 independent samples were drawn (a total of 2,500 samples (Merritt *et al.* 2003)). Estimates of the mean and SD for each flux parameter were derived from this sample set.

3.2.7. Data analysis

Statistical differences were determined using one-way analysis of variance (ANOVA). The difference was considered statistical significant when $p<0.05$.

3.3. Results

3.3.1. Plasma metabolite and hormone levels

Table 3.1 provides a summary of plasma metabolite and insulin levels along with body mass index (BMI), age and gender for all subjects. There were no significant differences in the plasma levels of insulin, C peptide, cholesterol, HDL cholesterol, LDL cholesterol, triglycerides and FFA between healthy control and either of the KTx patient groups. Homeostatic model assessment of insulin resistance (HOMA-IR), calculated using fasting plasma glucose and insulin, showed no significant differences among all the groups studied. All patients treated with CsA showed significant increases in plasma creatinine and ureic nitrogen relative to healthy controls. These observations likely reflect an impairment in kidney function due to the nephrotoxic effects of CsA (Myers *et al.* 1986).

TABLE 3.1: Characteristics of the different groups studied[&].

	Group 1 Controls	Group 2 Normoglycemic KTx patients treated with CsA	Group 3 Hyperglycemic KTx patients treated with CsA
Gender (male/female)	3/3	7/0	3/0
Age, yr	39 ± 6	45 ± 2	58 ± 4* #
BMI, kg/m²	26.2 ± 1.6	24.3 ± 1.0	30.5 ± 0.7* #
Glucose, mM	4.8 ± 0.2	4.7 ± 0.1	7.1 ± 0.5* ##
Insulin, μUi/mL	7.3 ± 2.9	10.7 ± 5.8	4.5 ± 0.2
C-peptide, nM	2.6 ± 0.9	3.0 ± 0.7	2.7 ± 0.3
Cholesterol, mg/dL	189.8 ± 14.8	217.7 ± 16.9	209.7 ± 18.7
HDL Cholesterol, mg/dL	51.8 ± 3.9	46.1 ± 5.6	65.0 ± 18.8
LDL Cholesterol, mg/dL	119.3 ± 13.3	141.6 ± 12.1	130.7 ± 29.5
Triglycerides, mg/dL	179.2 ± 80.6	166.0 ± 25.3	171.7 ± 50.5
Glycosylated Hemoglobin, %	5.7 ± 0.2	5.6 ± 0.2	7.2 ± 0.4*
Creatinine, mg/dL	1.0 ± 0.1	1.3 ± 0.1*	1.2 ± 0.0*
Ureic nitrogen, mg/dL	14.8 ± 1.5	25.9 ± 2.4**	21.7 ± 3.2*
Plasma free fatty acids, mmol/L	0.31 ± 0.07	0.39 ± 0.05	0.45 ± 0.12
HOMA-IR	1.7 ± 0.7	2.2 ± 1.2	1.4 ± 0.2

[&]Biochemical parameters corresponding to blood samples collected after 10h-fast and FFA plasma levels after 12h-fast. Results are shown as mean ± standard error mean (SEM); *$p<0.05$; **$p<0.01$ relative to controls; #$p<0.05$; ##$p<0.01$, relative to normoglycemic KTx patients treated with CsA.

Hyperglycemic patients had significantly higher fasting plasma glucose levels on the morning of the study as well as higher values of glycosylated hemoglobin. This indicates that the hyperglycemia in these patients was well established prior to the study. This group also had a significantly higher BMI and age average compared to both normoglycemic transplant patients and to the healthy control group.

3.3.2. ^{2}H-enrichment distribution of body water and urinary glucuronide

Steady-state body water enrichments were 0.53% ± 0.01% in the hyperglycemic obese KTx patients treated with CsA. This was significantly higher than that of controls, (0.43% ± 0.01%, $p < 0.01$) and of the normoglycemic KTx patients treated with CsA, (0.48% ± 0.02%, $p < 0.05$). These results are consistent with a reduction in body water and an increased body fat fraction for hyperglycemic posttransplant patients.

^{2}H NMR spectra of MAG derived from acetaminophen glucuronide generated well-resolved ^{2}H MAG resonances with the hydrogen 5 signal SNR ranging from 20:1 to 60:1 (Figure 3.3 and Table 3.2). Both the sample mass and the ^{2}H NMR spectra derived from healthy controls were consistent with those recently reported in a study of overnight-fasted healthy controls (Jones *et al.* 2006b). Enrichment of position 2, reflecting isotope equilibration with body water, was estimated to be 86% ± 12% that of body water. This indicates that the exchange between hydrogen 2 of hepatic G6P and that of body water *via* interconversion of G6P and F6P was essentially complete. This is in agreement with recent reports where it was found that after 5 hours of $^{2}H_2O$ incubation, plasma $^{2}H_2O$ and H2 were equilibrated (Jones *et. al* 2006). Other MAG ^{2}H-signals corresponding to positions 3, 4 and 5 of glucuronide were less intense, indicating dilution of ^{2}H-enrichment at these sites by G6P derived from unlabeled hepatic glycogen. As was previously observed with glucuronide enrichment distributions from $^{2}H_2O$ in healthy subjects and in type 1 diabetic patients, the hydrogen 4

and 5 positions were enriched to similar levels (Burgess *et al.* 2003, Jones *et al.* 2006b). The ratio of hydrogen 3 enrichment relative to hydrogen 2 (H3/H2) was significantly lower than that of H5/H2 (0.26 ± 0.02 *vs.* 0.47 ± 0.05, p <0.005 for controls; and 0.45 ± 0.04 *vs.* 0.62 ± 0.03, p <0.0002 for KTx patients). The difference in enrichment between positions 3 and 5 could be the result of incomplete exchange of *1*R-dihydroxyacetone phosphate (the precursor of G6P hydrogen 3) with body water deuterium *via* triose phosphate isomerase, possibly due to isotopic discrimination. If so, then hydrogen 3 enrichment would systematically underestimate the gluconeogenic contribution to HGP.

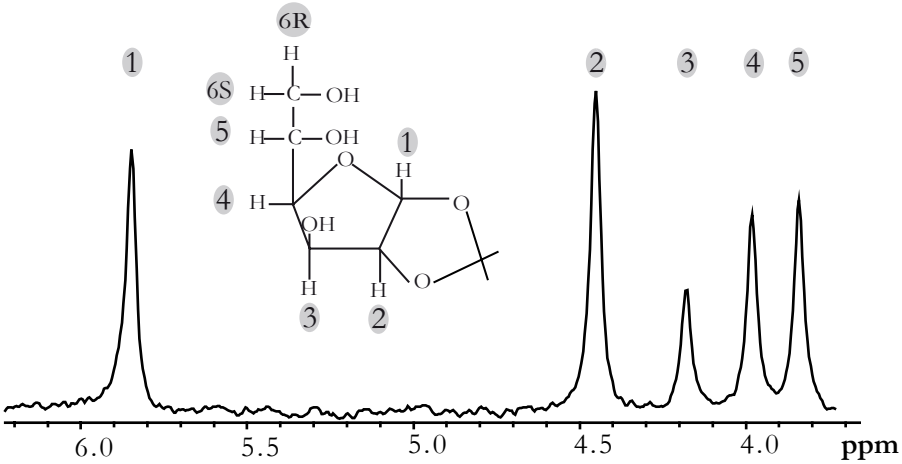

Figure 3.3. ^{2}H spectrum of MAG derived from urinary acetaminophen glucuronide. MAG molecule is represented and the respective protons identified.

In addition, the difference in enrichment between hydrogens 3 and 5 could also reflect transaldolase (TA) activity, which catalyzes the exchange of the 456 carbon fragment of F6P with free glyceraldehyde-3-phosphate (Stingl

et al. 2006, Jones *et al.* 2008). Since TA exchange results in the enrichment of unlabeled F6P (i.e., that derived from glycogenolysis) in positions 4, 5 and 6, this activity would contribute to hydrogen 5 enrichment of G6P independently of gluconeogenic flux, whereas hydrogen 3 enrichment would not be affected.

3.3.4. Gluconeogenesis and glycogenolysis contributions to hepatic glucose production by Bayesian/MCMC analysis

A summary of the Bayesian/MCMC estimates of the fractional contributions of gluconeogenesis and glycogenolysis to HGP for each subject is shown in Table 3.2, along with the SNR of the Fourier-transformed ^{2}H NMR spectrum of MAG. Generally, the precision of the flux estimates, as determined by the size of the SD, was highest for spectra with high SNR. These results also indicate that the precision of the Bayesian analysis is related to the relative intensities of the H5 and H2 signals independently of their individual SNR. As seen in Table 3.2, ^{2}H NMR spectra derived from controls and from hyperglycemic KTx patients had comparable SNR for H2 and H5. However, metabolic flux outputs from the spectra of the KTx patients had smaller SD compared to those of controls (5% ± 1% *vs.* 7% ± 2%). Aside from a higher H5/H2 intensity ratio (0.64 *vs.* 0.54), the spectra derived from the patients were similar to those of the control group in terms of signal linewidths and resolution. These results suggest that when the gluconeogenic contribution is low (i.e., less than 50% of HGP), the H5 signal SNR should be at least 60:1 in order to obtain reasonably low levels of uncertainty (i.e., a coefficient of variation of 10% or less). With higher gluconeogenic contributions (> 65% of HGP), a similar level of precision can be obtained from spectra with H5 SNR ratios of only ~30:1.

TABLE 3.2: Estimates of fractional gluconeogenesis and glycogenolysis contributions to HGP as determined by Bayesian analysis[#].

Subject	% HGP from gluconeogenesis	% HGP from glycogenolysis	H2 SNR	H5 SNR
Group 1: Controls				
AS	56 ± 10	44 ± 10	22.6	11.6
FP	55 ± 8	45 ± 8	66.4	33.1
IL	51 ± 7	49 ± 7	143.4	64.6
RC	43 ± 7	57 ± 7	69.7	35.7
RAC	55 ± 3	45 ± 3	130.9	63.5
TD	64 ± 9	36 ± 9	47.2	28.2
Average ± SD	**54 ± 7**	**46 ± 7**	-	-
Group 2: Normoglycemic KTx patients treated with CsA				
AB	54 ± 6	46 ± 6	80.2	46.5
AL	55 ± 6	45 ± 6	71.4	30.8
AM	69 ± 5	31 ± 5	80.6	52.8
AR	68 ± 4	32 ± 4	70.0	45.6
FO	70 ± 4	30 ± 4	55.1	44.0
LC	60 ± 5	40 ± 5	158.2	96.4
LS	58 ± 2	42 ± 2	86.2	51.7
Average ± SD	**62 ± 7**	**38 ± 7**	-	-
Group 3: Hyperglycemic KTx patients treated with CsA				
AM	69 ± 5	31 ± 5	30.9	22.2
AC	70 ± 4	30 ± 4	62.6	34.6
FS	65 ± 4	35 ± 4	95.2	59.6
Average ± SD	**68 ± 3***	**32 ± 3***	-	-

[#] Data presented as mean ± standard deviation of the Bayesian posterior probabilities (SDBPP) for each subject. Also shown are the SNR of deuterium 2 and 5 signals (H2 and H5) of MAG as determined after Fourier-transformation of the FID and applying 1 Hz of line-broadening using the NUTS NMR-processing software. Average ± SD are indicated for the groups studied; *p<0.05 relative to controls.

For the six control subjects, the mean contribution of gluconeogenesis and glycogenolysis to HGP was 54% ± 7% and 46% ± 7%, respectively. This is in good agreement with previous estimates of gluconeogenesis derived by the ^2H_2O method using ^2H NMR analysis of MAG derived from plasma glucose (Jones *et al.* 2001, Perdigoto *et al.* 2003, Burgess *et al.* 2003) as well as GC-MS analysis of plasma glucose (Landau *et al.* 1996, Chandramouli *et al.* 1997). These data are also in good agreement with values obtained by ^2H NMR analysis of MAG derived from urinary glucuronide (Burgess *et. al* 2003, Jones *et al.* 2006b).

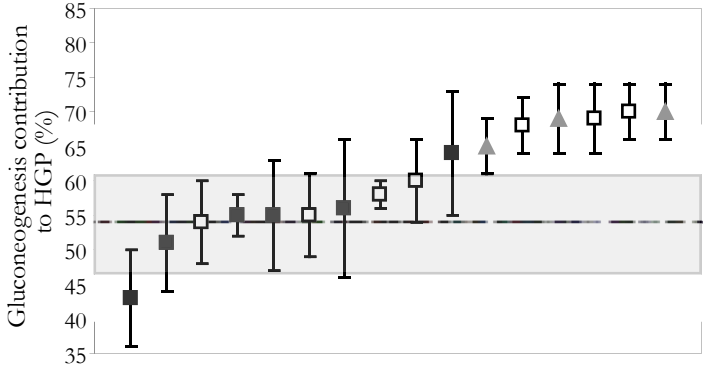

Figure 3.4. Percentage of hepatic glucose production from gluconeogenesis for each subject studied represented as mean ± standard deviation of the Bayesian posterior probabilities (SDBPP). The dotted line corresponds to the average of the gluconeogenic contribution to HGP of the subjects in the control group and the grey zone to the upper and lower limits of the respective standard deviation (SD). Black squares correspond to Group 1, the control group; white squares to Group 2, normoglycemic patients with a functional KTx with stable ongoing CsA-based therapy; and grey triangles to Group 3, hyperglycemic patients with a functional KTx and CsA-based therapy.

The gluconeogenic and glycogenolysis contribution to HGP for all the patients on CsA treatment is 64% ± 7% and 36% ± 7%, respectively (p <0.05, relative to controls). The lean normoglycemic KTx patients had a wider range of gluconeogenic contributions to HGP with a tendency towards a modestly increased gluconeogenic contribution to HGP (p = 0.06 relative to controls).

For the obese, hyperglycemic KTx patients, the gluconeogenic contribution to glucose production approached 70%. This estimate is somewhat higher than the value of 64% determined in healthy obese subjects by the ^2H_2O method but is in excellent agreement with the value of 68% obtained from obese subjects with type 2 diabetes (Gastaldelli *et al.* 2000) (Table 3.2 and Figure 3.4). There was no significant relationship between the fractional contribution of gluconeogenesis and any of the reported clinical parameters.

3.4. Discussion

The reported work demonstrates the feasibility and some limitations for quantifying fractional gluconeogenesis from Landau´s ^2H_2O method by Bayesian time-domain analysis of glucuronide enrichment in positions 5 and 2. As a result of the relatively large sample mass provided by glucuronide harvesting, ^2H NMR spectra with high SNR were obtained with a standard 11.75 T spectrometer and a 5 mm broadband probe. The accuracy precision of the Bayesian analysis is largely dependent on the SNR of the ^2H NMR spectrum. Among other things, this is a valuable tool for objectively determining the relationship between the sample collection time and statistical power of the analysis.

From the patient´s perspective, urinary glucuronide analysis is a more convenient and less invasive alternative to blood sampling. In addition, urinary glucuronide is far less susceptible than plasma glucose to degradation from delayed processing or storage above -80°C. Plasma glucose storage at -20°C for more than one month results in a marked decrease in glucose recovery as MAG whereas urinary glucuronide is stable for at least 4 months under these conditions. However, there are several disadvantages of acetaminophen glucuronide analysis compared to that of plasma glucose. The derivatization of acetaminophen glucuronide to MAG involves several additional steps compared to that of

plasma glucose and is therefore far less amenable for routine automation. In principle, the Bayesian analysis could be applied to ^{2}H NMR data of alternative glucuronides such as menthol glucuronide which can be more easily purified from urine and has fully resolved glucuronide ^{2}H-signals in its original form (Ribeiro *et al.* 2005, Mendes *et al.* 2006).

Compared to plasma glucose, the analysis of glucuronide ^{2}H-enrichment is less informative since the hexose position 6 hydrogens are removed during the conversion of UDP-glucose to glucuronide. The absence of position 6 ^{2}H-enrichment information means that the contributions of the TCA cycle and glycerol to gluconeogenesis, which relies on quantifying ^{2}H-enrichment in both position 5 and 6 (Landau *et al.* 1996), is not resolved. Gluconeogenesis measurement cannot be performed if there are contraindications to acetaminophen, such as advanced cirrhosis, or if the subject is inherently unable to synthesize significant levels of glucuronide, such as patients with uridine diphosphate (UDP)-glucuronosyl transferase deficiency (Demorais *et al.* 1992). There is additional uncertainty in the glucuronide sampling interval due to a 30-to 60-min lag time from its hepatic site of formation to reaching the bladder (Hellerstein *et al.* 1987). Moreover, hepatic glucuronide and glucose may exhibit different enrichment patterns from certain tracers as a result of hepatic metabolic zonation (Ekberg *et al.* 1995). Glycogen metabolism and glucuronide synthesis are both located in the pericentral region of the hepatic lobule whereas glucose secretion is predominantly in the periportal region (Jungermann 1986, Jungermann and Thurman 1992). To the extent that there is a difference in the gluconeogenic contribution to G6P synthesis in periportal *vs.* pericentral hepatocytes, plasma glucose and urinary glucuronide could report different fractional contributions of gluconeogenesis to HGP. For a small group of healthy subjects, plasma glucose and urinary glucuronide provided equivalent estimates of gluconeogenesis (Burgess *et al.* 2003), but this has not been tested in larger subject populations or in patients with disorders of glucose metabolism.

The results described in here suggest that the gluconeogenic contribution to HGP had a tendency to be modestly higher in lean normoglycemic KTx patients undergoing CsA-based immunosuppressant therapy compared to healthy controls, but this difference did not reach statistical significance in this study. Substrate selection for HGP can be modified by changes in insulin action as well as by the availability of oxidizable substrates such as FFA. Hepatic glycogenolysis is suppressed by insulin and enhanced by glucagon and is therefore sensitive to alterations in plasma insulin levels (Surmely *et al.* 1999). FFA can stimulate gluconeogenesis, possibly *via* augmentation of hepatic adenosine triphosphate (ATP) and reduced nicotinamide adenine dinucleotide (NADH) production (Chen *et al.* 1999, Boden *et al.* 2002). They may also increase the rate of glycogenolysis by impairing its suppression by insulin (Boden *et al.* 2002). While CsA has been reported to reduce pancreatic insulin secretion (Hjelmesaeth *et al.* 2007) possibly by inducing pancreatic β-cells apoptosis (Penfornis and Kury-Paulin 2006), neither the normo- nor the hyperglycemic CsA patients of this study had significantly different plasma insulin levels compared to healthy controls, at least under basal fasting conditions. Therefore, the data reported in here suggests that the observed alterations in HGP sources are not due to defective insulin secretion during fasting. Moreover, HOMA-IR indices for the three subject groups were similar suggesting that insulin sensitivity, as determined by this method, was not significantly modified in KTx patients. While plasma FFA levels were not significantly different between healthy, lean/normoglycemic and obese/hyperglycemic KTx patients, there was a tendency for FFA levels to be higher in the KTx patients, with the highest values found in the obese group.

3.5. Conclusions

In summary, for KTx patients undergoing CsA immunosuppressant therapy, the gluconeogenic contribution to HGP is significantly increased in the setting of PTDM. This metabolic alteration is most strongly associated with adiposity and BMI, but may also be associated with elevated plasma FFA. There was no association between the gluconeogenic contribution to HGP and either fasting plasma insulin levels or insulin sensitivity as determined by HOMA-IR. CsA treatment *per se* appears to provoke only modest alterations of HGP sources and is not associated with fasting hyperglycemia or hyperinsulinemia. Finally, the Bayesian analysis of urinary glucuronide ^{2}H-enrichment allows an objective evaluation of hepatic HGP sources to be easily integrated with other simple and practical measurements of human glucose homeostasis.

3.6. References

Boden G, Chen XH, Stein TP. Gluconeogenesis in moderately and severely hyperglycemic patients with type 2 diabetes *mellitus*. Am J Physiol Endocrinol Metab 2001;280(1):E23-E30.

Boden G, Cheung P, Stein TP, Kresge K, Mozzoli M. Free fatty acids cause hepatic insulin resistance by inhibiting insulin supression by glycogenolysis. Am J Physiol Endocrinol Metab 2002;283: E12-E19.

Burgess S, Schröer J, Kemp L. Detection of liver diseases by ^{2}H NMR analysis of glucose derivatives using a parallel automated sample preparation method. Chemspeed Technologies ed. 2002.

Burgess SC, Weis B, Jones JG, Smith E, Merritt ME, Margolis D, Sherry AD, Malloy CR. Noninvasive evaluation of liver metabolism by H-2 and C-13 NMR isotopomer analysis of human urine. Anal Biochem 2003;312(2):228-234.

Chandramouli V, Ekberg K, Schumann WC, Kalhan SC, Wahren J, Landau BR. Quantifying gluconeogenesis during fasting. Am J Physiol Endocrinol Metab 1997;36(6): E1209-E1215.

Chen X, Iqbal N, Boden G. The effects of free fatty acids on gluconeogenesis and glycogenolysis in normal subjects. J Clin Invest 1999; 103:365-72.

Chevalier S, Burgess SC, Malloy CR, Gougeon R, Marliss EB, Morais JA. The greater contribution of gluconeogenesis to glucose production in obesity is related to increased whole-body protein catabolism. Diabetes 2006;55(3):675-681.

Demorais SMF, Uetrecht JP, Wells PG. Decreased glucuronidation and increased bioactivation of acetaminophen in Gilberts-Syndrome. Gastroenterology 1992;102(2):577-586.

Ekberg K, Chandramouli V, Kumaran K, Schumann WC, Wahren J, Landau BR. Gluconeogenesis and glucuronidation in liver *in vivo* and the heterogeneity of hepatocyte function. J Biol Chem 1995;270(37):21715-21717.

Gastaldelli A, Baldi S, Pettiti M, Toschi E, Camastra S, Natali A, Landau BR, Ferrannini E. Influence of obesity and type 2 diabetes on gluconeogenesis and glucose output in humans - A quantitative study. Diabetes 2000;49(8):1367-1373.

Hellerstein MK, Greenblatt DJ, Munro HN. Glycoconjugates as noninvasive probes of intrahepatic metabolism. 1.Kinetics of label incorporation with evidence of a common precursor UDP-glucose pool for secreted glycoconjugates. Metab Clin Exp 1987;36(10):988-994.

Hjelmesaeth J, Hagen LT, Asberg A, Midtvedt K, Storset O, Halvorsen CE, Morkrid L, Hartmann A, Jenssen T. The impact of short-term ciclosporin A treatment on insulin secretion and insulin sensitivity in man. Nephrol Dial Transplant 2007;22(6):1743-1749.

Jindal RM, Sidner RA, Milgrom ML. Post-transplant diabetes *mellitus* - The role of immunosuppression. Drug Safety 1997;16(4):242-257.

Jones JG, Barosa C, Gomes F, Mendes AC, Delgado TC, Diogo L, Garcia P, Bastos M, Barros L, Fagulha A, Baptista C, Carvalheiro M, Caldeira MM. NMR derivatives for quantification of H-2 and C-13-enrichment of human glucuronide from metabolic tracers. J Carbohydr Chem 2006;25(2-3):203-217.

Jones JG, Fagulha A, Barosa C, Bastos M, Barros L, Baptista C, Caldeira MM, Carvalheiro M. Noninvasive analysis of hepatic glycogen kinetics before and after breakfast with deuterated water and acetaminophen. Diabetes 2006;55(8):2294-2300.

Jones JG, Garcia P, Barosa C, Delgado TC, Caldeira MM, Diogo L. Quantification of hepatic transaldolase exchange activity and its effects on tracer measurements of indirect pathway flux in humans. Magn Reson Med 2008;59(2):423-429.

Jones JG, Merritt M, Malloy C. Quantifying tracer levels of (H_2O)-H-2 enrichment from microliter amounts of plasma and urine by H-2 NMR. Magn Reson Med 2001;45(1):156-158.

Jones JG, Solomon MA, Cole SM, Sherry AD, Malloy CR. An integrated H-2 and C-13 NMR study of gluconeogenesis and TCA cycle flux in humans. Am J Physiol Endocrinol Metab 2001;281(4):E848-E856.

Jungermann K. Functional-heterogeneity of periportal and perivenous hepatocytes. Enzyme 1986;35(3):161-180.

Jungermann K, Thurman RG. Hepatocyte heterogeneity in the metabolism of carbohydrates. Enzyme 1992;46(1-3):33-58.

Landau BR, Wahren J, Chandramouli V, Schumann WC, Ekberg K, Kalhan SC. Contributions of gluconeogenesis to glucose production in the fasted state. J Clin Invest 1996;98(2):378-385.

Markell M. New-onset diabetes *mellitus* in transplant patients: Pathogenesis, complications, and management. Am J Kidney Dis 2004;43(6):953-965.

Markell MS. Post-transplant diabetes: Incidence, relationship to choice of immunosuppressive drugs, and treatment protocol. Adv Ren Replace Ther 2001;8(1):64-69.

Mendes AC, Caldeira MM, Silva C, Burgess SC, Merritt ME, Gomes F, Barosa C, Delgado TC, Franco F, Monteiro P, Providencia L, Jones JG. Hepatic UDP-glucose ^{13}C isotopomer from [U-^{13}C]glucose: a simple analysis of urinary menthol glucuronide. Magn Reson Med 2006;56(5):1121-5.

Merritt M, Bretthorst GL, Burgess SC, Sherry AD, Malloy CR. Sources of plasma glucose by automated Bayesian analysis of H-2 NMR spectra. Magn Reson Med 2003;50(4):659-663.

Myers BD, Sloan D, Garella S, Cohen JJ, Harrington JT, Spargo B, Coe F, Bushinsky D, Toback G, Hirsch S, Lau K. Cyclosporine nephrotoxicity. Kidney Int 1986;30(6):964-974.

Penfornis A, Kury-Paulin S. Immunosuppressive drug-induced diabetes. Diabetes Metab 2006;32(5):539-546.

Perdigoto R, Rodrigues TB, Furtado AL, Porto A, Geraldes CFGC, Jones JG. Integration of [U-C-13]glucose and (H_2O)-H-2 for quantification of hepatic glucose production and gluconeogenesis. NMR in Biomedicine 2003;16(4):189-198.

Ribeiro A, Caldeira MM, Carvalheiro M, Bastos M, Baptista C, Fagulha A, Barros L, Barosa C, Jones JG. Simple measurement of gluconeogenesis by direct H-2 NMR analysis of menthol glucuronide enrichment from (H_2O)-H-2. Magn Reson Med 2005;54(2):429-434.

Salvadori M, Bertoni E, Rosati A, Zanazzi M. Post-transplant diabetes *mellitus*. J Nephrol 2003;16(5):626-634.

Schwenk WF, Kahl JC. Acetaminophen glucuronidation accurately reflects gluconeogenesis in fasted dogs. Am J Physiol Endocrinol Metab 1996;34(3):E529-E534.

Stingl H, Chandramouli V, Schumann WC, Brehm A, Nowotny P, Waldhausl W, Landau BR, Roden M. Changes in hepatic glycogen cycling during a glucose load in healthy humans. Diabetologia 2006;49(2):360-368.

Surmely JF, Schneiter P, Henry S, Paquot N, Jequier E, Tappy L. Effects of glucagon in the control of endogenous glucose production in man. Nutrition 1999;15(4):267-273.

Weis BC, Margolis D, Burgess SC, Merritt ME, Wise H, Sherry AD, Malloy CR. Glucose production pathways by H-2 and C-13 NMR in patients with HIV-associated lipoatrophy. Magn Reson Med 2004;51(4):649-654.

Chapter 4

Hepatic glucose metabolism during glucose challenge

Effects of high fat dietary food intake and cyclosporine A treatment in rats

4.1. Introduction

Hepatic glucose metabolism plays an important role in whole body glucose homeostasis. In fasting, the liver accounts for the bulk of endogenous glucose production with glycogenolysis and gluconeogenesis both contributing to hepatic glucose production (HGP). After an overnight-fast gluconeogenesis and glycogenolsysis contribute equally to HGP whereas with increased fasting, hepatic glycogen stores are depleted and gluconeogenesis contribution is enhanced (Rothman *et al.* 1991, Landau *et al.* 1996).

During absorption of a meal, the liver receives a relatively high concentration of glucose *via* the portal vein. The increased glucose levels *per se* activate glucokinase to phosphorylate hepatic glucose to glucose-6-phosphate (G6P). The elevated G6P concentrations have a synergistic effect with glucose in promoting the inactivation of glycogen phosphorylase and inducing glycogen synthesis through glycogen synthase activation. Moreover, the increased glucose levels stimulate insulin secretion by pancreatic β-cells. Insulin further activates glucokinase by promoting its translocation from the nucleus to the cytoplasm whereas elevated plasma insulin to glucagon ratio activate glycogen synthase, inhibit glycogen phosphorylase and are also responsible for inactivation of some key gluconeogenic regulatory enzymes such as phosphoenolpyruvate kinase (PEPCK). Overall, hyperinsulinemia promotes hepatic glucose uptake, storage as glycogen, and suppression of HGP. After a glucose load, ~20% of the glucose is cleared by the liver and deposited as glycogen (Petersen *et al.* 2001).

In addition, glucose and insulin stimulate glucose uptake by insulin-sensitive peripheral tissues, including skeletal muscle and adipocytes. Hence, through the reduction of HGP and an increase in glucose disposal, plasma glucose levels are quickly restored to normal limits following carbohydrate ingestion and absorption. A defect in one or both of these mechanisms reduces the capacity for glucose homeostasis under these conditions and forms the definition of

glucose intolerance. In the clinical setting, glucose intolerance is interrogated by a glucose tolerance test (GTT). In humans, glucose can be administrated by means of an intravenous (i.v.) infusion, the intravenous glucose tolerance test (IVGTT), included in an oral glucose tolerance test (OGTT), or in the carbohydrate component of a mixed meal ingestion test. In small animal models, such as rats and mice, glucose intolerance may be assessed by IVGTT and OGTT protocols but the glucose load is also often delivered as an intraperitoneal (i.p.) injection, i.p. glucose tolerance test (IPGTT), because this method is more convenient compared to the other administration procedures.

In its current form, a glucose tolerance test can identify a defined level of glucose intolerance, but does not identify or resolve the underlying causes, which may include impaired glucose clearance, impaired suppression of HGP, or both. By introducing tracers into the load and analyzing their entry and clearance into plasma glucose and hepatic glycogen, the hepatic and peripheral components of glucose homeostasis can be resolved.

In this study, the fate of an i.p. glucose load enriched with [U-^{13}C]glucose and deuterated water ($^{2}H_2O$) was studied. Entry and clearance of the load through plasma glucose and the effects of the load on HGP were assessed by the analysis of plasma glucose enrichment from both tracers. This measurement was applied to Sprague-Dawley rats fasted for 6 hours. From the perspective of hepatic glucose metabolism, this fasting period corresponds to that of overnight-fasting in humans, the standard starting point for a glucose tolerance test in the clinical setting. The contribution of HGP to total body glucose was determined from the deuterium (^{2}H)-enrichment of plasma glucose position 2 relative to that of plasma water (PW) (Allick *et al.* 2006). The fraction of plasma glucose derived from gluconeogenic sources was quantified from the ^{2}H-enrichment levels at position 5 of plasma glucose relative to that of PW. The contribution of the i.p. load to plasma and total body glucose was estimated from the carbon 13 (^{13}C)-enrichment level of plasma [U-^{13}C]glucose relative to that of the load.

Enrichments of plasma glucose by [U-^{13}C]glucose and $^{2}H_2O$ were resolved by ^{2}H and ^{13}C Nuclear Magnetic Resonance (NMR) spectroscopy.

These measurements were applied to a group of healthy animals fed with a standard chow (SC) diet to obtain baseline estimates of glucose kinetics. To investigate the changes in glucose kinetics that accompany the onset of glucose intolerance induced by dietary or by pharmacological interventions, two further groups of animals were studied. In one group, glucose intolerance was induced as a result of high fat (HF) diet feeding. Previous studies have shown that rats placed on a HF diet show normal fasting blood glucose but when challenged with a glucose load they reveal glucose intolerance secondary to insulin resistance (Kraegen *et al.* 1986, Storlien *et al.* 1986). The underlying flux mechanisms that contribute to glucose intolerance have not yet been defined in this model. In the other group, glucose intolerance in normally-fed animals was induced after administration of Cyclosporine A (CsA). CsA is currently the most widely used agent for suppressing the host immune response following solid organ transplantation. It has recently been implicated in the promotion of glucose intolerance and posttransplant diabetes *mellitus* (PTDM), mainly through disruption of pancreatic β-cell function *in vivo* (Doyle *et al.* 2003). The effect of CsA on glucose clearance and HGP fluxes in relation to the development of glucose intolerance is not known.

4.2. Materials and Methods

4.2.1. Materials

[U-^{13}C]glucose (99%) and $^{2}H_2O$ (99.9%) were obtained from Cambridge Isotope Laboratories Inc. (Andover, MA, USA). CsA and other common chemicals were purchased from Sigma-Aldrich. The HF diet used contained 45% of calories from fat, 35% from carbohydrate and 20% derived from protein

(E15744-34, SSNIFF, Specialdiäten GmbH)®. SC diet contains 2.7% of fat, 60% carbohydrate and 16% protein.

4.2.2. Treatment protocol

The study was approved by the Institutional Animal Care and Use Committee. Male Sprague-Dawley rats were housed in a room on a 12-h light-dark cycle under constant temperature (22-25 ºC) and with *ad libitum* access to food and water. Animals were separated into different groups: Group 1, control animals maintained on a SC diet for 20 days; Group 2, animals maintained for 20 days on a HF diet; and Group 3, rats maintained on a SC diet and given daily an i.p. injection of CsA (15 mg/kg body weight). This dose was chosen according to previous studies in literature (Mazzoni *et al.* 1986). At the day of the study, all groups of animals were matched for body weight (Group 1, 318 ± 13 g; Group 2, 324 ± 20 g; Group 3, 313 ± 18 g). The number of animals for each experiment is indicated in the legend of the figures.

4.2.3. Intra-peritoneal glucose tolerance test protocol (IPGTT)

After 6-h fasting, rats were challenged with an i.p. glucose load (1.5 mg glucose/g body weight) 9.6 % enriched with [U-^{13}C]glucose and dissolved in 4 mL of 70% $^{2}H_2O$-saline. After the i.p. glucose load, control animals were sacrificed at different time points during a 60 min period. Animals on a HF diet or treated with CsA were sacrificed after 60 min and compared to the respective controls. At the pre-defined intervals, animals were anesthetized with isoflurane anesthetic, blood was immediately withdrawn from the descending aorta and the liver weighted, freeze-clamped and kept at -80ºC until further analysis. Blood glucose and plasma insulin levels were assessed using a standard glucometer and an ELISA kit from Lynco, respectively.

4.2.4. Blood processing

Blood was immediately deproteinized with a final volume of 4% perchloric acid (70%) and centrifuged at 13,000 *g* at 4ºC for plasma separation. The plasma supernatant was separated from erythrocytes and neutralized with concentrated KOH. Samples were further purified by anionic-cationic exchange chromatography and evaporated to dryness. The conversion of plasma glucose to monoacetone glucose (MAG) was performed according to the literature (Jones *et al.* 2001).

4.2.5. Liver Processing

Frozen livers were freeze-dried and then powdered. 30% KOH at 70ºC was added to each sample in 2:1 (v/v). After 30 minutes, 8 mL of Na_2SO_4 6% and 50 mL of absolute ethanol were added and the sample incubated overnight at 4ºC. The precipitated glycogen was separated from the supernatant by centrifugation at 3,000 *g* and dissolved in 5 mL of acetate buffer 0.05 M (pH 4.5). 16 U of amyloglucosidase were added to each sample and incubated for 10 hours at 55ºC. The containing glucose supernatant was then separated by centrifugation and derivatized to MAG according to literature (Jones *et al.* 2001).

4.2.6. Conversion of glucose to monoacetone glucose

A mixture of 0.5 mL acetone/mL of original plasma or 20 mL acetone/ liver and concentrated anhydrous H_2SO_4 (40 μL/mL acetone) was added to the sample and stirred vigorously for 4 h. 10 mL of H_2O were added and the pH adjusted to 2.2-2.3 followed by incubation at 40 ºC for 5 h. The samples pH was adjusted to ~8.0 and then evaporated to dryness. The dry residue was further extracted using ethyl acetate. MAG samples were then stored at room temperature until NMR analysis. MAG reflects plasma glucose and hepatic

glycogen glucose monomers labeling patterns but with completely resolved ^{2}H and ^{13}C NMR signals.

4.2.7. Nuclear Magnetic Resonance (NMR) Spectroscopy

4.2.7.1. ^{2}H NMR Spectroscopy

^{2}H NMR spectra from plasma MAG pooled samples and MAG from hepatic glycogen glucose monomers were obtained using a Varian 14.1 Tesla (T) spectrometer (Varian Instruments, Palo Alto, CA, USA). MAG was dissolved in 90% acetonitrile/10% water and shimming was performed on selected MAG proton (^{1}H) resonances. ^{1}H-decoupled ^{2}H NMR spectra were acquired at 50ºC using a 90º pulse, a 1.5 s acquisition time and 0.1 s interpulse delay. Typically 6,000-20,000 scans were averaged. For the determination of PW ^{2}H-enrichment, using the method described in Jones *et al.*, spectra were obtained at 25ºC using a 22.5º pulse and a 4 s acquisition time (Jones *et al.* 2001).

4.2.7.2. ^{13}C NMR Spectroscopy

Samples were dissolved in deuterated acetonitrile for ^{13}C NMR analysis. ^{1}H-decoupled ^{13}C NMR spectra were obtained with a Varian 11.75 T system (Varian Instruments, Palo Alto, CA, USA) equipped with a 5-mm broadband probe. Spectra were acquired at 25ºC using a 90º pulse and a 2.5 s acquisition time. 4,000-10,000 scans were averaged for each spectrum.

4.2.7.3. NMR Analysis

^{2}H and ^{13}C NMR spectra were analyzed using the curve-fitting routine supplied with the NUTS PC-based NMR spectral analysis program (Acorn NMR Inc., Fremont CA). In the MAG samples derived from the glucose monomers of hepatic glycogen, ^{2}H-enrichments were determined by comparison with the ^{2}H natural abundance (0.015%) signals of the acetone group of MAG whereas

in MAG samples from plasma glucose, ^{2}H-enrichments were quantified relative to an internal standard of dimethylsulfoxide (DMSO). ^{13}C-enrichments were determined relative to the natural abundance C1 singlet (1.11%).

4.2.8. Glucose from HGP and gluconeogenesis contribution

After the glucose load, it is assumed that total body glucose represents a combination of glucose absorbed from the load, HGP, and existent glucose from before the load (Jin *et al.* 2003). After providing $^{2}H_2O$, plasma glucose derived from HGP has ^{2}H incorporated into position 2 as a result of exchange between hepatic G6P and fructose-6-phosphate (F6P). Hence, the ratio of ^{2}H-enrichment in position 2 of glucose (H2) to that of PW reflects the fractional contribution of HGP to plasma glucose (Eq. 4.1). Note that this contribution formally includes glucose molecules that undergo futile cycling between blood and liver as a result of glucokinase and glucose-6-phosphatase (G6Pase) activites (Katz *et al.* 1975). ^{2}H-enrichment in position 2 of glucose was quantified by ^{2}H NMR analysis of the MAG derivative of plama glucose (Figure 4.1). MAG samples from animals of the same group at same time post-load were pooled in order to obtain better quality ^{2}H NMR spectra for confident quantification of the ^{2}H positional enrichments.

Plasma glucose derived from gluconeogenesis has deuterium incorporated in position 5 as a result of exchanges at the level of the triose phosphate precursors. The fraction of plasma glucose derived from gluconeogenesis can thus be determined from the ratio of ^{2}H-enrichment in position 5 of plasma glucose (H5) relative to the plasma water ^{2}H-enrichment (Eq. 4.2).

Percent of plasma glucose from HGP = (H2/PW) × 100 (%) *[Eq. 4.1]*

Percent of plasma glucose from gluconeogenesis = (H5/PW) × 100 (%) *[Eq. 4.2]*

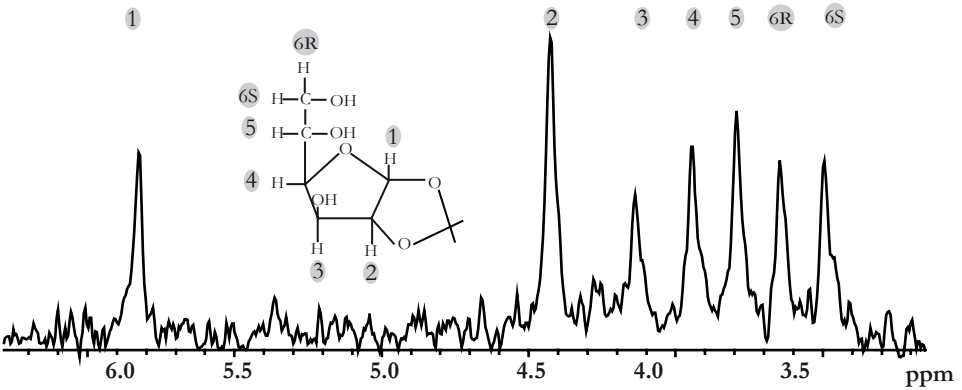

Figure 4.1. ^{2}H NMR spectrum of monoacetone glucose (MAG) derived from plasma glucose. The ^{2}H NMR spectrum shown corresponds to pooled MAG samples from control animals, 60 min after the i.p. glucose load (1.5 mg/g body weight) and administration of $^{2}H_{2}O$. Seven MAG aliphatic hydrogens derived from plasma glucose are shown and identified respectively.

4.2.9. Glucose and "recycled" glucose from the i.p. load

The contribution to total glucose from the i.p. load was estimated using ^{13}C NMR analysis following administration of [U-^{13}C]glucose. As the glucose load was only 9.6 % enriched with [U-^{13}C]glucose, the probability that two [U-^{13}C]trioses can be recombined to form [U-^{13}C]glucose is very low. Thus, it is assumed that all [U-^{13}C]glucose present in plasma glucose originated from the load (Jin *et al.* 2003). In the ^{13}C NMR spectra of MAG derived from plasma glucose, the ^{13}C resonances consist of singlet signals, mostly derived from ^{13}C natural-abundance, and the ^{13}C-^{13}C spin-spin coupled multiplets. In the carbon 1 resonance, it is possible to resolve the quartet (Q1 + Q2 + Q3 + Q4) corresponding to [U-^{13}C]glucose that is quantified relative to the 1.11% natural abundance singlet (Figure 4.2).

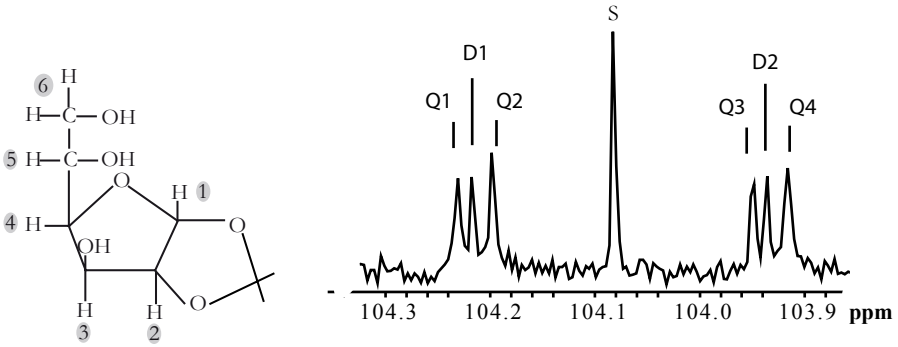

Figure 4.2. C1 ^{13}C NMR signals of monoacetone glucose (MAG) derived from plasma glucose 60 min after the i.p. glucose load (1.5mg/g body weight) in control animals. The singlet (S) corresponding to the natural abundance and the isotopomers resultant of [U-^{13}C]glucose (Q1-Q4) and recycled glucose (D1 and D2) are observed.

By accounting for the 9.6 % [U-^{13}C]glucose enrichment of the i.p. glucose load it is possible to estimate the contribution of the i.p. load to plasma glucose as follows:

Contribution to glucose from i.p. load =
[(Q1 + Q2 + Q3 + Q4) / S] × 1.11 / 0.096 (%) *[Eq. 4.3]*

The doublet signals (D1 and D2) in the ^{13}C NMR carbon 1 multiplet due to ^{13}C-^{13}C coupling between carbons 1 and 2 (but not carbon 5) represent the sum of [1,2,3-$^{13}C_3$]glucose and [1,2-$^{13}C_2$]glucose isotopomers. These represent "recycled" glucose molecules formed through the activity of the Cori cycle (i.e., glucose→pyruvate/lactate→glucose) since they are assumed to be derived from [1,2,3-$^{13}C_3$]pyruvate, the glycolytic product of [U-^{13}C]glucose. The generation of both [1,2,3-$^{13}C_3$]glucose and [1,2-$^{13}C_2$]glucose isotopomers from

[1,2,3-$^{13}C_3$]pyruvate is the result of tricarboxylix acids (TCA) cycle exchanges and pyruvate recycling fluxes (Jones *et al.* 1997). The abundance of these two isotopomers, corrected for dilution at the level of the TCA cycle, provides an estimate of the fraction of plasma glucose derived from recycling (Perdigoto *et al.* 2003, Sena *et al.* 2007) as follows:

Contribution of recycled glucose from i.p. load=
[(D1 + D2) / S] × 1.11 / 0.096 × 1.5 (%) *[Eq. 4.4]*

where 1.5 is a correction factor that accounts for dilution of the ^{13}C-label at the level of the hepatic TCA cycle (Perdigoto *et al.* 2003, Sena *et al.* 2007).

Previous studies have shown that the glucose entering the system is instantaneously mixed in ~16-20% of the animal body weight, the glucose mixing space (mL/kg) (Baker *et al.* 1959, Raman *et al.* 1990, McArthur *et al.* 1999). Using Eq. 4.5 is possible to determine the total body glucose considering the total glucose space, animals' body weight and the blood glucose concentration.

Total body glucose = glucose space × [blood glucose] × animal body weight *[Eq. 4.5]*

Thus, the absolute contributions (μmol) of HGP, gluconeogenesis, glucose and "recycled" glucose from the i.p. load to total body glucose are derived by multiplying relative percent contributions by total body glucose at each time point.

4.2.10. Hepatic glycogen synthesis

Hepatic glycogen content was determined 60 min following the i.p. glucose load by analyzing the amount of glucose after enzymatic hydrolysis of hepatic glycogen. Glucose concentrations were assessed enzymatically by the

glucose oxidase method using a commercial kit (Invitrogen). The percentage of newly synthesized hepatic glycogen after the glucose load can be quantified by analyzing the ^{2}H-enrichment in position 2 of MAG derivatized from hepatic glycogen following its enzymatic hydrolysis to glucose. Indirect pathway contributions to hepatic glycogen synthesis can be further assessed by calculating the ratio of ^{2}H-enrichments in position 5 and 2.

4.2.11. Statistical analysis

Data are presented as average ± standard deviation (SD). Statistical differences were determined using one-way analysis of variance (ANOVA) and considered to be statistical significant when $p < 0.05$.

4.3. Results

4.3.1. Blood glucose and plasma insulin during an i.p. glucose load

Blood glucose and plasma insulin levels attained during the i.p. glucose load for the groups studied are shown in Figure 4.3. Blood glucose peaked 15 min after the glucose load for control animals and decreased gradually thereafter, returning to basal levels 60 min after the load. The relatively high blood glucose levels attained may be partially attributed to the known effects of the anesthesia (Zuurbier *et al.* 2008). CsA-treated animals show significant elevated fasting hyperglycemia relative to control animals. HF diet and especially CsA treatment promoted impaired glucose tolerance (IGT) as compared with healthy animals. In addition, there is a trend for decreased glucose-stimulated insulin secretion in CsA-treated animals.

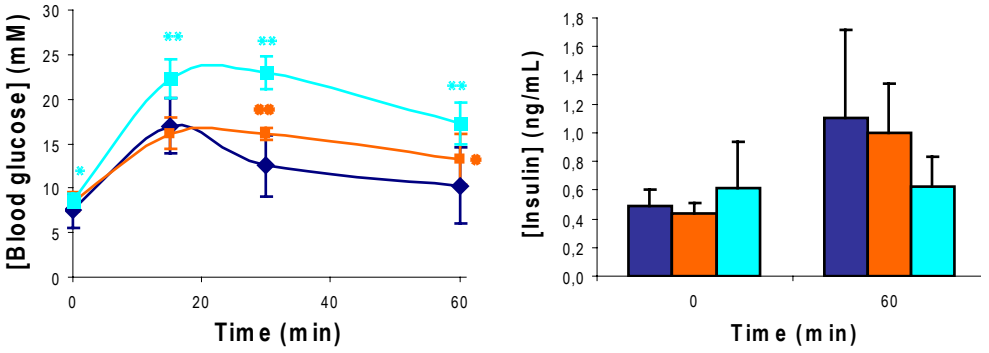

Figure 4.3. Blood glucose profiles and plasma insulin levels after the glucose load (1.5 mg/g body weight) for control animals (dark blue, n=8), rats on a HF diet (orange, n=5) and on CsA treatment (light blue, n=6). *p<0.05, **p<0.01 relative to controls, at each time point.

4.3.2. Plasma ^{2}H and [U-^{13}C]glucose enrichment kinetics

Following i.p. injection of 70% $^{2}H_2O$-saline solution, rat PW ^{2}H-enrichment rapidly reached isotopic steady-state within 4-7 minutes (Figure 4.4).

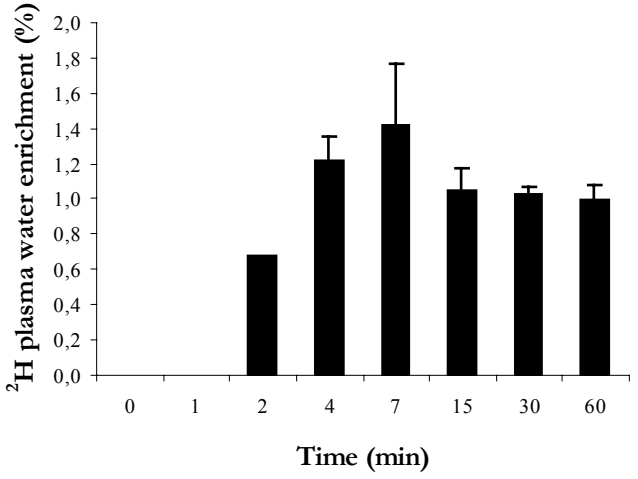

Figure 4.4. Plasma water ^{2}H-enrichment following i.p. injection of 70 % $^{2}H_2O$-saline solution in control rats.

Compared to the $^{2}H_2O$ tracer, [U-^{13}C]glucose enrichment of plasma glucose was much slower, peaking at 30 min after the i.p. glucose load (Figure 4.5). Moreover, the maximum enrichment levels attained were unexpectedly low (about one-third of the load enrichment), given the size of the glucose load (2,632 μmol) relative to the initial total body glucose pool size (442 μmol). The observed plasma [U-^{13}C]enrichment levels correspond to a ~37% contribution from the i.p. glucose load. Low plasma [U-^{13}C]glucose enrichments could result from reduced absorption rate of the i.p. glucose load or from dilution from unlabeled glucose generated *via* HGP. Previous studies with oral glucose loads show that 50% of plasma glucose in 6-h fasted rats was accounted for by the load at 60 minutes after (Smadja *et al.* 1988) while in 24-h fasted rats, the load contribution was 70-80% (Jin *et al.* 2003). Thus, the reduced contribution of the load glucose in the 6-h compared to 24-h fasting most probably reflects a higher initial glucose pool size and/or increased HGP at 6-h *vs.* 24-h fasting.

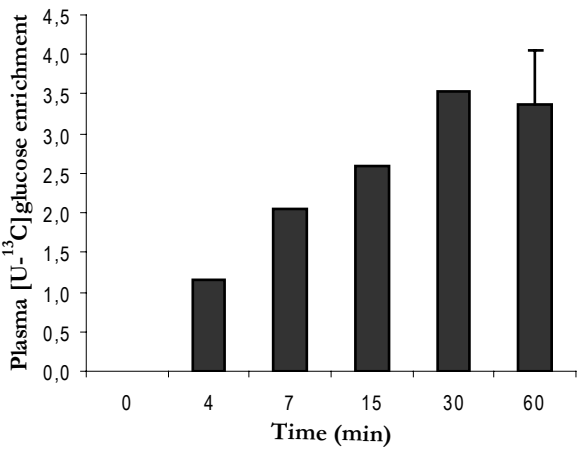

Figure 4.5. Plasma [U-^{13}C]glucose enrichment in control rats following i.p. injection of glucose (1.5 mg/g body weight) enriched with 9.6% [U-^{13}C]glucose.

4.3.3. Glucose from HGP and gluconeogenesis contribution

All plasma glucose derived from HGP (gluconeogenesis + glycogenolysis + glucose-G6P cycling) is labeled in position 2 as a result of F6P-G6P exchange. If HGP accounted for all the plasma glucose, the plasma glucose H2 enrichment level would be equal to that of PW. The glucose contributions from HGP to total glucose with time are shown in Figure 4.6. For control animals, HGP contributions were relatively constant and significant between 15 and 60 min after the i.p. glucose load.

Gluconeogenesis results in the labeling of H5 as well as H2 (while glycogenolysis and glucose-G6P cycling do not). Hence the fraction of plasma glucose derived from gluconeogenesis is given by H5/PW. If all plasma glucose was derived from gluconeogenesis, then the plasma glucose H5 enrichment level would be equal to that of PW. It would also necessarily mean that all HGP was derived from gluconeogenesis (i.e., H5/H2 = 1.0) and that all plasma glucose was derived from HGP since H5/H2 = 1.0, therefore H2 = PW (see Figure 4.1). From 15-60 minutes after the glucose load, gluconeogenesis was found to account for a minority (30-45%) of HGP.

4.3.4. Glucose and "recycled" glucose from the i.p. load

From the ^{13}C NMR analysis of plasma glucose ^{13}C-isotopomer levels, direct plasma glucose enrichment from the i.p. load, as determined from the enrichment of plasma [U-^{13}C]glucose, reached a peak at 30 min. At this point, 37% of total plasma and body glucose was accounted for by direct absorption from the load. At 60 min after the glucose load, direct absorption accounted for 34% of the load while HGP accounted for 55% of plasma glucose. The remaining 11% may represent the presence of a small amount of unlabeled glucose from before the load.

At 60 min post-load, "recycled" glucose accounted for 107 ± 35 μmol of total glucose and ~89% of the gluconeogenic HGP component. These data

suggest that during the i.p. glucose load, glucose recycling *via* the Cori cycle quantitatively accounts for almost all of the gluconeogenesis contribution to HGP. Thus, the glucose recycling fraction provides a good estimate of gluconeogenesis in this specific instance and in principle, would allow both the absorption and gluconeogenic contributions to plasma glucose levels to be determined from a single [U-^{13}C]glucose tracer.

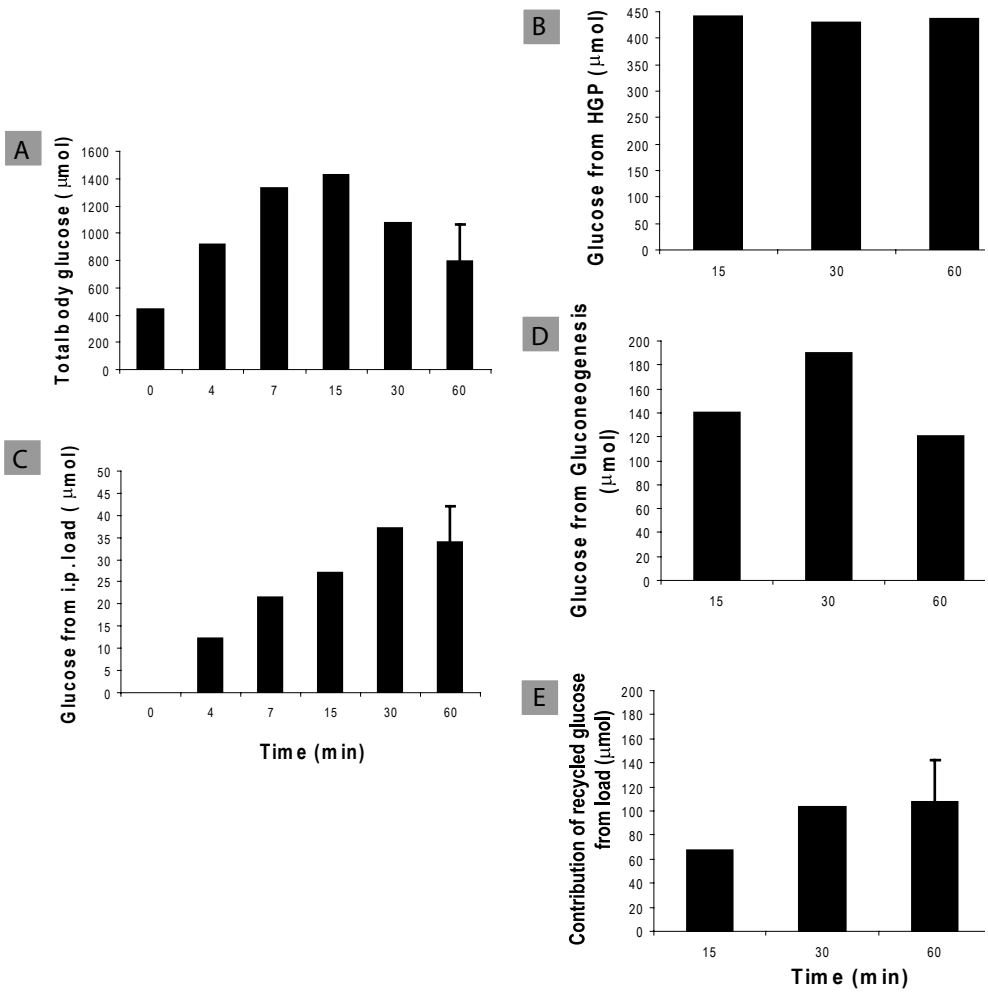

Figure 4.6. A. Total body glucose, B. glucose from HGP, C. glucose from the i.p. glucose load, D. glucose form gluconeogenesis and, E. recycled glucose from the load, in control animals at different times following the i.p. glucose load (1.5 mg/g body weight).

4.3.5. Effects of HF diet and CsA treatment in postprandial glucose metabolism

Postprandial metabolism of rats on a HF diet or CsA treatment for 20 days was further assessed during an i.p. glucose load test using ^{2}H and ^{13}C NMR spectroscopy following $^{2}H_2O$ and [U-^{13}C]glucose administration. Animals on a HF diet presented normal HGP, whereas CsA treated animals showed increased HGP and an increased contribution of the i.p. load to total glucose (Figure 4.7). Total body glucose and contributions from "recycled" glucose from load were not significantly altered in HF diet-fed and CsA-treated rats.

4.3.6. Hepatic glycogen synthesis

Hepatic glycogen content was assessed 60 min after the i.p. glucose load and found to account for 0.44 ± 0.13 mmol/g of liver wet weight in control animals. Hepatic glycogen content is not significantly altered in animals on a HF diet (0.37 ± 0.19 mmol/g liver wet weight) and CsA treatment (0.39 ± 0.09 mmol/g liver wet weight). Moreover, hepatic glycogen content was previously determined in healthy animals after 6-h fasting and found to account for 0.35 ± 0.10 mmol/g liver wet weight (Chapter 2). Thus, in 6-h fasted animals, hepatic glycogen content is not significantly altered after a glucose load which is in agreement with earlier studies (Smadja *et al.* 1988). Moreover, hepatic glycogen synthesis was quantified by measuring the incorporation of deuterium in hepatic glycogen and found to account only for ~2.5 % of total hepatic glycogen in control animals (~1 μmol/g liver during 60 min, data not shown). In these rats, indirect pathway contributed for ~64% of hepatic glycogen synthesis (data not shown).

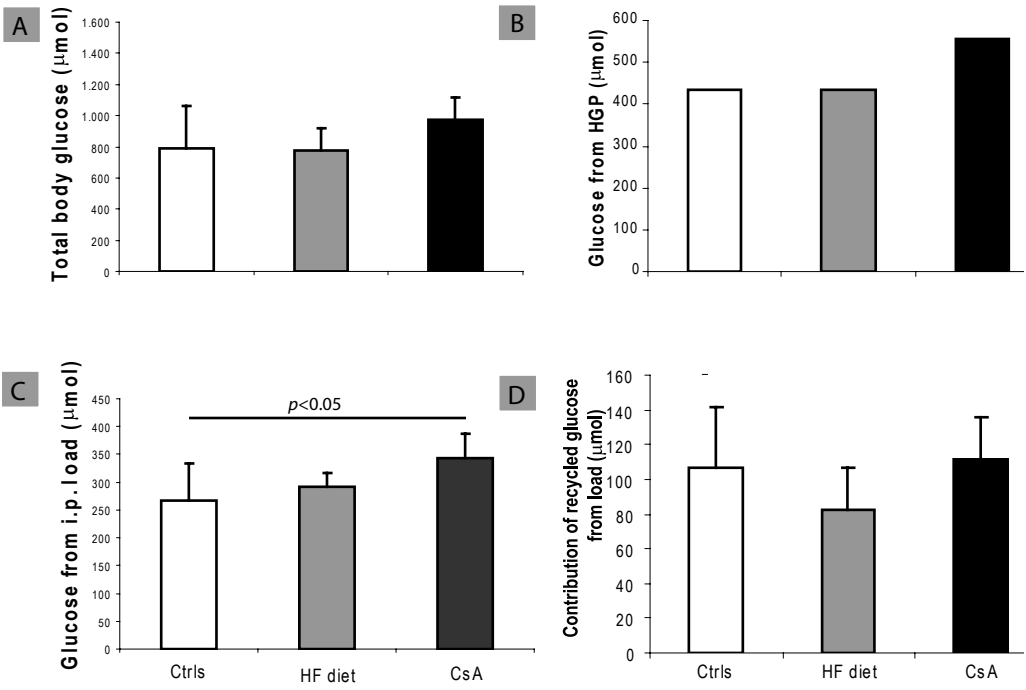

Figure 4.7. A. Total body glucose, B. glucose from HGP, C. glucose from the i.p. glucose load and, D. recycled glucose from the load 60 min after the i.p. glucose load (1.5 mg/g body weight) in animals on a HF diet, n=5 (grey) and CsA treatment, n=6 (black). $p<0.05$ is indicated as a result of comparison to healthy control animals group, n=8 (white).

4.4. Discussion

The disposition of an i.p. glucose load (1.5 mg glucose/g body weight) was assessed in 6-h fasted healthy control Sprague-Dawley rats. Contributions from HGP to total glucose, determined using ^2H_2O and ^2H NMR spectroscopy after the glucose load, were found to contribute substantially (~44% of the total glucose between 15-60 min after the load). Previously, HGP determined in 6-

h fasted control rats was found to be inhibited by 30% at 60 min following an oral glucose load of 2.4 mg/g body weight (Smadja *et al.* 1988), whereas in 24-h fasted rats HGP was not suppressed as a result of a glucose load (Smadja *et al.* 1990, Niewoehner *et al.* 1984). At 24 hours of fasting, the continuation of HGP in the presence of a glucose load may be an appropriate response to restore depleted carbohydrate stores in peripheral tissues.

To the extent that HGP as measured by the deuterated water method used in here includes contributions from glucose-G6P futile cycling, the true rates of HGP are overestimated. In hepatocytes, it was shown that futile cycling between glucose and G6P is extensive when glycogen content is elevated (i.e., fed animals) and relatively low in cells from starved rats (Katz *et al.* 1975). Considering that 6-h fasted animals demonstrated substantial G6Pase activity (as seen by the substantial contribution of HGP to whole body glucose) in the face of a large glucose load (which should stimulate glucokinase as a result of increased insulin levels), glucose-G6P cycling could be very active under these conditions and may contribute substantially to the estimated HGP.

Gluconeogenesis contribution to total glucose after a glucose load was determined by measuring the ratio of H5 to PW following administration of ^2H_2O and found to account for 30-45% of total glucose production. Previously, in 6-h fasted rats, gluconeogenesis was found to account for ~54% of HGP (Chapter 2). The observation that HGP sources are not drastically altered as a result of a glucose load is in agreement with previous studies where gluconeogenesis was found to account for ~80% of HGP in 24-h fasted rats, before (Jin *et al.* 2004) and after a glucose load (Jin *et al.* 2003). Moreover, the glucose-G6P cycling activity may also explain the relatively low gluconeogenic contribution (30-45%) to HGP that was measured.

Given the abundance of hepatic glycogen after 6 hours of fasting (~0.35 mmol/g liver wet weight) (Chapter 2) contributions from glycogenolysis to HGP cannot be ruled out. However, the fact that hepatic glycogen levels at 60 minutes

post-load were essentially equal to baseline levels indicates that there was no net loss or gain of hepatic glycogen as a result of the glucose load. In addition, ^{2}H incorporation into newly synthesized hepatic glycogen was residual implying that after a glucose load, hepatic glycogen synthesis is negligible in 6-h fasted rats. This is in agreement with a study by Smadja *et al.*, where liver glycogen concentration remained unchanged during the glucose load despite a normal capacity for glycogen synthesis (Smadja *et al.* 1988).

The contribution of plasma glucose from the i.p. load as estimated using ^{13}C NMR analysis following administration of [U-^{13}C]glucose was found to contribute ~34% for total glucose, 60 minutes after the glucose load. The reduced contribution of the load glucose in 6-h fasted rats most probably reflects a high initial glucose pool size and/or increased HGP. "Recycled" glucose from Cori cycle contribution was determined and found to be similar to the gluconeogenesis contribution to total glucose. Thus, lactate from "recycled" glucose through Cori cycle in peripheral tissues is probably the major gluconeogenic substrate following a glucose load (Niewoehner *et al.* 1984). The glucose recycling fraction provides a good estimate of gluconeogenesis and in principle allows both the absorption and gluconeogenic contributions to plasma glucose levels to be determined from a single [U-^{13}C]glucose tracer.

Finally, sources of total glucose after an i.p. glucose load were evaluated in animals on a HF diet for 20 days and with ongoing CsA treatment. Both groups of animals showed IGT relative to controls. HF diet did not promote impaired contribution from HGP and insulin secretion by pancreatic β-cells was not affected. Thus, the IGT of HF-fed animals can be attributed to decreased whole body glucose disposal secondary to peripheral insulin resistance rather than impaired HGP suppression. With CsA-treated animals the observed IGT was associated with a higher HGP contribution to plasma glucose levels, suggesting that in this model impaired HGP suppression was a significant component of IGT.

4.5. References

Allick G, van der Crabben SN, Ackermans MT, Endert E, Sauerwein HP. Measurement of gluconeogenesis by deuterated water: the effect of equilibration time and fasting period. Am J Physiol Endocrinol Metab 2006;290(6):E1212-E1217.

Baker N, Shipley RA, Clark RE, Incefy GE. C14 studies in carbohydrate metabolism: glucose pool size and rate of turnover in the normal rat. Am J Physiol - Legacy Content 1959;196(2):245-252.

Doyle ME, Egan JM. Pharmacological agents that directly modulate insulin secretion. Pharmacol Rev 2003;55(1):105-131.

Jin ES, Jones JG, Merritt M, Burgess SC, Malloy CR, Sherry AD. Glucose production, gluconeogenesis, and hepatic tricarboxylic acid cycle fluxes measured by nuclear magnetic resonance analysis of a single glucose derivative. Anal Biochem 2004;327(2):149-155.

Jin ES, Uyeda K, Kawaguchi T, Burgess SC, Malloy CR, Sherry AD. Increased hepatic fructose 2,6-bisphosphate after an oral glucose load does not affect gluconeogenesis. J Biol Chem 2003;278(31):28427-28433.

Jones JG, Solomon MA, Cole SM, Sherry AD, Malloy CR. An integrated H-2 and C-13 NMR study of gluconeogenesis and TCA cycle flux in humans. Am J Physiol Endocrinol Metab 2001;281(4):E848-E856.

Jones JG, Naidoo R, Sherry AD, Jeffrey FM, Cottam GL, Malloy CR. Measurement of gluconeogenesis and pyruvate recycling in the rat liver: a simple analysis of glucose and glutamate isotopomers during metabolism of [1,2,3-(13)C_3]propionate. FEBS Lett 1997;412(1):131-137.

Katz J, Wals PA, Golden S, Rognstad R. Recycling of glucose by rat hepatocytes. Eur J Biochem 1975;60(1):91-101.

Kraegen EW, James DE, Storlien LH, Burleigh KM, Chisholm DJ. *In vivo* insulin resistance in individual peripheral tissues of the high fat fed rat: assessment by euglycaemic clamp plus deoxyglucose administration. Diabetologia 1986;29(3):192-198.

Landau BR, Wahren J, Chandramouli V, Schumann WC, Ekberg K, Kalhan SC. Contributions of gluconeogenesis to glucose production in the fasted state. J Clin Invest 1996;98(2):378-385.

McArthur MD, You D, Klapstein K, Finegood DT. Glucose effectiveness is the major determinant of intravenous glucose tolerance in the rat. Am J Physiol Endocrinol Metab 1999;276(4):E739-E746.

Mazzoni G, Mazzoni P. Reversibility of graft rejection following a short cyclosporin-A administration 5 days after grafting. Microsurgery 1986;7(3):114-116.

Niewoehner CB, Gilboe DP, Nuttall FQ. Metabolic effects of oral glucose in the liver of fasted rats. Am J Physiol Endocrinol Metab 1984;246(1):E89-E94.

Perdigoto R, Rodrigues TB, Furtado AL, Porto A, Geraldes CFGC, Jones JG. Integration of [U-C-13]glucose and (H_2O)-H-2 for quantification of hepatic glucose production and gluconeogenesis. Nmr in Biomedicine 2003;16(4):189-198.

Petersen KF, Cline GW, Gerard DP, Magnusson I, Rothman DL, Shulman GI. Contribution of net hepatic glycogen synthesis to disposal of an oral glucose load in humans. Metabolism 2001;50(5):598-601.

Raman M, Radziuk J, Hetenyi G, Jr. Distribution and kinetics of glucose in rats analyzed by noncompartmental and compartmental analysis. Am J Physiol Endocrinol Metab 1990;259(2):E292-E303.

Rothman DL, Magnusson I, Katz LD, Shulman RG, Shulman GI. Quantitation of hepatic glycogenolysis and gluconeogenesis in fasting humans with ^{13}C NMR. Science 1991;254(5031):573-576.

Sena CM, Barosa C, Nunes E, Seica R, Jones JG. Sources of endogenous glucose production in the Goto-Kakizaki diabetic rat. Diabetes & Metabolism 2007;33(4):296-302.

Smadja C, Morin J, Ferre P, Girard J. Metabolic fate of a gastric glucose load in unrestrained rats bearing a portal vein catheter. Am J Physiol Endocrinol Metab 1988;254(4):E407-E413.

Smadja C, Morin J, Ferre P, Girard J. Initial glucose kinetics and hormonal response to a gastric glucose load in unrestrained post-absorptive and starved rats. Biochem J 1990;270(2):505-510.

Storlien LH, James DE, Burleigh KM, Chisholm DJ, Kraegen EW. Fat feeding causes widespread in vivo insulin resistance, decreased energy expenditure, and obesity in rats. Am J Physiol Endocrinol Metab 1986;251(5):E576-E583.

Zuurbier CJ, Keijzers PJM, Koeman A, Van Wezel HB, Hollmann MW. Anesthesia's effects on plasma glucose and insulin and cardiac hexokinase at similar hemodynamics and without major surgical stress in fed rats. Anesth Analg 2008;106(1):135-142.

Chapter 5

Hepatic glucose metabolism during glucose challenge in humans

5.1. Introduction

Hepatic glycogen metabolism is regulated by substrate and hormonal availability according to the nutritional conditions. In the fasting state, when plasma glucose levels are low, glycogen phosphorylase is activated and glycogen is converted to glucose *via* glucose-1-phosphate (G1P) and glucose-6-phosphate (G6P). The released glucose contributes substantially to hepatic and endogenous glucose production (EGP). Following ingestion of a meal and carbohydrate absorption, plasma glucose levels increase and promote the secretion of insulin by pancreatic β-cells. Insulin enhances glycogen synthesis from hepatic G6P primarily by activating glycogen synthase and inhibiting glycogen phosphorylase. The G6P used for hepatic glycogen synthesis is derived from two distinct pathways: direct conversion from glucose *via* glucokinase and indirect synthesis involving 3-carbon precursors (Newgard *et al.* 1983, Newgard *et al.* 1984) (Figure 5.1). The 3-carbon sources for the indirect pathway may originate from hepatic glycolysis of glucose as well as from non-glucose (gluconeogenic) precursors such as lactate, amino acids and glycerol. Direct and indirect pathway contributions to hepatic glycogen synthesis can be examined following ingestion of a tracer and analysis of plasma glucose and hepatic uridine diphosphate-glucose (UDP-glucose) enrichments.

In humans, when a xenobiotic agent (i.e., acetaminophen or peppermint oil) is provided, the enrichment distributions of hepatic UDP-glucose are also reflected in the respective urinary glucuronide conjugate (i.e., acetominophen or menthol glucuronide (Hellerstein *et al.* 1986, Landau *et al.* 1991, Ribeiro *et al.* 2005, Mendes *et al.* 2006)) since the glucose moiety of UDP-glucose is converted to glucuronide by a single dedicated pathway. To date, contributions of direct and indirect pathways to hepatic glycogen synthesis have been estimated using [1-^{13}C]glucose or deuterated water ($^{2}H_2O$) in conjunction with acetaminophen. With these methods, the indirect pathway was found to contribute substantially

(30-50 %) to hepatic glycogen synthesis in healthy subjects following a mixed meal (Taylor *et al.* 1996, Bischof *et al.* 2002, Jones *et al.* 2006) or a glucose load (Napoli *et al.* 1992, Petersen *et al.* 2001).

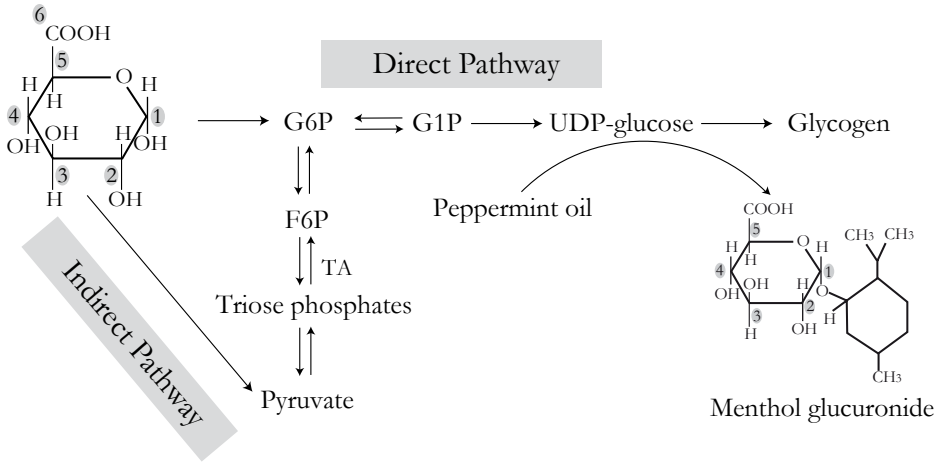

Figure 5.1. Hepatic glycogen synthesis metabolism and sampling by menthol glucuronide after a meal. G6P. glucose-6-phosphate; F6P. fructose-6-phosphate; G1P. glucose-1-phosphate; UDP-glucose. uridine diphosphate-glucose. TA. Transaldolase.

The oral glucose tolerance test (OGTT) is a widely used test for whole body glucose clearance and represents a significant substrate challenge to the liver. Surprisingly, given the pivotal role of the liver in splanchnic glucose metabolism, there have been few studies to date on the role and mechanism of hepatic glucose disposal in this setting. Therefore, the goal of this study was to evaluate direct and indirect pathway contributions to hepatic glycogen synthesis in healthy volunteers during an OGTT. Direct and indirect pathway contributions were estimated by carbon 13 (^{13}C) Nuclear Magnetic Resonance (NMR) analysis of plasma glucose and urinary menthol glucuronide excess enrichments following ingestion of peppermint oil and an oral glucose load enriched with a stable isotope tracer. Compared to the rather laborious purification and derivatization methods required for analysis of acetominophen glucuronide (Magnusson *et al.*

1987, Burgess *et al.* 2003), menthol glucuronide can be directly analyzed by NMR spectroscopy after a simple isolation protocol (Ribeiro *et al.* 2005, Mendes *et al.* 2006).

A variety of carbon and hydrogen tracers can be used to follow the metabolism of glucose to hepatic UDP-glucose (Napoli *et al.* 1992, Jones *et al.* 2006), with [1-^{13}C]glucose being the most widely used at this time (Hwang *et al.* 1995, Petersen *et al.* 2001). The main disadvantages of [1-^{13}C]glucose are that: 1) a relatively large amount (~10 grams) is required to generate sufficient excess enrichment of the UDP-glucose and glucuronide pools so that glucuronide ^{13}C-enrichment can be reliably quantified above the background 1.11% ^{13}C-enrichment level and 2) the effects of glucose recycling on glucose and glucuronide ^{13}C-enrichments have to be accounted for since [1-^{13}C]glucose metabolism *via* the Cori cycle can produce [1-^{13}C]glucuronide and regenerate [1-^{13}C]glucose.

Therefore, the use of two tracers that effectively eliminate background effects and are non-recyclable were focused in here. With the first tracer, [U-^{13}C]glucose, the background ^{13}C-contribution becomes negligible due to the tiny probability (0.0116) of a naturally-occurring glucose molecule containing six ^{13}C-atoms. The [U-^{13}C]glucose precursor and [U-^{13}C]glucuronide product generate resolvable signals in the ^{13}C spectrum allowing direct quantification by ^{13}C NMR (Hwang *et al.* 1995, Mendes *et al.* 2006) and whole body glucose recycling does not regenerate significant levels of [U-^{13}C]glucose. Moreover, this tracer is already widely used in plasma kinetic studies of glucose disposal and is less expensive than [1-^{13}C]glucose. The second tracer, [U-$^{2}H_{7}$]glucose, has the advantage of a low background level of deuterium (^{2}H) (0.015%). Since some of the deuterium labels are removed during the conversion of [U-$^{2}H_{7}$]glucose to glucuronide, each ^{2}H-enrichment site has to be independently monitored during this metabolic sequence. This can be achieved by ^{2}H NMR as the ^{2}H-enrichments of both glucose (in the form of monoacetone glucose (MAG)) and glucuronide are fully resolved in their respective ^{2}H NMR spectra. The ^{2}H-enrichment in position 3

can be considered to be non-recyclable since it is quantitatively removed during glycolysis. Finally, since the presence of [U-$^{2}H_{7}$]glucose does not interfere with the NMR analysis of [U-^{13}C]glucose metabolism or *vice versa*, enrichment from both tracers can be analyzed from a common blood or urine sample and therefore studied in the same experiment.

5.2. Materials and methods

5.2.1. Human Studies

Six lean healthy volunteers (4 men and 2 women; age 47 ± 10 years; body mass index 26 ± 4 kg/m^{2}) without known endocrine-metabolic pathology were studied. The study protocol was approved by the University Hospital of Coimbra Ethics Committee and was performed in accordance with the ethical standards laid down in the Helsinki Declaration. Subjects were studied in the Department of Endocrinology, Metabolism and Diabetes in the University Hospital of Coimbra after obtained informed consent.

5.2.2. Oral glucose tolerance test (OGTT)

Fasting was started at 20:00 h (24-h clock) of the previous evening after a normal dinner meal. At 8:30 h of the following day, blood was withdrawn for standard biochemical analysis, and subjects were asked to ingest 200 mg of peppermint oil. At 9:30 h, a 75 g glucose load, enriched with 6.7% [U-^{13}C]glucose and 3.3% [U-$^{2}H_{7}$]glucose was provided to each subject. At 10:30 h, a second dose of 200 mg peppermint oil was given to the healthy volunteers. Blood samples were collected at 11:30 and 12:30 h. Finally, urine samples from 11:30 to 13:30 h were collected and kept frozen until further treatment. Plasma glucose and insulin levels were assessed each 30 min for 3 hours after the glucose load for assessment of glucose tolerance (Figure 5.2).

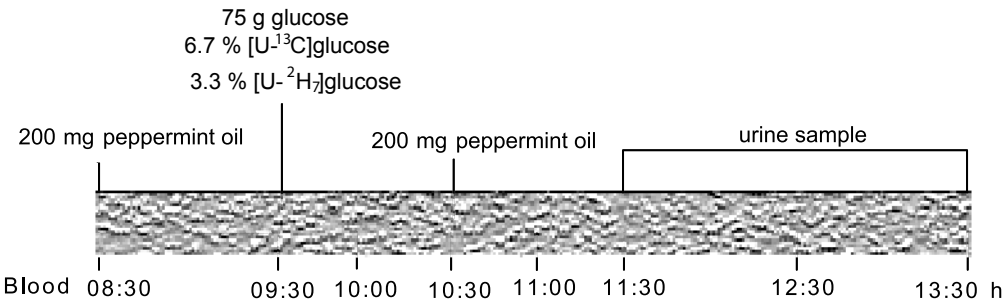

Figure 5.2. Oral glucose tolerance test (OGTT) protocol design. Overnight fasted healthy subjects were given a glucose challenge (75 g glucose enriched with 6.7% [U-^{13}C]glucose and 3.3% [U-$^{2}H_7$]glucose).

5.2.3. Biochemical analysis

Fasting plasma glucose, insulin, C peptide, cholesterol, high-density lipoprotein (HDL) cholesterol, low-density lipoprotein (LDL) cholesterol, triglycerides and glycosylated hemoglobin levels, were analyzed at the laboratories of the University Hospital of Coimbra.

5.2.4. Sample processing

5.2.4.1. Urine samples

Urine samples were concentrated by evaporation reducing to a final volume of 10-20 mL, and the pH of the supernatant adjusted to 1.5 after centrifugation. Samples were eluted with ether in a solid phase extraction column. After evaporation to dryness, the extracted menthol glucuronide was further purified by preparative High Performance Liquid Chromatography (HPLC).

5.2.4.2. Blood samples

Blood that was collected at 2 and 3 h after the glucose load, was immediately deproteinized with an equal volume of 0.3 N $ZnSO_4$ and neutralized with twice

the volume of 0.3 N $Ba(OH)_2$. After centrifugation at 13,000 *g* at 4ºC, the plasma supernatant was further purified by anionic-cationic exchange chromatography and evaporated to dryness. The conversion of isolated plasma glucose to monoacetone glucose (MAG) was performed according to the literature (Jones *et al.* 2001). A mixture of 0.5 mL acetone/mL original plasma and concentrated anhydrous H_2SO_4 (40 μL/mL acetone) was added to the sample and stirred vigorously for 4 h. Afterwards, samples were hydrolyzed by incubation at 40ºC and pH 2.2-2.3 for 5 h. After pH neutralization, the solution was evaporated to dryness. MAG was further extracted from the dry residue with boiling ethyl acetate, followed by removal of insoluble salts by centrifugation, and evaporation of ethyl acetate. MAG molecules show the same labeling patterns as plasma glucose but with completely resolved ^{2}H and ^{13}C NMR signals.

5.2.5. Nuclear Magnetic Resonance (NMR) spectroscopy

5.2.5.1. ^{13}C NMR spectroscopy

Samples were dissolved in deuterated acetonitrile for ^{13}C NMR analysis. Proton (^{1}H)-decoupled ^{13}C NMR spectra were obtained using a Varian 14.1 Tesla (T) system (Varian Instruments, Palo Alto, CA, USA). Spectra were acquired at 25ºC using a 90º pulse and a 2.5 s acquisition time.

5.2.5.2. ^{2}H NMR spectroscopy

^{2}H NMR spectra were acquired with a Varian 14.1 T spectrometer (Varian Instruments, Palo Alto, CA, USA). Samples were dissolved in acetonitrile and shimming was performed on selected ^{1}H resonances. ^{1}H-decoupled ^{2}H NMR spectra were acquired without field-frequency lock at 50ºC using a 90º pulse, a 1.6 second acquisition time with a pulse delay (D_1) of 0.1 second. Since these conditions resulted in the partial saturation of the internal ^{2}H-enrichment pyrazine standard (T_1 ~0.7 seconds), standard samples of MAG and menthol glucuronide

containing the pyrazine standard were acquired under ambient conditions and under non-saturating conditions (D_1=5 and 15 seconds). By comparing the ratio of pyrazine to analyte signals under both acquisition conditions, a correction factor for partial saturation was obtained.

5.2.5.3. NMR Analysis

NMR spectra were analyzed using the curve-fitting routine supplied with the NUTS PC-based NMR spectral analysis program (Acorn NMR Inc., Fremont CA). ^{13}C-enrichments were quantified relative to the natural abundance signals (1.11%) whereas ^{2}H-enrichments were determined by comparison to an internal pyrazine ^{2}H-enrichment standard after correction for relaxation time (T_1).

5.2.6. Quantification of direct and indirect pathway contributions to glycogen synthesis with [U-^{13}C]glucose and [U-$^{2}H_7$]glucose

After ingestion of [U-^{13}C]glucose, [U-^{13}C]glucuronide is formed by direct pathway whereas by indirect pathway, the [U-^{13}C]glucose carbon skeleton is broken and there is further dilution by unlabeled gluconeogenic precursors. Thus, the probability of forming [U-^{13}C]glucuronide isotopomers by indirect pathway is negligible (Schwenk *et al.* 1996). Hence, quantification of the fractional ^{13}C-enrichment of [U-^{13}C]glucuronide divided by the ^{13}C-enrichment of the plasma [U-^{13}C]glucose precursor provides an estimate of the direct pathway contribution to hepatic glycogen synthesis (Eq. 5.1).

$$\text{Direct pathway} = \frac{\text{fractional enrichment of [U-}^{13}\text{C]glucuronide}}{\text{fractional enrichment of [U-}^{13}\text{C]glucose}} \times 100 \ (\%) \qquad \textit{[Eq. 5.1]}$$

$$\text{Indirect pathway} = 100 - \text{direct pathway} \quad (\%) \qquad \textit{[Eq. 5.2]}$$

When [U-$^2H_7$]glucose is metabolized through the indirect pathway, the ^2H-label in position 3 is assumed to be quantitatively removed following conversion of [U-$^2H_7$]glucose-6-phosphate to triose phosphates and pyruvate, hence, UDP-glucose or glucuronide that is subsequently synthesized *via* indirect pathway is not enriched with ^2H in this position. Meanwhile, direct pathway metabolism of [U-$^2H_7$]glucose and the involvement of the hexose phosphate intermediates in exchange reactions does not remove the ^2H-enrichment of position 3 (H3). Therefore, the direct pathway contribution can be estimated as the ratio of glucuronide and plasma glucose H3 enrichment (Eq. 5.3).

$$\text{Direct pathway} = \frac{\text{Glucuronide H3}}{\text{Glucose H3}} \times 100 \ (\%) \qquad \textit{[Eq. 5.3]}$$

$$\text{Indirect pathway} = 100 - \text{direct pathway} \ (\%) \qquad \textit{[Eq. 5.4]}$$

5.2.7. Quantification of transaldolase exchange activity from analysis of [U-$^2H_7$]gluronide enrichment from [U-$^2H_7$]glucose

Transaldolase (TA) catalyzes the exchange of the 456 carbon fragment of fructose-6-phosphate (F6P) and glyceraldehyde-3-phosphate (G3P). Thus, TA exchange activity results in a loss of ^2H-enrichment in position 5 relative to positions 3 hence the ratio of ^2H-enrichment in position 5 relative to position 3 (H5/H3) of menthol glucuronide reflects the fraction of direct pathway flux that participated in TA exchange (Eq. 5.5).

$$\text{Percent direct pathway flux involved in TA exchange} = [1-(H5/H3)] \times 100 \ (\%) \qquad \textit{[Eq. 5.5]}$$

5.2.8. Correcting the direct pathway estimates derived from [U-^{13}C] glucose for transaldolase exchange

The direct pathway contribution to hepatic glycogen synthesis as estimated with [U-^{13}C]glucose (Eq. 5.1) was corrected for TA exchange activity as derived from the [U-$^{2}H_{7}$]glucose tracer (Eq. 5.5) as follows:

Corrected direct pathway =
direct pathway contribution + [(direct pathway contribution × TA exchange)/100] (%)
[Eq. 5.6]

Corrected indirect pathway = 100 – corrected direct pathway (%) *[Eq. 5.7]*

Exchanges of the hydrogen moieties during the direct pathway metabolism of glucose will be further revealed and quantified in the Discussion section.

5.3. Results

5.3.1. Plasma metabolite and hormone levels

Table 5.1 summarizes plasma metabolite and hormone levels of the subjects studied. All subjects presented normal fasting blood glucose levels and normal glycosylated haemoglobin, indicative of long-term normoglycemia. After a glucose challenge, all subjects show normal glucose tolerance, as indicated by plasma glucose levels of less than 11.1 mM at 2 h post- load. Plasma glucose and insulin profiles during the OGTT are shown in Figure 5.3.

TABLE 5.1: Plasma metabolite and hormone levels [#].

Patients	JJ	CB	RC	MC	CN	AT	Average ± SD
Fasting glucose, mM	5.6	4.8	5.2	4.3	5.4	4.6	5.0 ± 0.5
C peptide, nM	2.3	2.7	2.3	1.8	4.2	2.4	2.6 ± 0.8
Glycosylated hemoglobin, %	5.3	5.4	5.5	5.5	5.5	5.2	5.4 ± 0.1
Cholesterol, mg/dL	182	234	163	220	181	-	196 ± 30
HDL Cholesterol, mg/dL	61	86	51	65	60	29	59 ± 19
LDL Cholesterol, mg/dL	114	141	116	151	125	186	139 ± 27
Triglycerides, mg/dL	92	177	106	102	122	-	120 ± 34

[#]Average values ± standard deviation (SD) are shown. (–) Not determined.

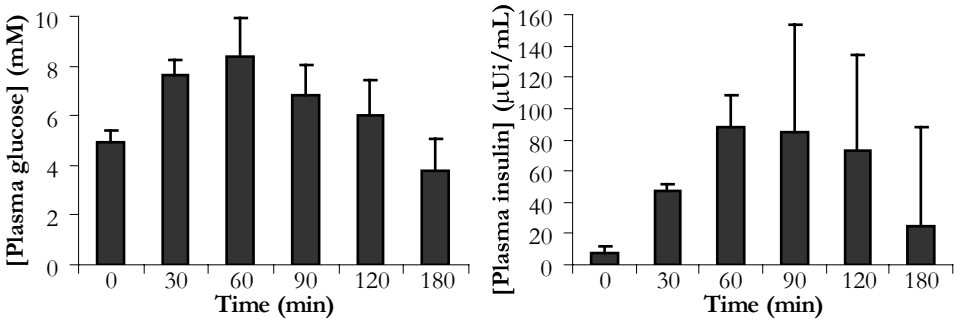

Figure 5.3. Plasma glucose and insulin profiles during OGTT. Values are shown as mean ± SD.

5.3.2. Enrichment patterns of plasma glucose and urinary glucuronide from [U-^{13}C]glucose and [U-$^{2}H_{7}$]glucose

^{13}C NMR spectra of MAG derivatized from plasma glucose (Figure 5.4) and of purified urinary menthol glucuronide (Figure 5.5) generated well-resolved ^{13}C-signals. Plasma glucose and urinary menthol glucuronide ^{13}C resonances consist of singlet signals, mostly derived from natural abundance ^{13}C (1.11%), and the ^{13}C-^{13}C spin-spin coupled multiplets. In the C1 resonance of MAG, [U-^{13}C]glucose is detected as a doublet of doublets arising from the splitting due to

coupling between positions 1 and 2, and 1 and 5 of MAG (Perdigoto *et al.* 2003). Plasma [U-^{13}C]glucose enrichments attained relatively constant levels; reaching the glucose load enrichment, at 2 and 3 hours after the load (7.0% ± 0.4% and 6.5% ± 0.4%, respectively) (Table 5.2). This indicates that the bulk of plasma glucose (~90%) was derived from the load with minimal dilution from EGP.

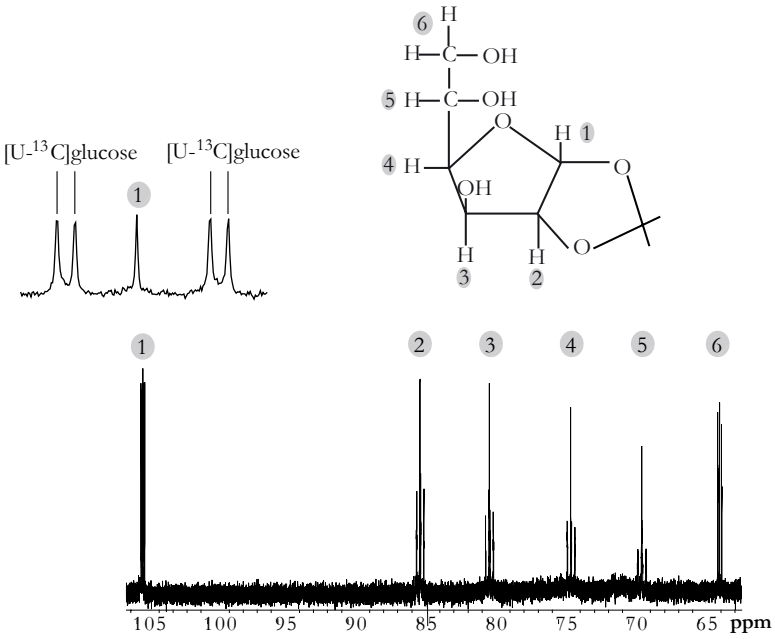

Figure 5.4. ^{13}C NMR spectrum of monoacetone glucose (MAG) derived from plasma glucose collected 3 h post-load. ^{13}C NMR signals from carbons 1-6 of MAG are indicated. In the inset, C1 signals are expanded and the singlet corresponding to the natural abundance and the isotopomers resultant of [U-^{13}C]glucose are observed.

In the ^{13}C NMR spectrum of menthol glucuronide, the multiplets observed represent a mixture of glucuronide ^{13}C isotopomers derived from hepatic metabolism of [U-^{13}C]glucose. In carbon 1 of menthol glucuronide, [U-^{13}C]glucuronide corresponds to the quartet arising from coupling between carbons 1 and carbons 2, 3 and 6 ($J_{1,2}$= 47.6 Hz, $J_{1,3}$= 4.7 Hz, and $J_{1,6}$= 5.5 Hz

(Mendes *et al.* 2006)). [U-^{13}C]glucuronide enrichment from 2-4 h after the glucose load was 2.5% ± 0.8%. Using Equation 5.1, the direct pathway contribution to hepatic glycogen synthesis was found to account for only 36% ± 12% of hepatic glycogen synthesis.

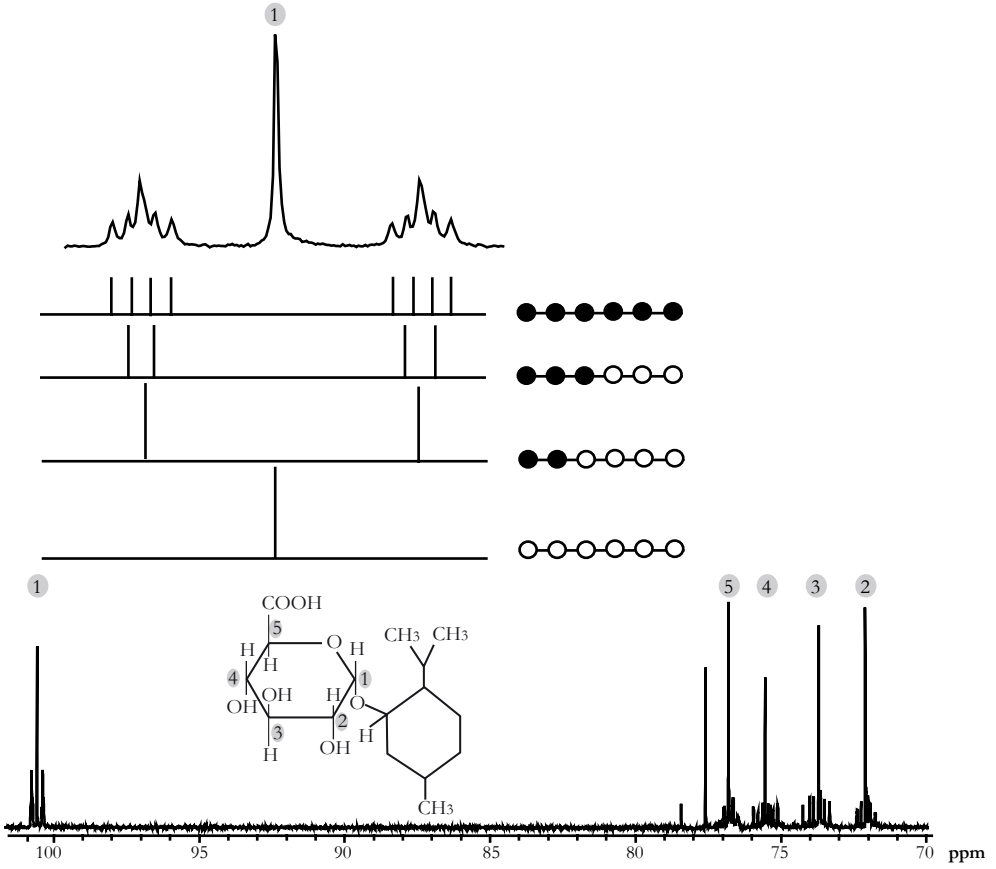

Figure 5.5. ^{13}C NMR spectrum of urinary menthol glucuronide collected 2-4 h post-load. ^{13}C NMR signals from carbons 1-5 of menthol glucuronide are indicated. In the inset, C1 signals are expanded and the isotopomers resultant of hepatic glucose metabolism assigned.

^{2}H NMR analysis of glucose enrichment from [U-$^{2}H_{7}$]glucose present in the load revealed that the plasma glucose H3 enrichment was ~80% that of the precursor oral glucose load indicating that the majority of plasma glucose was derived from the load and resembling the enrichment pattern observed with [U-^{13}C]glucose (Figure 5.6). While the dilution of both tracers after ingestion was relatively small, the extent of [U-$^{2}H_{7}$]glucose dilution was slightly, but systematically higher compared to [U-^{13}C]glucose. This is most likely the result of the different methodologies used to determine the ^{13}C and ^{2}H-enrichment levels from the NMR spectra. As shown in Table 5.2, glucuronide H3 enrichment was only about half that of plasma glucose, consistent with a significant amount of dilution by unlabeled hexoses derived *via* indirect pathway flux. From analysis of the glucose and glucuronide H3 enrichment ratios (Eqs. 5.3 and 5.4) the indirect pathway was estimated to contribute about half of the total glycogen synthesis flux. This estimate tended to be lower and closer to literature values of 30-50% (Napoli *et al.* 1992, Petersen *et al.* 2001) compared to the 64% derived from [U-^{13}C]glucose. Due to the large inter-individual variations in direct pathway estimates obtained with both methods, the differences in estimates were not statistically significant for this group of subjects.

While the ^{2}H-enrichment levels of plasma glucose were relatively constant across all seven positions, enrichment of the glucuronide hydrogens showed marked variations in ^{2}H-enrichment levels. During the conversion of UDP-glucose to glucuronide, the position 6 hydrogens are removed through the oxidation of carbon 6. Removal of ^{2}H from the remaining positions can be attributed to hexose phosphate exchanges that occur during the conversion of glucose to UDP-glucose. There are three main exchange reactions that can remove ^{2}H during direct pathway conversion of [U-$^{2}H_{7}$]glucose to glycogen. Firstly, G6P-F6P exchange catalyzed by G6P-isomerase results in the loss of ^{2}H at position 2 (Landau *et al.* 1991). Secondly, G6P-F6P- mannose-6-phosphate (M6P) exchange catalyzed by G6P and M6P-isomerases results in the loss of ^{2}H

at position 1 (Chandramouli *et al.* 1999), and thirdly, exchange of F6P carbons 4, 5 and 6 with those of glyceraldehyde-3-phosphate *via* TA results in the loss of ^{2}H at positions 4, 5 and 6 (Jones *et al.* 2008). Therefore, with the exception of position 3, these exchanges deplete ^{2}H from all other positions of G6P and the extent of each exchange activity can be estimated by comparing the ^{2}H-enrichment levels of the exchangeable hydrogen with that of position 3.

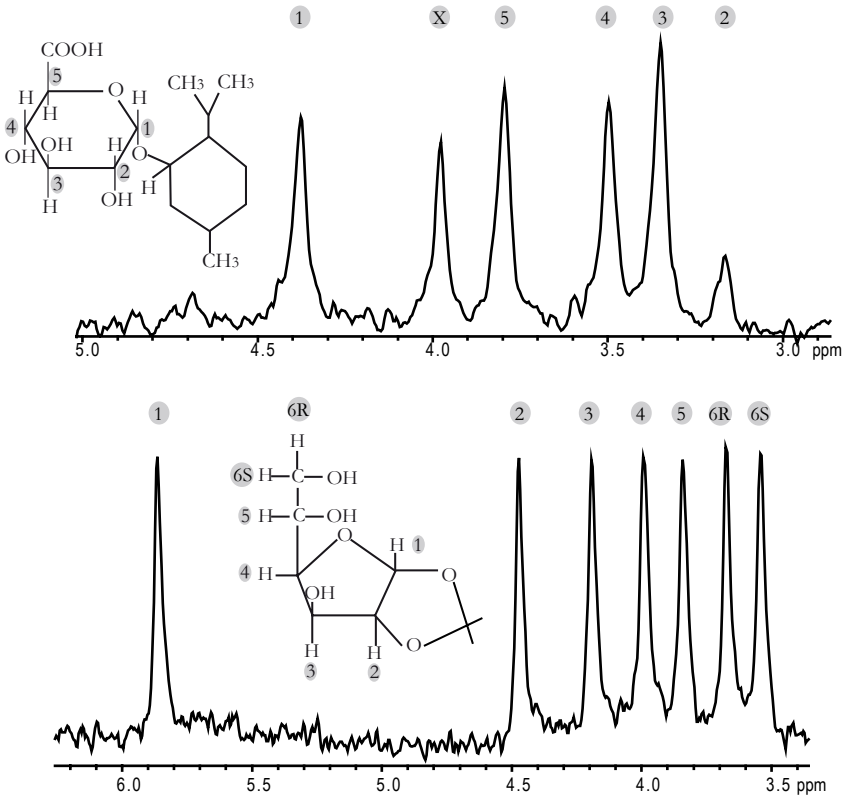

Figure 5.6. ^{2}H NMR spectra of monoacetone glucose (MAG) derived from plasma glucose collected post-load (bottom) and from menthol glucuronide collected 2-4 h post-load (upper). ^{2}H NMR signals from protons 1-6 of MAG and 1 to 5 of menthol glucuronide are indicated.

TABLE 5.2: Direct and indirect pathway contributions to hepatic glycogen synthesis[#].

Subjects	JJ	CB	RC	MC	CN	AT	Average ± SD
Plasma [U-^{13}C]glucose enrichment (2h post-load), %	7.5	6.9	7.5	6.5	6.7	6.6	7.0 ± 0.4
Plasma [U-^{13}C]glucose enrichment (3h post-load), %	6.9	6.8	6.3	6.7	5.9	-	6.5 ± 0.4
Urinary [U-^{13}C]glucuronide enrichment, %	1.2	2.7	3.5	3.0	2.4	1.9	2.5 ± 0.8
Direct pathway, %	17	51	37	46	38	29	36 ± 12
Indirect pathway, %	83	49	63	54	62	71	64 ± 12
Plasma [3-^{2}H]glucose enrichment (2h post-load), %	2.5	3.2	2.8	2.1	2.7	3.7	2.8 ± 0.6
Plasma glucose [3-^{2}H]enrichment (3h post-load), %	3.2	2.4	2.0	1.8	2.9	-	2.5 ± 0.6
Urinary glucuronide [3-^{2}H]enrichment, %	1.1	1.8	1.3	1.3	1.4	1.1	1.3 ± 0.3
Direct pathway, %	40	63	54	67	48	29	50 ± 14
Indirect pathway, %	60	37	46	33	52	71	50 ± 14

[#] Integral areas of the ^{13}C and ^{2}H-signals from monoacetone glucose (MAG) and urinary menthol glucuronide were calculated from the respective ^{13}C and ^{2}H NMR spectra. Average values of plasma [U-^{13}C]glucose and [3-^{2}H]glucose enrichment for 2 and 3 h post-load were used for direct and indirect pathway quantification. (-) Not determined.

The vestigial signal at position 2, corresponding to an average excess ^{2}H-enrichment level of 0.13% is consistent with the extensive loss of ^{2}H from this position by exchange of G6P and F6P *via* G6P-isomerase (Landau *et al.* 1991). The position 2 to position 3 enrichment ratio was 0.10 ± 0.06 indicating that exchange of hydrogen 2 with that of body water was ~90%. Average enrichment levels of position 1 (0.96% ± 0.30%) are consistently inferior to enrichments in position 3 (1.25% ± 0.28%) most probably due to G6P-M6P isomerization (Chandramouli *et al.* 1999). The position 1 to position 3 enrichment ratio was

0.76 ± 0.18 indicating that exchange of hydrogen 1 with that of body water *via* M6P was ~24%. Finally, enrichment levels of both 4 and 5 positions of glucuronide were also systematically lower than that of hydrogen 3, consistent with TA exchange activity. From the ^{2}H NMR analysis of the H5/H3 menthol glucuronide ^{2}H-enrichments (see Equation 5.5), 21% ± 10% of the direct pathway flux participated in TA exchange.

5.4. Discussion

5.4.1. Sources of hepatic glycogen synthesis during OGTT: comparison with previously published studies

Direct and indirect pathway contributions to hepatic glycogen synthesis were evaluated during an OGTT in healthy subjects following ingestion of two different tracers incorporated in the load, [U-^{13}C]glucose and [U-$^{2}H_{7}$]glucose, and peppermint oil for the chemical biopsy of hepatic UDP-glucose as urinary menthol glucuronide. Direct and indirect pathway contributions were then estimated from the dilution of the enrichment between plasma glucose and UDP-glucose. Various exchange reactions at the level of hepatic G6P can modify the enrichment of glucuronide independently of direct and indirect pathway fluxes and therefore may significantly add to the uncertainty of the measurement. Since these exchanges involve specific G6P carbons and/or hydrogens, their effects can in principle be corrected for, or even avoided, by choosing the appropriate labeled glucose precursor. To unravel the extent and effects of these exchanges, the application of ^{2}H NMR to monitor the conversion of [U-$^{2}H_{7}$]glucose to glucuronide represents a significant advance since the fate of each individual deuterium label of glucose can be monitored in a single measurement.

Since the position 3 deuterium of glucose is the only label that is unaffected by exchange reactions involving hepatic hexose phosphates, direct and indirect pathway contributions were determined through the dilution of

^{2}H-enrichment in this position during the conversion of [U-$^{2}H_{7}$]glucose to glucuronide. This analysis revealed an indirect pathway contribution of ~50%, an unexpectedly high contribution considering that the preceding "meal" was 100% glucose.

Previously, Petersen *et al.* reported an indirect pathway contribution of 36-38% to glycogen synthesis during an OGTT using [1-^{13}C]glucose and acetaminophen (Petersen *et al.* 2001). Apart from methodological differences, including the different analysis technique used (i.e. NMR *vs.* Gas-Chromatography-Mass Spectrometry (GC-MS), the different biopsy agent used (i.e., peppermint oil *vs.* acetominophen), use of a different tracer (i.e., [U-$^{2}H_{7}$]glucose and [U-^{13}C[glucose *vs.* [1-^{13}C]glucose), the glucose load was significantly different in both studies (i.e., 75 g *vs.* 98 g). Moreover, the plasma glucose levels attained after the glucose load in the study by Petersen *et al.* are relatively lower than the ones reported in here (~7.5 mM at 30 min *vs.* 8.4 mM at 60 min) probably reflecting healthier controls. The relative contributions of direct and indirect pathways to hepatic glycogen synthesis are dependent on plasma glucose concentrations and emphasize the predominance of the indirect pathway of glycogen synthesis for higher values of plasma glucose (Lang *et al.* 1986). Thus, it is speculated that the different estimated values for indirect pathway contribution are probably due to lower plasma glucose levels attained by the subjects used by Petersen *et al.*.

In any event, given that the liver only extracts ~20% of splanchnic glucose while the majority is taken up and metabolized by peripheral tissues, notably skeletal muscle, it is hypothesized that the Cori cycle is the major contributor to indirect pathway flux following OGTT, as a result of peripheral tissue glycolysis of the majority (~80%) of the glucose load. This activity is consistent with the reported increase of blood lactate concentrations during OGTT in healthy subjects (Prando *et al.* 1988).

5.4.2. Carbon exchanges during the direct pathway metabolism of glucose to glycogen and their effect on direct and indirect pathway estimates using [U-^{13}C]glucose

[U-^{13}C]glucose is a potentially highly informative tracer of hepatic metabolism since unlike hydrogen tracers, the ^{13}C-label can be followed through the glycolytic pathway and into the acetyl-CoA and tricarboxylic acids (TCA) cycle pools. In humans, these can be noninvasively interrogated alongside the hepatic UDP-glucose pool by providing phenylacetate or phenylbutyrate to bind and sample hepatic glutamine as urinary phenyalcetylglutamine (PAGN) (Cline *et al.* 1994). While beyond the scope of this Thesis, ^{13}C NMR analysis of PAGN obtained from these experiments revealed measurable levels of ^{13}C-enrichment and therefore the potential for interrogating hepatic acetyl-CoA and TCA cycle fluxes and integrating this information with that of hepatic glycogen synthesis (data not shown).

Estimates of indirect pathway contribution derived from the analysis of [U-^{13}C]glucose were found to be systematically higher compared to those derived from the analysis of [3-^{2}H]glucose dilution following its conversion to [3-^{2}H]glucuronide. This difference may in part be accounted for by TA exchange. Since TA exchange involves the transfer of hexose carbon as well as hydrogen moieties, TA activity can modify the enrichment of [U-^{13}C]hexose phosphates and UDP-glucose independently of direct and indirect pathway fluxes. Specifically, [U-^{13}C]glucose that is metabolized *via* the direct pathway is converted to [1,2,3-$^{13}C_3$]glucose as a result of TA exchange. Therefore, to the extent that TA exchange is active, the enrichment level of the [U-^{13}C]glucuronide product is reduced hence the direct pathway contribution is underestimated, while the indirect pathway fraction is correspondingly overestimated. From the ^{2}H-enrichment analyses, it was estimated that 21% ± 10% of direct pathway flux participated in TA exchange. Therefore, as a result of TA exchange activity, the direct pathway contribution reported by [U-^{13}C]glucose is underestimated by

~20% while the indirect pathway contribution is correspondingly overestimated. After correcting for this level of TA exchange, (Eqs. 5.6 and 5.7) direct pathway estimates of 44% ± 14% and indirect pathway contributions of 56% ± 14% were obtained from the [U-^{13}C]glucose tracer analysis. These values correlate well with the 50% ± 14% estimate obtained from the [3-^{2}H]glucose/glucuronide analysis.

In summary, novel ^{13}C and ^{2}H glucose tracers were used to determine direct and indirect pathway contributions to hepatic glycogen synthesis during OGTT by NMR analysis of plasma glucose and urinary glucuronide enrichments. Exchanges of both carbon and hydrogen moieties during the direct pathway metabolism of glucose were further revealed and quantified. Enrichment of glucuronide from any glucose tracer that is enriched in carbons 4, 5 and 6 (including [U-^{13}C]glucose) will be modified by TA exchange in addition to direct and indirect pathway fluxes. During OGTT, ~20 % of direct pathway flux was involved in this exchange hence the values derived from the [U-^{13}C]glucose tracer resulted in underestimates of the direct pathway contribution. For glucose enriched with ^{2}H, the position 3 label is unaffected by hexose phosphate exchanges hence direct pathway estimates based on [3-^{2}H]glucose/glucuronide enrichment ratios are insensitive to TA exchange and therefore reflect true direct/indirect pathway fluxes. As conclusions, the results presented in here demonstrate that during an OGTT in healthy humans, half of hepatic glycogen synthesis is derived from 3-carbon precursors rather than directly from the glucose load.

5.5. References

Bischof MG, Bernroider E, Krssak M, Krebs M, Stingl H, Nowotny P, Yu C, Shulman GI, Waldhausl W, Roden M. Hepatic glycogen metabolism in type 1 diabetes after long-term near normoglycemia. Diabetes 2002;51(1):49-54.

Burgess SC, Weis B, Jones JG, Smith E, Merritt ME, Margolis D, Sherry AD, Malloy CR. Noninvasive evaluation of liver metabolism by H-2 and C-13 NMR isotopomer analysis of human urine. Anal Biochem 2003;312(2):228-234.

Chandramouli V, Ekberg K, Schumann WC, Wahren J, Landau BR. Origins of the hydrogen bound to carbon 1 of glucose in fasting: significance in gluconeogenesis quantitation. Am J Physiol Endocrinol Metab 1999;277(4):E717-E723.

Cline GW, Rothman DL, Magnusson I, Katz LD, Shulman GI. ^{13}C-nuclear magnetic resonance spectroscopy studies of hepatic glucose metabolism in normal subjects and subjects with insulin-dependent diabetes *mellitus*. J Clin Invest 1994;94(6):2369-2376.

Hellerstein MK, Greenblatt DJ, Munro HN. Glycoconjugates as noninvasive probes of intrahepatic metabolism: Pathways of glucose entry into compartmentalized hepatic UDP-glucose pools during glycogen accumulation. PNAS 1986;83(18):7044-7048.

Hwang JH, Perseghin G, Rothman DL, Cline GW, Magnusson I, Petersen KF, Shulman GI. Impaired net hepatic glycogen synthesis in insulin-dependent diabetic subjects during mixed meal ingestion. A ^{13}C nuclear magnetic resonance spectroscopy study. J Clin Invest 1995;95(2):783-787.

Jones JG, Fagulha A, Barosa C, Bastos M, Barros L, Baptista C, Caldeira MM, Carvalheiro M. Noninvasive analysis of hepatic glycogen kinetics before and after breakfast with deuterated water and acetaminophen. Diabetes 2006;55(8):2294-2300.

Jones JG, Garcia P, Barosa C, Delgado TC, Caldeira MM, Diogo L. Quantification of hepatic transaldolase exchange activity and its effects on tracer measurements of indirect pathway flux in humans. Magn Reson Med 2008;59(2):423-429.

Jones JG, Solomon MA, Cole SM, Sherry AD, Malloy CR. An integrated H-2 and C-13 NMR study of gluconeogenesis and TCA cycle flux in humans. Am J Physiol Endocrinol Metab 2001;281(4):E848-E856.

Landau BR. Noninvasive approaches to tracing pathways in carbohydrate metabolism. J Parenter Enteral Nutr 1991;15(3):74S-777.

Lang CH, Bagby GJ, Blakesley HL, Johnson JL, Spitzer JJ. Plasma glucose concentration determines direct *versus* indirect liver glycogen synthesis. Am J Physiol Endocrinol Metab 1986;251(5):E584-E590.

Magnusson I, Chandramouli V, Schumann WC, Kumaran K, Wahren J, Landau BR. Quantitation of the pathways of hepatic glycogen formation on ingesting a glucose load. J Clin Invest 1987;80(6):1748-1754.

Mendes AC, Caldeira MM, Silva C, Burgess SC, Merritt ME, Gomes F, Barosa C, Delgado TC, Franco F, Monteiro P, Providencia L, Jones JG. Hepatic UDP-glucose ^{13}C isotopomers from [U-^{13}C]glucose: a simple analysis by ^{13}C NMR of urinary menthol glucuronide. Magn Reson Med 2006;56(5):1121-1125.

Napoli R, Capaldo B, Picardi A, Piscione F, Bigazzi MC, D'Ascia C, Sacca L. Indirect pathway of liver glycogen synthesis in humans is predominant and independent of beta-adrenergic mechanisms. Clin Physiol 1992;12(6):641-652.

Newgard CB, Hirsch LJ, Foster DW, Mcgarry JD. Studies on the mechanism by which exogenous glucose is converted into liver glycogen in the rat. A direct or an indirect pathway? J Biol Chem 1983;258(13):8046-8052.

Newgard CB, Moore SV, Foster DW, Mcgarry JD. Efficient hepatic glycogen synthesis in refeeding rats requires continued carbon flow through the gluconeogenic pathway. J Biol Chem 1984;259(11):6958-6963.

Perdigoto R, Rodrigues TB, Furtado AL, Porto A, Geraldes CFGC, Jones JG. Integration of [U-C-13]glucose and (H_2O)-H-2 for quantification of hepatic glucose production and gluconeogenesis. NMR in Biomedicine 2003;16(4):189-198.

Petersen KF, Cline GW, Gerard DP, Magnusson I, Rothman DL, Shulman GI. Contribution of net hepatic glycogen synthesis to disposal of an oral glucose load in humans. Metabolism 2001;50(5):598-601.

Prando R, Cheli V, Buzzo P, Melga P, Ansaldi E, Accoto S. Blood lactate behavior after glucose load in diabetes *mellitus*. Acta Diabetol Lat 1988;25(3):247-256.

Ribeiro A, Caldeira MM, Carvalheiro M, Bastos M, Baptista C, Fagulha A, Barros L, Barosa C, Jones JG. Simple measurement of gluconeogenesis by direct H-2 NMR analysis of menthol glucuronide enrichment from (H_2O)-H-2. Magn Reson Med 2005;54(2):429-434.

Schwenk WF, Kahl JC. Acetaminophen glucuronidation accurately reflects gluconeogenesis in fasted dogs. Am J Physiol Endocrinol Metab 1996;34(3):E529-E534.

Taylor Roy, Magnusson I, Rudenski AS, Cline GW, Caumo Andrea, Cobelli C, Shulman GI. Direct assessment of liver glycogen storage by ^{13}C nuclear magnetic resonance spectroscopy and regulation of glucose homeostasis after a mixed meal in normal subjects. J Clin Invest 1996;97:126-132.

Chapter 6

Hepatic lipid metabolism

Effects of high fat dietary food intake in rats

This chapter is based on:

Delgado TC, Pinheiro D, Caldeira M, Castro MMCA, Geraldes CFGC, Lopez-Larrubia P, Cerdán S, Jones JG. Sources of hepatic triglyceride accumulation during high-fat feeding in the healthy rat. NMR in Biomedicine (in press).

6.1. Introduction

The high fat (HF) level of the typical western style diet is considered to be an important factor in the development of type 2 diabetes (T2D) (McGarry 2001, Unger and Zhou 2001, Unger and Orci 2001). In this setting, there is an initial phase often referred to as the "prediabetic state" which is characterized by weight gain, an increase in the body fat fraction and the development of glucose intolerance. In addition to an overall gain in body fat, there is increased deposition of ectopic triglycerides, particularly in liver and skeletal muscle. Since these lipid pools may play a key role in the development of insulin resistance (IR) at an early and possibly reversible stage of T2D, there is an increased interest in the study of ectopic lipid dynamics both in order to better understand the pathogenesis of IR and also as a clinical marker for identifying people that may be at an elevated risk of developing T2D. There is particular focus on the study of ectopic hepatic triglycerides (HTG) as they are highly sensitive to dietary fat intake. Moreover, elevated HTG is tightly associated with glucose intolerance and decreased insulin sensitivity (Ryysi *et al.* 2000, Anderwald *et al.* 2002). Elevated HTG levels are prevalent in patients with established T2D (Ryysi *et al.* 2000, Anderwald *et al.* 2002, Mayerson *et al.* 2002, Kelley *et al.* 2003, Petersen *et al.* 2005), in animal models of T2D and are associated with features of the metabolic syndrome (Kotronen *et al.* 2008).

Rodent models are important for understanding the relationship between HTG and the development of IR and glucose intolerance in the "prediabetic" state. These models enable the design of prospective diet studies on HTG levels with the effects being observed within a few days or weeks. Non-diabetic healthy rats placed on a HF diet accumulate HTG (Samuel *et al.* 2004, Gauthier *et al.* 2006) and this is associated with significantly impaired insulin action, reduced whole body glucose disposal rates and hepatic IR (Kraegen *et al.* 1986, Storlien *et al.* 1986, Kraegen *et al.* 1991, Oakes *et al.* 1997a, Oakes *et al.* 1997b).

However, the time-scale and reversibility of HTG levels induced by HF diet and its associated effects on glucose homeostasis are not as well defined in rats compared to humans. This is because noninvasive methods such as Magnetic Resonance Spectroscopy (MRS)/Imaging (MRI) that have been developed and applied for monitoring longitudinal changes of human HTG levels have not yet been widely applied in rats. Localized proton (^{1}H) MRS is a noninvasive technique that has been shown to be a precise tool for quantification of HTG content (Szczepaniak *et al.* 1999, Szczepaniak *et al.* 2005, Thomas *et al.* 2005). With appropriate high-field Magnetic Resonance (MR) systems (7 Tesla (T) or above) was possible the quantification of HTG in mice (Garbow *et al.* 2004) and in the Zucker diabetic fatty (ZDF) rat, a model of T2D (Kuhlmann *et al.* 2003). Additionally, this measurement is well suited for longitudinal measurements of HTG in a single animal.

HTG can be derived from extra-hepatic fatty acids that are taken up and esterified to triglycerides following hepatic uptake or can also be formed *in situ via* hepatic *de novo* lipogenesis (DNL) of fatty acids from acetyl-CoA. Given the capacity of the liver to synthesize, import and export triglycerides, the accumulation of HTG may arise through an imbalance between triglyceride import and export and/or imbalance between triglyceride synthesis and utilization. In this study, total HTG were quantified by *in vivo* localized proton (^{1}H) MRS measurement and the lipogenic and non-lipogenic contributions resolved by integrating the MRS measurement with a novel and simple measurement of DNL by *ex vivo* deuterium (^{2}H) Nuclear Magnetic Resonance (NMR) analysis of HTG ^{2}H-enrichment from ^{2}H-enriched body water. This approach was applied to study the effects of altering dietary fat content on both HTG levels and sources in healthy male Sprague Dawley rats.

6.2. Materials and methods

6.2.1. Experimental design

Male Sprague-Dawley rats (180-220 g) were housed in a room on a 12-h light-dark cycle (08:00-20:00 h light) under constant temperature (22-25 ºC) and with *ad libitum* access to food and water. Animals were divided in three distinct study groups. In study 1, animals were studied during 20 days and divided in two different subgroups fed either with a HF diet (n=5) containing 45% of calories from fat, 35% from carbohydrate and 20% derived from protein (E15744-34, SSNIFF, Specialdiäten GmbH)® or with a standard chow (SC) diet (2.7% fat, 60% carbohydrate and 16% protein) (n=6). On day 8 and 15, the two subgroups were assessed in terms of HTG content and on the last day of experiment blood was withdrawn from 6-h fasted animals for determination of blood glycemia, plasma free fatty acids (FFA) and triglyceride content. These animals were challenged by a glucose tolerance test consisting of an intraperitoneal (i.p.) injection of glucose (1.5 mg glucose/g of body weight) and blood glycemia was assessed during 60 min after the glucose load, in pre-determined intervals. Blood glucose concentration was measured with a standard glucometer whereas plasma FFA and triglyceride levels were assessed using biochemical assay kits commercially available from Wako Chemicals GmbH and Sigma, respectively.

In study 2, a group of animals (n=5) was maintained during 35 days on HF diet feeding, and on the last day assayed for HTG content by ^{1}H MRS and compared to a group of animals fed with a SC diet (n=4). On the afternoon of day 35, animals were given an i.p. injection of 8 mL of 99.9% deuterated water ($^{2}H_2O$) (Sigma-Aldrich) in physiological saline. At this point, the drinking water was also enriched with 3% $^{2}H_2O$ to maintain constant body water enrichment until the end of the study. On day 37, animals were sacrificed at 14:00 h (24-h clock), livers were collected and freeze-clamped for lipid analysis, blood withdrawn and immediately centrifuged for plasma separation. Plasma was quickly stored at

-80ºC. 6-h fasting plasma glucose and insulin were also measured. Insulin was measured using an ELISA assay from Linco Research.

In study 3, Five rats were maintained on a HF diet during 8 days and afterwards switched back to a SC diet. On day 1, 8 and 15 of experiment, liver ^{1}H MRS was performed to assess HTG levels in each animal.

6.2.2. ^{1}H Magnetic Resonance Imaging and Spectroscopy (MRI/MRS)

In vivo MRI and ^{1}H MRS studies were performed on a 7 T Bruker Pharmascan system using a whole body coil for radiofrequency transmitting and signal receiving. Animals were placed in their prone position, kept at 37ºC and anesthetized with isoflurane anesthetic and maintained under 1.0-1.5% isoflurane-oxygen (v/v) during the imaging and spectroscopy experiments. Transverse images of the liver were used to ensure accurate positioning of the cubic voxel size of 5 mm in the region of interest (ROI) of liver (Figure 6.1). Single-voxel volume-localized ^{1}H MR spectra were obtained using a point-resolved spectroscopy (PRESS) sequence (repetition time, TR=1000 ms and echo time, TE=28 ms) without water saturation and with 128 average scans (Kuhlmann *et al.* 2003).

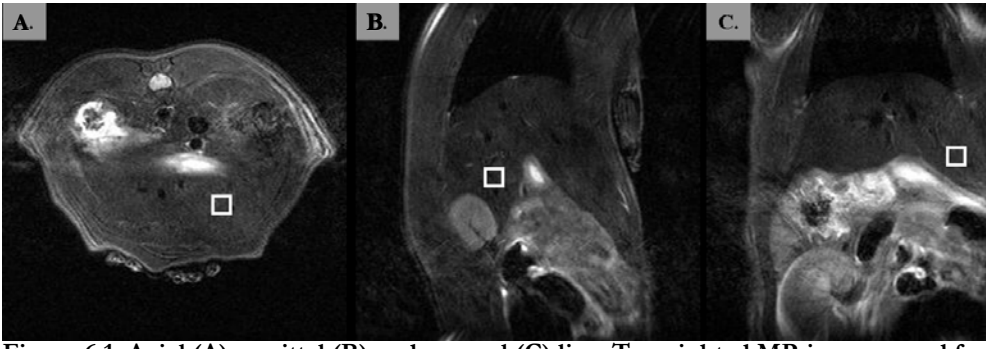

Figure 6.1. Axial (A), sagittal (B) and coronal (C) liver T_2-weighted MR images used for hepatic localization and voxel placement.

Spectra were analyzed using the NMR data processing program, MestreC (Mestrelab Research S.L., Spain), where peak areas for all resonances were obtained and the lipid resonance corresponding to the methylene group, $(CH_2)_n$, arising from aliphatic fatty acid chains of triglycerides was quantified with reference to the water resonance (Kuhlmann *et al.* 2003, Garbow *et al.* 2004).

6.2.3. Liver triglyceride extraction protocol

Hepatic lipids from freeze-clamped livers were separated by a Folch extraction (Folch *et al.* 1957) adding 20 mL of a chloroform/ethanol solution 2/1 (v/v) for each gram of liver powder under 15 min stirring at room temperature. After centrifugation, the supernatant was collected and diluted in NaCl (0.9%) in 5/1 (v/V) with vigorous agitation. Finally, after another centrifugation, the lower lipid-containing phase was collected, evaporated to dryness and dissolved in chloroform with pyrazine as an internal standard for NMR analysis.

6.2.4. ^1H and ^2H Nuclear Magnetic Resonance (NMR) analysis

^1H and ^2H NMR spectra were acquired at 11.75 T with a Varian spectrometer equipped with a 5-mm broadband "switchable" probe with z-gradient (Varian, Palo Alto, CA, USA). Proton-decoupled ^2H NMR spectra were acquired without field-frequency lock at 25ºC using a 90º pulse, a 2.0 second acquisition time and a 2.0 second pulse delay. ^2H-enrichment of the aggregate triglyceride methyl hydrogens, CH_3, was quantified by comparing the composite HTG methyl ^2H-signal with that of an internal pyrazine deuterated standard. The fraction of HTG derived from DNL was estimated as HTG ^2H-methyl/body water ^2H-enrichment. ^2H body water enrichment was determined in each plasma sample using ^2H NMR spectroscopy (Jones *et al.* 2001).

6.2.5. Estimating hepatic triglyceride synthesis from *de novo* lipogenesis by the analysis of acyl methyl hydrogen ^{2}H-enrichment from ^{2}H-enriched body water

During DNL, the methyl hydrogens of the acyl moiety are directly derived from those of acetyl-CoA and do not participate in the desaturation and chain elongation reactions that occur during lipogenesis. To our knowledge, there have been no direct measurements of acetyl-CoA enrichment from ^{2}H-enriched body water. Assuming that pyruvate is the main source of lipogenic acetyl-CoA and given that the exchange of pyruvate methyl protons with those of water is 80-95% complete (Rognstad *et al.* 1974, Kuwajima *et al.* 1986), the enrichment of body water is a good approximation for that of the immediate acetyl-CoA precursor. Assuming that body water enrichment is equal to that of the acetyl-CoA precursor, the fraction of triglyceride acyl groups derived from DNL (HTG lipogenic fraction) is simply the triglyceride enrichment divided by body water enrichment, given by Eq. 6.1.

$$\text{HTG lipogenic fraction (\%)} = 100 \times \frac{^{2}\text{H acyl methyl enrichment}}{^{2}\text{H body water enrichment}} \qquad \textit{[Eq. 6.1]}$$

In the ^{2}H NMR spectrum, methyl signals from palmitoyl (C16) and stearoyl (C18) chains co-resonate (Zhang *et al.* 2006) hence the NMR measurement reports the methyl enrichment from both C16 and C18 acyl moieties. A significant portion of stearyl acyl units are derived by an independent chain elongation reaction of palmitoyl-CoA (Bassilian *et al.* 2002). However, since the chain is elongated at the carboxyl end of the acyl moiety, the methyl hydrogens of these elongated acyl moieties still represent the original lipogenic C16 moiety. Therefore, the ^{2}H-enrichment level represents the total population of acyl units (C16 plus C18) derived from lipogenesis.

6.2.6. Data analysis

Data are presented as mean ± standard error mean (SEM). Statistical differences were determined using the paired or unpaired bilateral Student's t test, where $p < 0.05$ was considered to be statistically significant.

6.3. Results

6.3.1. Study groups characteristics

Table 6.1 shows the average weight gain for the 20 and 35 day study groups (study 1 and 2) in addition to fasting blood glucose, plasma insulin, FFA and triglyceride levels. HF diet-fed animals initially show an increased weight gain compared to the controls but after 35 days of HF diet, these animals showed a decreased average weight gain relative to animals on a SC diet for the same time period. HF diet was previously shown to reduce appetite in rodents (Liu *et al.* 2005), and therefore it can be speculated that the lower net weight gain in HF diet-fed animals was likely due to diminished food intake. Fasting blood glucose, plasma insulin, FFA and triglyceride concentrations were not significantly modified in animals placed on the HF diet compared to those maintained on SC.

TABLE 6.1: Biochemical and physical characteristics of the different groups of animals studied [#].

	Study 1- Day 20		Study 2- Day 35	
	SC diet	**HF diet**	**SC diet**	**HF diet**
n	6	5	4	5
Weight gain, g	110 ± 3	131 ± 3 *	191 ± 7	138 ± 8*
Blood glucose, mM	7.7 ± 0.2	8.4 ± 0.4	8.3 ± 0.6	9.7 ± 0.3
Insulin, ng/mL	-	-	0.27 ± 0.07	0.34 ± 0.11
Free fatty acids (FFA), mM	9.23 ± 0.81	12.31 ± 1.19	-	-
Triglycerides, mg/dL	76.4 ± 5.0	70.4 ± 7.3	-	-

[#] Data are presented as mean ± SEM; * $p<0.05$ relative to the control group for each study. (-) Not determined. SC. standard chow ; HF. high fat diet-fed animals.

Plasma glucose disposal following a glucose challenge was less efficient in HF diet fed animals compared to their SC counterparts as shown in Figure 6.2. In postprandial SC fed animals, blood glucose levels peaked at 15 minutes and returned to basal values (9.4 ± 0.8 mM) within 60 minutes of a glucose challenge. In comparison, postprandial HF diet-fed rats attained maximum plasma glucose levels at 15 minutes after the challenge but subsequently, plasma glucose levels failed to return to basal levels by 60 minutes (60 minutes plasma glucose = 13.3 ± 1.3 mM, $p<0.05$ compared to SC fed animals).

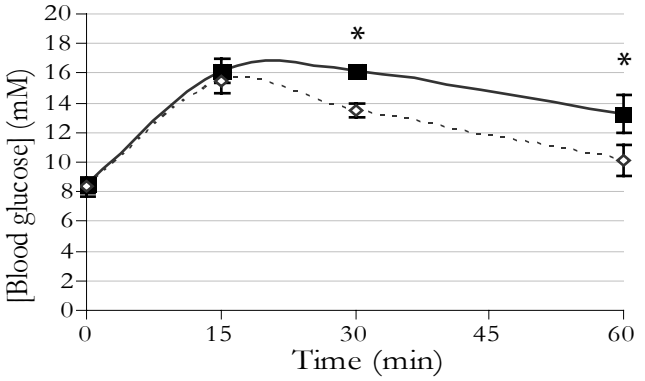

Figure 6.2. Glucose challenge profile during 60 min after the glucose load. Animals fed with a high fat (HF) diet (n=5) (black squares), and rats given a standard chow (SC) diet (n=4) (white diamonds). $p<0.05$ relative to controls.

6.3.2. Hepatic triglyceride content

Single-voxel ^{1}H MRS was previously validated *in vivo a*gainst the gold standard histological detection of HTG content, providing good correlation parameters (Szczepaniak *et al.* 1999, Garbow *et al.* 2004). The spectroscopic data reported here using a 7 T system allows the confident quantification of lipid, $(CH_2)_n$, and H_2O signals. ^{1}H MR liver spectra obtained from an animal on day 1 and day 8 of HFD are shown in Figure 6.3. The resonances from methylene

protons of triglyceride acyl chains appear between 1.0 and 1.6 parts *per* million (ppm). The composite acyl $(CH_2)_n$ signal was used for calculation of intracellular triglyceride content due to its higher signal intensity compared with the acyl methyl (CH_3) resonance.

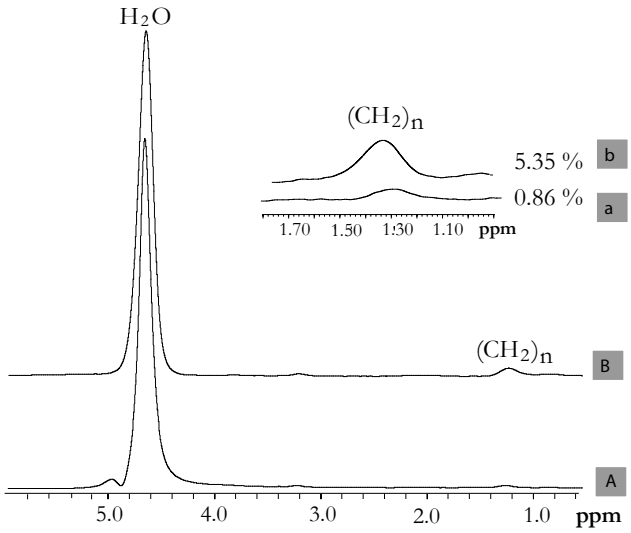

Figure 6.3. Hepatic ^{1}H Magnetic Resonance spectra of an animal for 1 (A) and 8 days (B) on a HF diet. H_2O is the water signal, whereas $(CH_2)_n$ corresponds to the methylene protons of triglyceride acyl chains that are shown expanded in the inset **a** and **b**, respectively for 1 and 8 days of HF diet.

Eight days of a HF diet promoted a significant increase in HTG levels in comparison to animals fed with a SC diet (3.85% ± 0.60% *vs.* 2.13% ± 0.34%, $p<0.05$). Interestingly, when the animals were continued on the HF diet, HTG levels did not show any further increases over SC fed rats (3.98% ± 0.86% *vs.* 1.55% ± 0.18%, $p<0.05$ on day 15; 3.30% ± 0.60% *vs.* 1.12% ± 0.30%, $p<0.05$ on day 35). In a group of rats that were fed for 7 days on a HF diet and then subsequently weaned on a SC diet for 7 days, HTG levels increased approximately three-fold following the change to HF diet, attaining comparable levels (3.33%

± 0.51%) to that observed at the same stage for the other HF groups. After 7 days of weaning on SC diet, HTG levels returned to basal values (0.76% ± 0.06%), as shown in Figure 6.4.

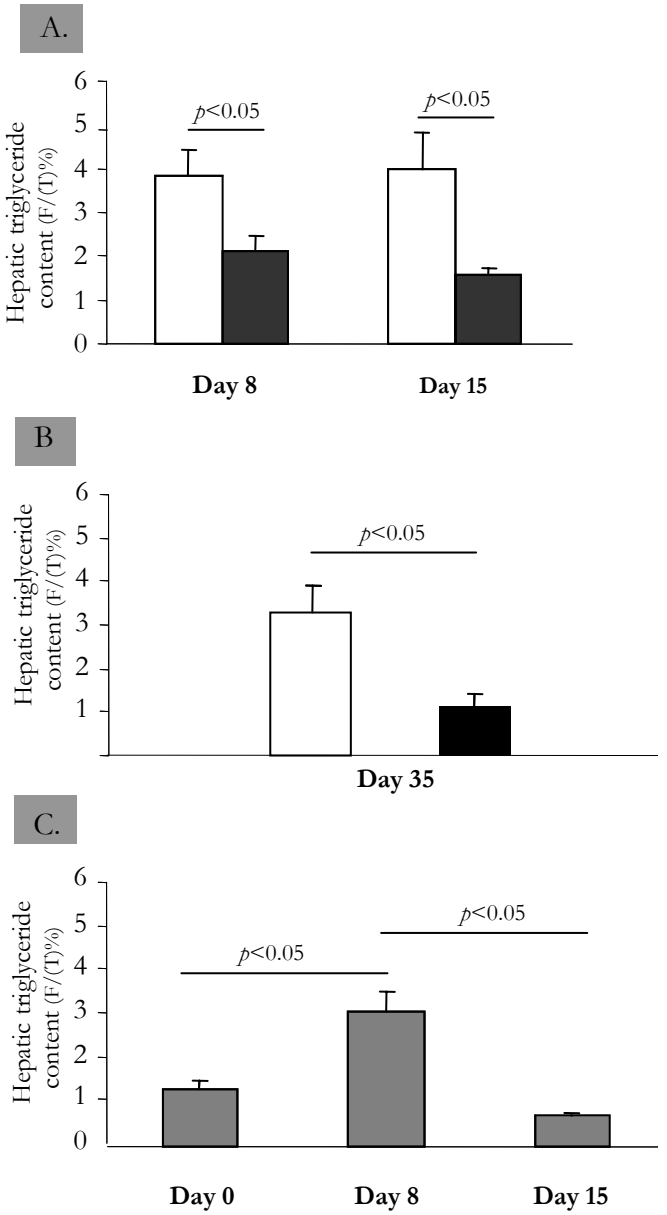

Figure 6.4. Hepatic triglyceride levels presented as mean ± SEM. A. Study 1**:** HTG content on day 8 and day 15 of rats maintained for 20 days on a high fat (HF) diet (n=5) and compared to a control group given a standard chow (SC) diet (n=6); **B.** Study 2: HTG levels of rats maintained for 35 days on a HF diet (n=5) and compared with a control group given a SC diet (n=4); **C.** Study 3: HTG content of a group of animals maintained for 7 days of a HF diet and then switched back to a SC diet (n=5). White columns correspond to animals fed with a HF diet, black columns to SC diet fed animals and grey columns to animals maintained 7 days on a HF diet and then switched back to SC diet. Values of $p < 0.05$ are indicated.

6.3.3. Contribution of *de novo* lipogenesis to hepatic triglycerides

The enrichment of HTG methyl hydrogens from ^{2}H-enriched body water provides a measure of the contribution of DNL to the total HTG pool. The triglyceride methyl hydrogens are directly traceable to the original acetyl-CoA precursor and they are also well resolved in the ^{2}H NMR spectrum of hepatic triglycerides isolated by a simple Folch extraction. The intensity of the methyl ^{2}H NMR signal reflects both the ^{2}H-enrichment at that site and the quantity of triglycerides in the NMR tube. Therefore, with constant triglyceride amounts, differences in ^{2}H-signal intensities between two samples reflect different levels of ^{2}H-enrichment. The spectra shown in Figure 6.5 represent 175 μmol portions of hepatic triglycerides extracted from livers of a SC and a HF diet-fed animal (Figure 6.5 A and B, respectively). The two samples had equivalent amounts of triglycerides, as shown by the equal triglyceride ^{1}H NMR signal intensities of their ^{1}H NMR spectra. However, the ^{2}H NMR signal intensities were ~10-fold higher in SC compared to HF diet-fed animals, indicating that the extent of ^{2}H-incorporation into the triglyceride of the SC fed animal was much greater compared to that of its HF diet-fed companion. From the ^{1}H and ^{2}H NMR data, triglyceride methyl ^{2}H-enrichment levels were estimated as described in the methods. By relating these enrichment values to that of body water, the fraction of HTG derived from *de novo* lipogenesis was derived (see Table 6.2). Body water enrichment was slightly but significantly elevated in HF fed animals relative to SC which may reflect a higher body lipid fraction in the former group. In animals

given a SC diet, 10.9% ± 1.0% of total HTG was derived from lipogenesis over a 48 h period while the remaining 89.1% ± 1.0% was either obtained from dietary sources or was present before the administration of deuterated water. With HF diet, the lipogenic fraction was reduced approximately 10-fold, accounting for only 1.0% ± 0.2% of total HTG ($p < 0.01$ compared to the lipogenic contribution in SC fed animals).

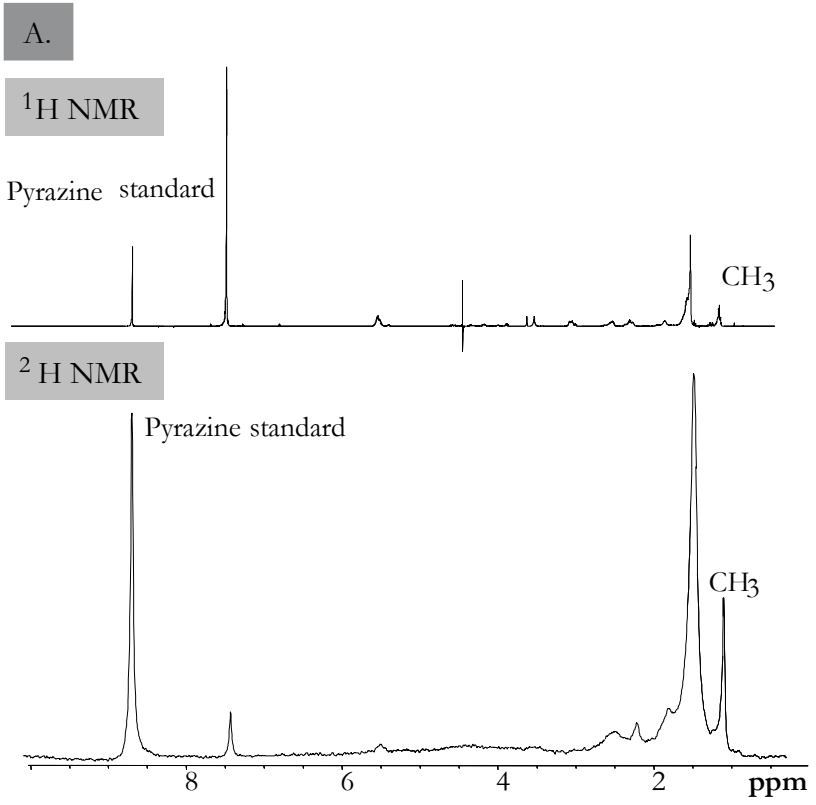

Figure 6.5.A. ^{1}H and ^{2}H NMR spectra of extracted liver triglycerides from an animal fed with a standard chow diet for 35 days. Pyrazine and triglycerides methyl signals are indicated.

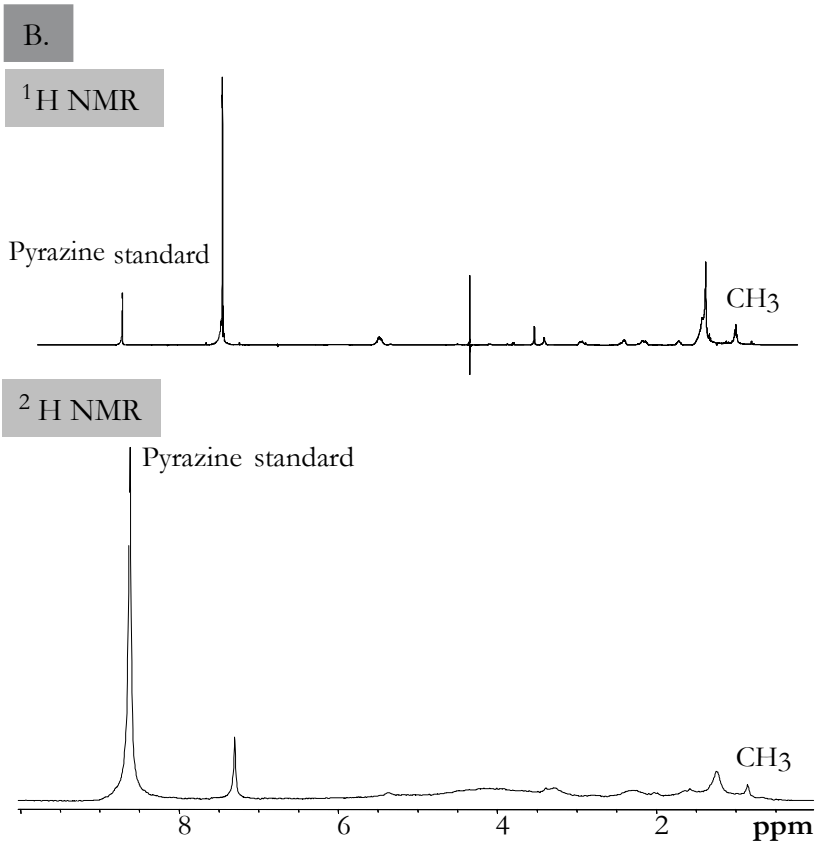

Figure 6.5. B. ^{1}H and ^{2}H NMR spectra of extracted liver triglycerides from an animal fed with a high fat diet for 35 days. Pyrazine and triglycerides methyl signals are indicated.

TABLE 6.2: ^{2}H body water enrichments and 48 h hepatic *de novo* lipogenesis fractional synthetic rates for high fat (HF) (n=5) and standard chow (SC) diet (n=4) fed animals for 35 days[#].

	SC diet	HF diet
^{2}H body water enrichment, %	1.59 ± 0.04	1.76 ± 0.03 *
^{2}H triglyceride methyl enrichment, %	1.78 ± 0.15	0.18 ± 0.03 *
HTG lipogenic fraction, %	10.9 ± 1.0	1.0 ± 0.2 **
HTG non-lipogenic fraction, %	89.1 ± 1.0	99.0 ± 0.2 **

[#] Data are presented as mean ± SEM; * p<0.05 and ** p<0.01, relative to SC fed animals.

6.4. Discussion

6.4.1. Effect of diet on hepatic triglyceride levels

When rats were placed on a HF diet for 5 weeks, HTG levels increased around 3-fold within the first week but then stabilized over the remaining four weeks. The results presented in here resemble previous studies of HTG levels in rats placed on a HF diet where HTG, measured by the gold-standard *post-mortem* enzymatic assay, increased by 200% in the first two weeks of HF diet (Gauthier *et al.* 2006). In a separate study, a 3-fold increase in HTG was found after 3 days of placement on a HF diet (Samuel *et al.* 2004) whereas others only showed a ~30% increase in HTG after 4 weeks of a diet containing 40% of the total calories as lard (Hudgins *et al.* 1996). A 3-fold increase in HTG is a relatively modest change when compared to HTG levels in patients with non-alcoholic steatohepatitis (NASH), the most severe form of non-alcoholic fatty liver disease (NAFLD), or in rat models of diet-induced NASH. Normal human HTG levels are similar to that of the rat (1-2%) while NASH subjects with or without T2D have HTG ranging from 10-50%. In rat models of diet-induced NASH (rats placed on a choline-deficient diet), HTG accumulates to ~40% of liver mass (Grattagliano *et al.* 2003).

These studies showed that elevated HTG levels induced by HF diet feeding quickly reverted to basal values when the rats were weaned on a SC diet, thus demonstrating the reversibility of this process and the high sensitivity of HTG to diet modification. The findings reported in here are analogous to recent observations in T2D patients, where elevated HTG levels were restored to normal values in a relatively short time by dietary intervention (Petersen *et al.* 2005). Alterations in rat HTG levels were not accompanied by changes in plasma triglycerides, suggesting that the liver may play a role as a systemic buffer in the face of dietary fat overload. These observations also demonstrate that an increase in HTG is among the earliest observable change in whole body lipid status when

rats are challenged by HF diet feeding and the utility of localized single-voxel ^{1}H MRS for noninvasively monitoring this change. However, even though single-voxel ^{1}H MRS was validated *in vivo* against histological and enzymatic assays of HTG content (Szczepaniak *et al.* 1999, Garbow *et al.* 2004), possible caveats include the presence of focal steatosis (Timlin and Parks 2005), where HTG concentrations measured by localized MR might differ from the mean value measured by *post-mortem* enzymatic assay.

6.4.2. Sources of hepatic triglycerides

The fatty acid components of HTG can be derived from outside the liver or can be synthesized within by DNL. While the contribution of DNL to systemic fatty acid synthesis has been determined in both rats and humans by various tracer methods, there are no reports on its contribution to HTG levels. Even though DNL rates are quite small in relation to total body lipid mass, they assume much higher significance in relation to the much smaller HTG pool size and could therefore play an important role in the regulation of HTG levels.

The association between DNL flux assessed by whole body fatty acid synthesis rates, HF feeding, and HTG has been explored in both healthy rats and T2D models. Placement of both healthy rats and the lean littermates of ZDF rats on a HF diet resulted in a reduction of DNL activity (Pichon *et al.* 2006) whereas in the obese ZDF rats, with elevated HTG content (Kuhlmann *et al.* 2003), DNL rates were unchanged (Lee *et al.* 2000). Since HTG levels reflect the balance between fatty acid import, DNL and triglycerides export, the relationship between DNL fluxes and the contribution of DNL to HTG levels is not known. The studies presented in here indicate that DNL contributions to HTG are modest for healthy animals on a SC diet but are essentially negligible when they are placed on a HF diet. Therefore, the increase in HTG levels during HF diet feeding is almost entirely driven by uptake and esterification of extra-hepatic fatty acids.

The effects of diet and pathophysiology on DNL in rats have strong parallels with observations of DNL in humans. In humans, the fractional contribution of DNL to hepatic lipid synthesis was noninvasively inferred from the analysis of triglyceride derived from the plasma fraction of very low density lipoproteins (VLDL) (Hudgins *et al.* 1996, Timlin and Parks 2005). In healthy humans, HF feeding over 25 days resulted in a sharply reduced DNL contribution to VLDL triglyceride compared to subjects given a low fat diet (Hudgins *et al.* 1996). These observations bear a strong resemblance to the results in rats presented in here and indicate that for both healthy rats and humans, DNL is highly attenuated by short term HF diet feeding. The effects of longer term HF feeding on DNL rates have not been characterized in humans. In subjects with NAFLD, a common endpoint of excessive long term dietary fat intake, DNL contributions were found to be chronically elevated under both fed and fasting conditions (Donnelly *et al.* 2005). These observations suggest that the regulation of DNL by dietary substrates was not functional, and resemble the absence of dietary DNL regulation observed in obese ZDF rats. Overall, these studies indicate a strong similarity in DNL between rats and humans and support the use of rat models for investigating the effects of diet, endocrine status and interventions on DNL.

Deuterated water is a highly convenient tracer for quantifying DNL, as steady-state enrichment in plasma is achieved within minutes after an i.p. injection bolus (see Chapter 4) which can then be maintained indefinitely by providing a maintenance level of $^{2}H_{2}O$ enrichment in drinking water. However, the measurement relies on some untested assumptions. It was considered that pyruvate was the main source of lipogenic acetyl-CoA and that the exchange of pyruvate methyl protons with those of the water is essentially complete (Rognstad *et al.* 1974, Kuwajima *et al.* 1986). Thus, the ^{2}H-enrichment of body water is assumed to be equal to that of acetyl-CoA and hence can be used as the precursor enrichment. To the extent that the methyl hydrogens of acetyl-CoA

are not fully exchanged with those of body water, the DNL contribution will be underestimated. With Mass Spectrometry (MS) measurements of ^{2}H lipid enrichment, a correction factor, known as the N value, corresponding to the average number of deuterium atoms incorporated into palmitate, is applied to account for incomplete exchange (Diraison *et al.* 1996). For *in vivo* rat studies, N was determined to be 22, corresponding to an exchange fraction of 22/31, or ~75% complete. Acetyl-CoA precursors, such as pyruvate, exchange extensively with bulk water, hence fatty acyl hydrogens derived directly from acetyl-CoA, including the terminal methyl hydrogens, may have a somewhat higher enrichment level (Rognstad *et al.* 1974, Kuwajima *et al.* 1986). Assuming a 75% rather than a 100% extent of ^{2}H-incorporation into acetyl-CoA, the reported DNL estimates would increase from 10.9% to 14.3% for the SC fed rats and from 1.0% to 1.3% for the HF diet group.

The other key assumption behind our estimates of lipogenic and non-lipogenic contribution to HTG is that the HTG pool turned over completely during the 72 hour exposure to $^{2}H_{2}O$. To the extent that HTG was incompletely turned over, this measurement underestimates the DNL contribution. In healthy humans, 9.2 grams of triglycerides *per* day are exported as VLDL (Vedala *et al.* 2006). Assuming a liver mass of 1.5 kg and HTG levels of 1%, giving a HTG pool size of 15 grams, the daily output represents ~60% of HTG, hence the pool is completely replaced in less than 2 days. Given the faster basal metabolic rate of the rat, it was assumed that under this study conditions, HTG were completely turned over within the 72 hour period of ^{2}H body water enrichment. However, triglyceride turnover in steatotic livers may be longer, given the increased pool size, hence under these conditions, the period of body water ^{2}H-enrichment may need to be extended.

6.4.3. Relationship between hepatic triglycerides and glycemic status

In animal models, glycemic control and IR are highly associated with the accumulation of triglycerides in liver and skeletal muscle (Oakes *et al.* 1997a, Oakes *et al.* 1997b). These sites have a selective contribution to the pathogenesis of IR and hyperglycemia in that the accumulation of intramyocellular lipid (IMCL) in skeletal muscle impairs the action of insulin on the whole body disposal of glucose, while increased hepatic triglyceride is associated with an impairment of endogenous glucose production (EGP). During the transition to HF diet feeding, the hepatic triglyceride pool - because of its relatively small mass and high turnover – is likely to be modified faster and by a larger degree compared to IMCL. Therefore at this early stage, the reduced ability of insulin to suppress postprandial EGP could play an important role in the development of glucose intolerance.

Studies in healthy animals following 3 days on a HF diet showed that, while insulin-stimulated glucose disposal and basal EGP were not different from control animals maintained on a SC diet, under hyperinsulinemic clamp conditions there was an impaired suppression of EGP, indicative of hepatic IR (Gauthier *et al.* 2006). In this study, the extent of glucose intolerance induced by 35 days of HF feeding was relatively modest, as seen by comparable fasting blood glucose and insulin levels to animals maintained on the SC diet. A previous study reported enhanced IR and glucose intolerance after 4 weeks of a HF diet (Srinivasan *et al.* 2004). Seven weeks of a HF diet in healthy rats was also associated with higher blood glucose 2 hours after the oral glucose challenge (Huang *et al.* 2004). The mild loss of glucose tolerance that it was observed in this study may reflect the relatively small increment of HTG levels in comparison to that observed in T2D rat animal models with severe glucose intolerance (Garbow *et al.* 2004). In comparison to the clamp measurement, a glucose tolerance test does not provide direct measurements of insulin action on glucose production and disposal fluxes and therefore may not resolve hepatic and peripheral IR. However, as with ^{1}H

MRS analysis of HTG, a glucose tolerance test can in principle be repeated in the same animal and may therefore be useful for relating longitudinal changes in HTG with alterations in glycemic status for individual animals.

6.5. Conclusions

In healthy rats, hepatic triglyceride levels can be acutely raised or lowered by altering the dietary fat content and these changes can be effectively monitored by ^{1}H MRS. During HF feeding, essentially all of the hepatic triglyceride is derived from dietary lipid with very little contribution from DNL. ^{1}H MRS is a noninvasive and accurate technique suitable for longitudinal studies of evaluation of hepatic triglyceride content in animal models and can be used for assessing the effects of dietary interventions. The novel ^{2}H NMR measurement of hepatic triglyceride ^{2}H-enrichment from $^{2}H_2O$ reported in here, in spite of requiring further validation, is a simple and practical approach for assessing the contribution of *de novo* lipogenesis to hepatic triglyceride levels.

6.6. References

Anderwald C, Bernroider E, Krssak M, Stingl H, Brehm A, Bischof MG, Nowotny P, Roden M, Waldhausl W. Effects of insulin treatment in type 2 diabetic patients on intracellular lipid content in liver and skeletal muscle. Diabetes 2002;51(10):3025-3032.

Bassilian S, Ahmed S, Lim SK, Boros LG, Mao CS, Lee W-NP. Loss of regulation of lipogenesis in the Zucker diabetic rat. II. Changes in stearate and oleate synthesis. Am J Physiol Endocrinol Metab 2002;282(3):E507-E513.

Diraison F, Pachiaudi C, Beylot M. *In vivo* measurement of plasma cholesterol and fatty acid synthesis with deuterated water: Determination of the average number of deuterium atoms incorporated. Metab Clin Exp 1996;45(7):817-821.

Donnelly K.L., Smith C.I., Schwarzenberg S.J., Jessurun J., Boldt M.D., Parks E.J. Sources of fatty acids stored in liver and secreted *via* lipoproteins in patients with nonalcoholic fatty liver disease. J Clin Invest 2005;115(5):1343-1351.

Folch J, Lees M, Stanley GHS. A simple method for the isolation and purification of total lipids from animal tissues. J Biol Chem 1957;226(1):497-509.

Garbow JR, Lin X, Sakata N, Chen Z, Koh D, Schonfeld G. *In vivo* MRS measurement of liver lipid levels in mice. J Lipid Res 2004;45(7):1364-1371.

Gauthier MS, Favier R, Lavoie JM. Time course of the development of non-alcoholic hepatic steatosis in response to high-fat diet-induced obesity in rats. Br J Nutr 2006;95(2):273-281.

Grattagliano I, Caraceni P, Portincasa P, Domenicali M, Palmieri VO, Trevisani F, Bernardi M, Palasciano G. Adaptation of subcellular glutathione detoxification system to stress conditions in choline-deficient diet induced rat fatty liver. Cell Biol Toxicol 2003;19(6):355-366.

Hudgins LC, Hellerstein MK, Seidman C, Neese RA, Diakun J, Hirsch LJ. Human fatty acid synthesis is stimulated by a eucaloric low fat, high carbohydrate diet. J Clin Invest 1996;97(9):2081-2091.

Huang BW, Chiang MT, Yao HT, Chiang W. The effect of high-fat and high-fructose diets on glucose tolerance and plasma lipid and leptin levels in rats. Diabetes Obes Metab 2004;6(2):120-126.

Jones JG, Merritt M, Malloy C. Quantifying tracer levels of (H_2O)-H-2 enrichment from microliter amounts of plasma and urine by H-2 NMR. Magn Reson Med 2001;45(1):156-158.

Kelley DE, McKolanis TM, Hegazi RAF, Kuller LH, Kalhan SC. Fatty liver in type 2 diabetes *mellitus*: relation to regional adiposity, fatty acids, and insulin resistance. Am J Physiol Endocrinol Metab 2003;285(4):E906-E916.

Kotronen A, Seppala-Lindroos A, Bergholm R, Yki-Jarvinen H. Tissue specificity of insulin resistance in humans: fat in the liver rather than muscle is associated with features of the metabolic syndrome. Diabetologia 2008;51(1):130-138.

Kraegen EW, Clark PW, Jenkins AB, Daley EA, Chisholm DJ, Storlien LH. Development of muscle insulin resistance after liver insulin resistance in high-fat-fed rats. Diabetes 1991;40(11):1397-1403.

Kraegen EW, James DE, Storlien LH, Burleigh KM, Chisholm DJ. *In vivo* insulin resistance in individual peripheral tissues of the high fat fed rat: assessment by euglycaemic clamp plus deoxyglucose administration. Diabetologia 1986;29(3):192-198.

Kuhlmann J, Neumann-Haefelin C, Belz U, Kalisch J, Juretschke HP, Stein M, Kleinschmidt E, Kramer W, Herling AW. Intramyocellular lipid and insulin resistance: a longitudinal *in vivo* ^{1}H-spectroscopic study in Zucker diabetic fatty rats. Diabetes 2003;52(1):138-144.

Kuwajima M, Golden S, Katz J, Unger RH, Foster DW, Mcgarry JD. Active hepatic glycogen-synthesis from gluconeogenic precursors despite high tissue-levels of fructose 2,6-bisphosphate. J Biol Chem 1986;261(6):2632-2637.

Lee WNP, Bassilian S, Lim S, Boros LG. Loss of regulation of lipogenesis in the Zucker diabetic (ZDF) rat. Am J Physiol Endocrinol Metab 2000;279(2):E425-E432.

Liu R, Sun CH, Weng Y. The study on mechanism of appetite regulation in diet-induced obesity resistant rats. Zhonghua Yu Fang Yi Xue Za Zhi 2005;39(2):119-121.

Mayerson AB, Hundal RS, Dufour S, Lebon V, Befroy D, Cline GW, Enocksson S, Inzucchi SE, Shulman GI, Petersen KF. The Effects of Rosiglitazone on insulin sensitivity, lipolysis, and hepatic and skeletal muscle triglyceride content in patients with type 2 diabetes. Diabetes 2002;51(3):797-802.

McGarry JD. Banting Lecture 2001: Dysregulation of fatty acid metabolism in the etiology of type 2 diabetes. Diabetes 2002;51(1):7-18.

Oakes ND, Bell KS, Furler SM, Camilleri S, Saha AK, Ruderman NB, Chisholm DJ, Kraegen EW. Diet-induced muscle insulin resistance in rats is ameliorated by acute dietary lipid withdrawal or a single bout of exercise: parallel relationship between insulin stimulation of glucose uptake and suppression of long-chain fatty acyl-CoA. Diabetes 1997;46(12):2022-2028.

Oakes ND, Cooney GJ, Camilleri S, Chisholm DJ, Kraegen EW. Mechanisms of liver and muscle insulin resistance induced by chronic high-fat feeding. Diabetes 1997;46(11):1768-1774.

Petersen KF, Dufour S, Befroy D, Lehrke M, Hendler RE, Shulman GI. Reversal of nonalcoholic hepatic steatosis, hepatic insulin resistance, and hyperglycemia by moderate weight reduction in patients with type 2 diabetes. Diabetes 2005;54(3):603-608.

Pichon L, Huneau JF, Fromentin G, Tome D. A high-protein, high-fat, carbohydrate-free diet reduces energy intake, hepatic lipogenesis, and adiposity in rats. J Nutr 2006;136(5):1256-1260.

Rognstad R, Clark DG, Katz J. Glucose synthesis in tritiated-water. Eur J Biochem 1974;47(2):383-388.

Ryysy L, Hakkinen AM, Goto T, Vehkavaara S, Westerbacka J, Halavaara J, Yki-Jarvinen H. Hepatic fat content and insulin action on free fatty acids and glucose metabolism rather than insulin absorption are associated with insulin requirements during insulin therapy in type 2 diabetic patients. Diabetes 2000;49(5):749-758.

Samuel VT, Liu ZX, Qu XQ, Elder BD, Bilz S, Befroy D, Romanelli AJ, Shulman GI. Mechanism of hepatic insulin resistance in non-alcoholic fatty liver disease. J Biol Chem 2004;279(31):32345-32353.

Srinivasan K, Patole PS, Kaul CL, Ramarao P. Reversal of glucose intolerance by Pioglitazone in high fat diet-fed rats. Methods Find Exp Clin Pharmacol 2004;26(5):327-333.

Storlien LH, James DE, Burleigh KM, Chisholm DJ, Kraegen EW. Fat feeding causes widespread *in vivo* insulin resistance, decreased energy expenditure, and obesity in rats. Am J Physiol Endocrinol Metab 1986;251(5):E576-E583.

Szczepaniak LS, Babcock EE, Schick F, Dobbins RL, Garg A, Burns DK, McGarry JD, Stein DT. Measurement of intracellular triglyceride stores by ^{1}H spectroscopy: validation *in vivo*. Am J Physiol Endocrinol Metab 1999;276(5):E977-E989.

Szczepaniak LS, Nurenberg P, Leonard D, Browning JD, Reingold JS, Grundy S, Hobbs HH, Dobbins RL. Magnetic resonance spectroscopy to measure hepatic triglyceride content: prevalence of hepatic steatosis in the general population. Am J Physiol Endocrinol Metab 2005;288(2):E462-E468.

Thomas EL, Hamilton G, Patel N, O'Dwyer R, Dore CJ, Goldin RD, Bell JD, Taylor-Robinson SD. Hepatic triglyceride content and its relation to body adiposity: a magnetic resonance imaging and proton magnetic resonance spectroscopy study. Gut 2005;54(1):122-127.

Timlin MT, Parks EJ. Temporal pattern of *de novo* lipogenesis in the postprandial state in healthy men. Am J Clinical Nutrition 2005;81(1):35-42.

Unger RH, Orci L. Diseases of liporegulation: new perspective on obesity and related disorders. FASEB J 2001;15(2):312-321.

Unger RH, Zhou Y. Lipotoxicity of beta-cells in obesity and in other causes of fatty acid spillover. Diabetes 2001;50(90001):S118-S121.

Vedala A, Wang W, Neese RA, Christiansen MP, Hellerstein MK. Delayed secretory pathway contributions to VLDL-triglycerides from plasma NEFA, diet, and *de novo* lipogenesis in humans. J Lipid Res 2006;47(11):2562-2574.

Zhang BL, Pionnier S, Buddrus S. Deuterium NMR study of the origin of hydrogen in fatty acids produced *in vivo* by chicken. Eur J Lipid Sci Tech 2006;108(2):125-133.

Chapter 7

Concluding Remarks

CONCLUDING REMARKS

Alterations in hepatic metabolic fluxes play an important role in the loss of glucose homeostasis that is associated with certain nutritional imbalances (i.e., high fat (HF) or sugar feeding) or pharmacological interventions (i.e., immunosuppressant drugs such as glucocorticoids and calcineurin inhibitors).

To better define the relationship between hepatic metabolic fluxes and the development of whole body insulin resistance (IR) and glucose intolerance in these settings, novel noninvasive assays of hepatic glucose and lipid fluxes were developed and applied to both human subjects and animal models. These measurements were accompanied by standard clinical assessments of plasma insulin and glucose levels, thus allowing whole body glucose tolerance and insulin sensitivity to be correlated with hepatic metabolic activity. In particular, the insulin-mediated rates of hepatic glucose production (HGP) under both basal fasting conditions and in the face of a glucose challenge were assessed to provide a measure of hepatic insulin resistance. HGP was resolved into its gluconeogenic and glycogenolytic components in order to define the role of these pathways in sustaining normal and abnormal HGP rates.

In 6-h fasted healthy animals, tracer measurements revealed that all plasma glucose was derived from HGP with equal contributions from hepatic gluconeogenesis and glycogenolysis fluxes. At 60 minutes after a glucose load, HGP contribution dropped to 55% of total plasma glucose, but this was not accompanied by a shift in HGP source fluxes. Thus, in healthy animals, while a glucose load diluted the contribution of HGP to total plasma glucose, it did not result in a significant reorganization of HGP source fluxes. Lactate derived from Cori cycle metabolism of the administered glucose load was the principal hepatic gluconeogenic precursor. Hepatic glycogen synthesis accounted for a very minor portion (<2%) of the total glucose load disposal. Surprisingly, given

the sole presence of glucose and the absence of other substrates, the indirect pathway contributed to the majority (~60%) of hepatic glycogen synthesis. Fasting and postprandial plasma glucose and insulin concentrations were similar to those reported in previous rodent studies of glucose loading. On this basis, the observed hepatic fluxes are representative of the standard physiological and endocrine responses to a glucose load.

In comparison, overnight-fasted humans also derived all plasma glucose from HGP with similar gluconeogenic and glycogenolytic contributions to that observed in 6-h fasted rats. After an oral glucose load, HGP contributed to a much smaller fraction of plasma glucose (< 15%) suggesting that HGP was suppressed more efficiently in the human compared to the rat studies. Through the noninvasive assay of uridine diphosphate-glucose (UDP-glucose) enrichment, direct and indirect pathway contributions to hepatic glycogen synthesis were evaluated and found to contribute ~50% of hepatic glycogen synthesis flux. Fasting and postprandial plasma glucose and insulin concentrations were similar to those reported in previous human studies and reflected normal glucose tolerance and insulin sensitivity as determined by the Homeostasis model assessment of insulin resistance (HOMA-IR).

Healthy animals placed on a HF diet for 20 days showed normal fasting glycemia. Consistent with previous reports of loss of insulin sensitivity secondary to HF diet feeding, there was mild glucose intolerance after a glucose challenge, as seen by systematically higher plasma glucose levels from 20-60 minutes after the glucose load. HGP rates and source contributions (gluconeogenesis and glycogenolysis) were not significantly different from animals fed on a standard chow (SC) diet and postprandial hepatic glycogen levels were also similar. Therefore the observed glucose intolerance is not the result of altered hepatic fluxes but rather a consequence of peripheral insulin resistance.

Hepatic insulin resistance is highly associated with increased hepatic triglycerides (HTG). By using *in vivo* proton (^{1}H) Magnetic Resonance

Spectroscopy (MRS), HTG levels were shown to be highly sensitive to dietary alterations. As a result of 8 days HF diet feeding, HTG increased relative to the controls and returned to basal values after weaning on a SC diet for the same time period. Although HF diet caused a tripling of HTG levels relative to controls (~3 % *vs.* ~1% by weight), these changes are very modest compared with animal models of induced hepatic stetatosis, where HTG levels can exceed 40% of total liver weight. The modest changes in HTG levels that accompanied HF diet feeding were not accompanied by alterations in hepatic glucose and glycogen metabolism. In accord with the low dietary carbohydrate to fat ratio, the contribution of hepatic *de novo* lipogenesis to HTG was suppressed under these conditions and HTG were almost entirely derived from dietary lipid. In other animal models of hepatic steatosis, *de novo* lipogenesis may have a far more significant role in escalating HTG. The novel methods developed in here for measurement of hepatic *de novo* lipogenesis can be easily transferred to the clinical setting by providing deuterated water (^2H_2O) together with sulfamethoxazole (SMX) following analysis of the plasma very low density lipoprotein triglycerides and urinary SMX conjugates enrichments.

Fasting hyperglycemia and glucose intolerance in normally-fed animals were induced after administration of CsA, a widely used immunosuppressant drug. After a glucose challenge, CsA-treated rats were less able to suppress HGP relative to control animals. A tendency for decreased insulin secretion was observed which is consistent with the known impairment of pancreatic insulin secretion by CsA. Thus, it is speculated that in CsA-treated rats, alterations in hepatic glucose metabolism (i.e., hepatic insulin resistance) in addition to diminished insulin secretion contribute to glucose intolerance. In addition, a bigger contribution from the glucose load to total glucose was observed in CsA-treated rodents which could result from changes in glucose absorption and/or clearance profiles.

In the clinical setting, CsA treatment is associated with the development

of posttransplant diabetes *mellitus* (PTDM). However, posttransplant patients also typically gain weight following the transplant and the extent to which PTDM is associated with weight gain *per se*, as compared to the effects of CsA alone, are unclear.

Sources of postabsorptive HGP were studied in lean and obese posttransplant patients with ongoing CsA immunosuppressant therapy and compared to healthy controls. For posttransplant patients undergoing CsA immunosuppressant therapy, the gluconeogenic contribution to fasting HGP was significantly increased in the setting of PTDM. This metabolic alteration was most strongly associated with increased body mass index whereas CsA treatment *per se* provoked only modest alterations of HGP sources and was not associated with fasting hyperglycemia or hyperinsulinemia. Thus, in posttransplant humans, alterations in hepatic glucose fluxes that contribute to the development of glucose intolerance and PTDM are more strongly associated with obesity than with CsA.

In conclusion, this Thesis advanced our understanding of hepatic glucose and lipid metabolic fluxes in both normal and glucose intolerant conditions induced by diet and by CsA. Among other things, defining the sources and contribution of HGP to hyperglycemia could prove useful for evaluating the efficacy of new antihyperglycemic drugs that function by inhibiting the activities of specific HGP enzymes.

ACKNOWLEDGEMENTS/AGRADECIM(I)ENTOS

To Doctor John Jones, my scientific mentor, I express deep gratitude for the guidance throughout these years, the sharing of your expertise, and your friendship.

Ao Professor Carlos Geraldes agradeço a supervisão e orientação. Obrigada por me ter recebido com amizade no Grupo de RMN e pela oportunidade de realizar esta projecto de Doutoramento contando sempre com o seu apoio e vasto conhecimento científico.

Al Doctor Sebastián Cerdán mi reconocimiento por la supervisión de mi doctorado, y por haberme recibido en su laboratorio donde encontré todos los medios y ayuda necesaria para realizar una larga parte de los experimentos descritos en esta Tesis.

À Doutora Margarida Castro agradeço profundamente todo o apoio e amizade.

Já diz o fado que "Coimbra tem mais encanto na hora da despedida". É este estranho encanto que faz com que os que partem desta cidade voltem para rever as amizades que fizeram em Coimbra. Um obrigada especial à Claúdia, Cristina, Daniela, Isabel, Doutora Madalena e Patrícia, cuja colaboração foi fundamental na realização desta Tese. Não podia também deixar de agradecer a algumas pessoas que desde o primeiro dia me acarinharam: Carla, Giovannia, Liliana e Pedro Coxito. Um abraço aos membros do Departamento de Bioquímica de Faculdade de Ciências e Tecnologia da Universidade de Coimbra, do Centro de Neurociências e Biologia Celular de Coimbra e em especial aos do Laboratório de RMN deste Centro com os quais convivi diariamente nos últimos anos. Obrigada a todos pelos bons momentos partilhados.

Querría dejar también una palabra de amistad a algunas personas del Instituto de Investigaciones Biomédicas "Alberto Sols", que siempre me ayudaron, y más que todo me hicieron sentir siempre uno mas de ellos: Alejandra, Guti, Inês, Javi, Jesús, Laura, Marina, Marisa, Patri, Pilar, Rocío, Rosa, Rui, Santiago, Tere, Tiago y Valeria.

Ao serviço de Endocrinologia, Diabetes e Metabolismo do Hospital Universitário de Coimbra, e principalmente à Doutora Manuela Carvalheiro, Dra. Margarida Bastos e Dra. Carla Baptista o meu agradecimento por este anos de trabalho em conjunto. Obrigada a todos os Enfermeiros e funcionários deste serviço que sempre me auxiliaram em todos os estudos clínicos realizados. A minha gratidão ao Doutor Alfredo Mota do serviço de Transplantes Renais deste mesmo Hospital.

To Doctors Craig Malloy, Matthew Merritt and Shawn Burgess, my gratitude for receiving me in the Advanced Imaging Research Center at the Texas University Southwestern Medical Center in Dallas, Texas, USA. Thank you to all of the laboratory members, especially Angela and Chuck, for sharing their expertise with me.

To Doctor Lidia Szczepaniak, from the Texas University Southwestern Medical Center, thank you for the excellent opportunity to learn about *in vivo* Magnetic Resonance techniques.

To Doctors Donald Scott and Robert O'Doherty, from the University of Pittsburgh Medical School, thank you for revealing me novel approaches for studying diabetes.

Um agradecimento especial a todos os voluntários que participaram nos estudos clínicos apresentados nesta Tese.

Edgar e Ana, obrigada por esta experiência inesquecível que foi viver com vocês.

Aos meus amigos.
A mis amigos.
To my friends.
Als meus amics.

À minha família.

E finalmente, às pessoas mais importantes da minha vida a quem dedico esta Tese. Pai, mãe e Guida, obrigada por acreditarem em mim.

In the last decades, insulin resistance and type 2 diabetes (T2D) are becoming more prevalent mainly due to alterations in dietary and life-styles. Posttransplant diabetes *mellitus* (PTDM) has also become a subject of interest and importance in the wake of increased numbers and survival rates of solid organ transplantations. Hepatic glucose and lipid metabolism disruptions appear to play a central role in the onset of insulin resistance, T2D and PTDM. Changes in hepatic glucose and lipid fluxes using stable isotope tracers and Nuclear Magnetic Resonance (NMR) analysis both in animal models and patients with insulin resistance, T2D or PTDM were addressed in this Thesis. Moreover, further developments of techniques for the study of hepatic glucose metabolism from fasting to dynamic situations were challenged as well as for the integrated analysis of hepatic glucose and lipid metabolism.